11-13-2019 5:00 PM

The Impact of Scaphoid Malunion on Wrist Kinematics & Kinetics: A Biomechanical Investigation

Spencer B. Chambers
The University of Western Ontario

Supervisor
Suh, Nina
The University of Western Ontario
Johnson, James
The University of Western Ontario

Graduate Program in Surgery
A thesis submitted in partial fulfillment of the requirements for the degree in Master of Science

Abstract

Scaphoid fractures are very common injuries that can have serious sequelae if pathologic healing ensues. Although there is agreeance regarding the importance of a non-united scaphoid, the impact of a malunited scaphoid is less clear. This is based on a paucity in the literature and the lack of understanding of the natural history of scaphoid malunion. This study aims to elucidate this question by investigating the impact of scaphoid malunion on joint kinetics, as well as the impact of scaphoid malunion on carpal bone kinematics. This was accomplished using a combination of *in-silico*, as well as *in-vivo* modelling based of cadaveric results derived from an active motion simulator. Our results showed that increasing scaphoid malunion was associated with increasing joint contact at the radioscaphoid joint. There was no significant relationship between scaphoid motion and scaphoid malunion severity; however, there was a significant change in lunate motion, as well as motion between the scaphoid and lunate ($p<0.05$).

This work serves as the framework for understanding the complex motion of the carpus and emphasizes the potential importance of establishing a good reduction of the scaphoid following fracture. The clinical importance of this finding has yet to be elucidated, but by understanding this relationship future clinical studies can be targeted at identifying features of patients who may benefit from therapy and intervention.

Keywords: Scaphoid; Malunion; Biomechanics; Computational Modelling**;** Biomechanical modelling.

Lay Summary

The wrist is a complex joint made up of eight bones. These bones are uniquely shaped to fit together in a way that allows for many different gripping positions. One of the bones, the scaphoid, is particularly important because it coordinates movement of all the other wrist bones. For this reason, if the shape of the scaphoid is changed by an injury, the entire wrist can be impacted. This leads to painful and limited motion that can result in arthritis. The most common injury that results in a change to a scaphoids shape is when it is broken and heals in the wrong position; this is called a malunion. Some of these injuries heal with standard medical treatment, but others have a difficult recovery. With the number of these injuries being so large in Ontario, numerous individuals who have this injury will go on to have lifelong wrist pain, limited movement, and loss of strength. Currently, the importance of this injury is not known. There have been many reports of patients with this injury having limited painful movement that improves after surgery to correct this. Other reports have argued that this change in shape is not important to normal function. The overall picture is unclear because the changes to wrist motion caused by a scaphoid malunion have never been studied. This makes it difficult for surgeons to decide the best treatment for patient with this injury.

The objective of this project was to investigate how increasing severity of scaphoid malunion changes wrist motion. By understanding this relationship we plan to identify target future clinical research that may eventually help create guidelines to assist surgeons make decisions about the best treatment for a patient with this injury.

Co-Authorship Statement

Chapter 1:

Sole Authorship: Spencer B Chambers
Manuscript Review: Nina Suh, James Johnson

Chapter 2:

Study Design: Nina Suh, Clare Padmore, Spencer B Chambers, Jim Johnson
Computational Specimen Preparation: Clare Padmore, Spencer B Chambers
Data Analysis: Clare Padmore, Spencer B Chambers
Statistical Analysis: Clare Padmore
Manuscript Preparation: Spencer B Chambers, Clare Padmore
Manuscript Review: Nina Suh, James Johnson

Chapter 3:

Study Design: Spencer B Chambers, Clare Padmore, Nina Suh, James Johnson
Specimen Preparation: Spencer B Chambers, Clare Padmore, Stacy Fan, Nina Suh
Data Collection: Spencer B Chambers, Clare Padmore, Stacy Fan, Brendan McNeely
Data Analysis: Spencer B Chambers, Clare Padmore
Statistical Analysis: Clare Padmore
Manuscript Preparation: Spencer B Chambers, Clare Padmore
Manuscript Review: Nina Suh, James Johnson

Chapter 4:

Sole Authorship: Spencer B Chambers
Manuscript Review: Nina Suh, James Johnson

Acknowledgments

The preparation and completion of this manuscript was made possible through the contributions and assistance of numerous individuals. Firstly, I would like to thank my supervisors Dr. Nina Suh and Dr. James Johnson, both of whom offered immense support and insight. Their availability throughout the design and implementation of this study has been invaluable and I truly could not have done it without them.

Clare Padmore was instrumental throughout the testing, data analysis, and engineering components of this project. The magnitude of her assistance cannot be overstated. I am truly fortunate to have had the opportunity to work with her. The long days in the lab and seemingly insurmountable task that was this work became possible with her assistance.

I also want to thank the RM|HULC lab, including those who have completed work before me that laid the groundwork for this research. Duncan Iglesias, Emily Lalone, Helen Stoesser, and Diana Isa are among the few whose work laid the foundation of the production of this paper.

Last but not least I want to extend a sincere thanks to my fiancé, parents, and family. My success was not borne out my efforts alone and it is truly remarkable the luck I have had to know and garnered support from such a remarkable group of people

Table of Contents

List of Tables

List of Figures

List of Appendices

List of Abbreviations

APL	Abductor Pollicis Longus
CT	Computed Tomography
Dif.	Difference
DRTL	Dorsal Radial Triquetrum Ligament
DCA	Dorsal Cortical Angle
ECRL	Extensor Carpi Radialis Longus
ECRB	Extensor Carpi Radialis Brevis
EDC	Extensor Digitorum Communis
EDQ	Extensor Digit Quinti
ECU	Extensor Capri Ulnaris
EPL	Extensor Pollicis Longus
EPB	Extensor Pollicis Brevis
EIP	Extensor Indicis Proprius
FCR	Flexor Carpi Radialis
FCU	Flexor Carpi Ulnaris
FDS	Flexor Digitorum Superficialis
FPL	Flexor Pollicis Longus
H/L	Height-to-length ratio
IPj	Interphalangeal Joint
K-Wire	Kirschner Wire
LRLL	Long radiolunate ligaments
LISA	Lateral Intra-Scaphoid Angle
MCPj	Metacarpal Phalangeal Joint
MRI	Magnetic Resonance Imaging
PL	Palmaris Longus
PQ	Pronator Quadratus
RSCL	Radioscaphoid-Capitate Ligament
RSL	Radioscaphoid Ligament

SD	Standard Deviation
SL	Scapho-lunate
SRLL	Short radiolunate ligaments
STL	Stereolithography
SCL	Scapho-capitate ligament
STTL	Scaphoid-trapezium-trapezoid ligament
TFCC	Triangular Fibrocartilage Complex
UCL	Ulnar Capitate Ligament
UTL	Ulnar triquetral Ligament
ULL	Ulnar lunate ligament

Chapter 1

1 Introduction

This chapter introduces the current state of knowledge of wrist mechanics, with a particular focus to the role of the scaphoid. The anatomy of this bone and its surrounding soft tissues are reviewed. The current understanding of the scaphoid's contribution to wrist motion, as well as a brief overview of clinical entities that impact this motion are discussed. Finally, the current methods used to evaluate wrist motion and joint contact mechanics will be reviewed. The objective, purpose, rationale, and hypothesis of this work are also given.

1.1 Anatomy of the Hand and Wrist

The wrist is one of the most anatomically complex joints in the body and is comprised of numerous osseous, tendinous, and ligamentous structures that connects the hand to the forearm. The hand and wrist are comprised of 27 bones **(Figure** 1.1**)**. The forearm is composed of 2 bones: the radius and ulna. The wrist includes 8 bones: the scaphoid, lunate, triquetrum, pisiform, trapezium, trapezoid, capitate, and hamate, and the hand is composed of 19 bones: 4 bones for each of the 4 digits (1 metacarpal, 3 phalanges), and 3 bones for the thumb (1 metacarpal and 2 phalanges). The carpal bones work as a construct that allows for positioning of the hand in a variety of positions while maximizing gripping stability and power. This wide range of motion is accomplished with limited soft tissue attachment because the osseous anatomy of the carpus maintains a delicate inter-bone relationship to provide stability.

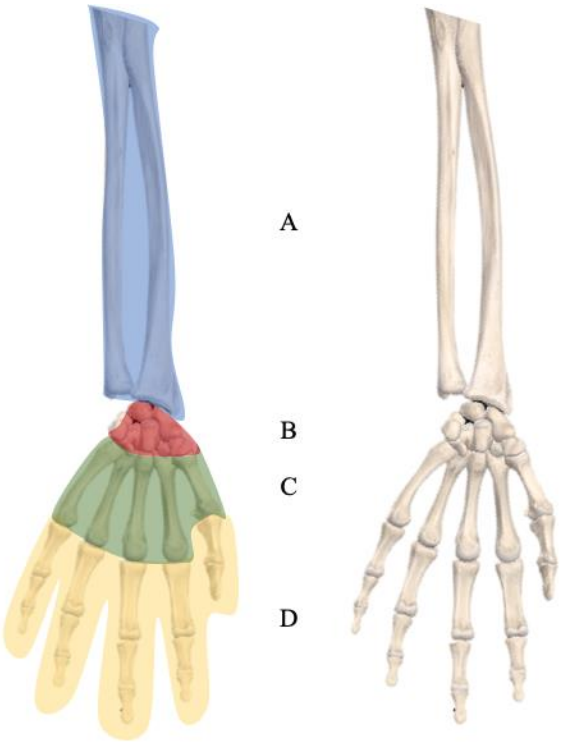

Figure 1.1: Osseous Anatomy of the Forearm, Hand and Wrist. Bony anatomy of the right forearm, wrist, and hand demonstrating groupings of bones of interest. (A) Radius and Ulna, (B) Carpals, (C) Metacarpals, and (D) Phalanges.

1.2 Carpal Bones

The carpal bones are organized into proximal and distal rows (**Figure** 1.2)**.** From the radial to ulnar side, the proximal row is comprised of the scaphoid, lunate, triquetrum, and pisiform. The scaphoid, lunate, and triquetrum are the primary bones, as the pisiform is a sesamoid bone with minimal joint articulation.[1] The distal row is comprised of the trapezium, trapezoid, capitate, and lunate. The scaphoid is unique in its position because it bridges these two rows and coordinates movement between them.[2] Each bone is comprised of a cancellous core, surrounded by a tough cortex. With the exception of the pisiform, all carpal bones have 6 surfaces for articulation or muscular attachments. For the purpose of this work, only the scaphoid will be discussed in detail and minor discussion will be presented regarding the bones that articulate immediately with the scaphoid (lunate, capitate, trapezium, and trapezoid).

Figure 1.2: The Carpal Bones. Anterior view of the carpal bones. The carpal bones are organized into two rows; the proximal carpal row is composed of the Scaphoid (S), Lunate (L), Triquetrum (Tq), and Pisiform (P). The distal carpal row is composed of the Trapezium (Tm), Trapezoid (Td), Capitate (C), and Hamate (H).

1.2.1 Osteology of the Scaphoid

The scaphoid is the second largest of the carpal bones and is positioned at the radial side of the carpus bridging the proximal and distal carpal row (**Figure** 1.3). Its shape is similar to that of a boat hence its name (*skaphos 'boat' latin*) with the superior surface being convex and the inferior surface concave. Approximately 80% of its entire surface is covered in cartilage to facilitate articulations with four neighboring carpal bones.[1,3] These facets include: the oval facet on the distal medial concave that articulates with the capitate, the medial semi-lunar facet that articulates with the lateral aspect of the lunate, the proximal-lateral convex facet that articulates with the radius at the scaphoid fossa, and the distal convex articular surface which interacts with the trapezoid and trapezium. There are 2 primary locations for attachments of ligaments on the scaphoid: on the proximal volar surface lies the scaphoid tubercle which is a rounded projection oriented volarly and serves as the attachment for the transverse carpal ligament, and a small ridge on the inferior aspect runs the length of the bone and serves as the attachments of numerous ligaments such as the radial collateral ligament. These areas are also of importance because these are the primary locations at which the scaphoid receives vascular supply.[1]

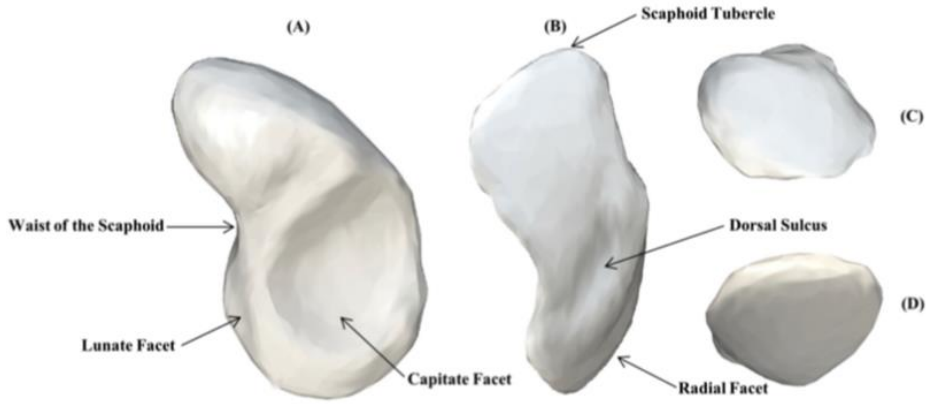

Figure 1.3: Osseous Anatomy of the Scaphoid. Bony anatomy of the left scaphoid with associated landmarks. (A) Medial View, (B) Dorsal View, (C) Distal Articular Surface, (D) Proximal Articular Surface.

1.2.2 Osteology of the Lunate

The lunate is a wedge or moon shaped bone (*luna 'moon' latin*) that resides in the central aspect of the proximal row (**Figure** 1.4). Two common types of lunates described. Type I has a total of 4 articulations; proximally with the radius at the radio-lunate fossa, ulnarly with the proximal scaphoid pole, at the distal radial aspect with the trapezoid, and at the distal central aspect with the capitate. Type II additionally has an articulation at the distal ulnar aspect of the hamate, for a total of 5 articulations. In general, the volar and dorsal aspects of the lunate are non-articulating surfaces and serve as the site of attachments of numerous soft tissue structures as well as the site of vascular ingrowth.[1]

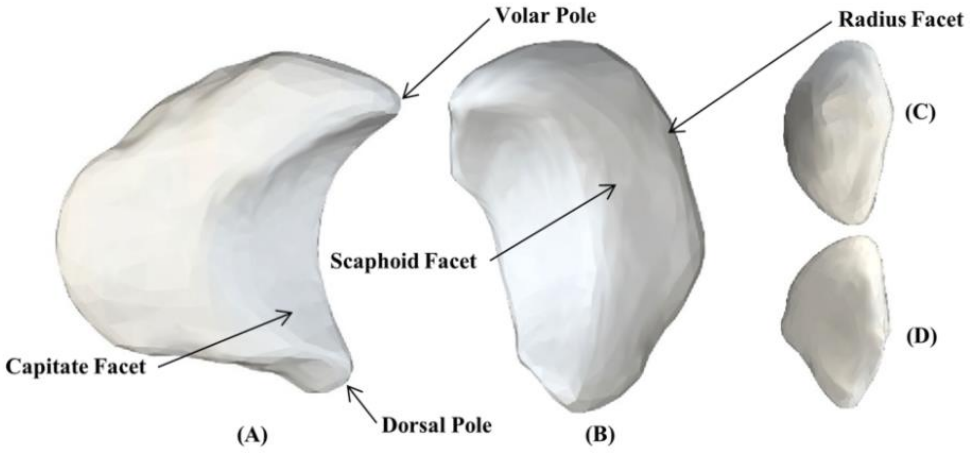

Figure 1.4: Osseous Anatomy of the Lunate. Bony anatomy of a left lunate with landmarks highlighted. (A) Distal Articular Surface, (B) Proximal Articular Surface, (C) Medial View, (D) Lateral View

1.2.3 Osteology of the Capitate

The capitate is the largest carpal bone and resides centrally in the distal carpal row (**Figure** 1.5). It comprises the basis of the transverse carpal arch forming a rigid central column of the hand and wrist. Distally it articulates with the third and fourth metacarpal. There is minimal motion at this joint and functionally the capitate acts as an extension of the base of the third metacarpal. On the radial aspect of the capitate lies the scapho-capitate joint. On the ulnar aspect, the capitate articulates with the hamate. Proximally, the capitate sits within the lesser convexity of the lunate, which allows for flexion and extension at the mid-carpal joint.

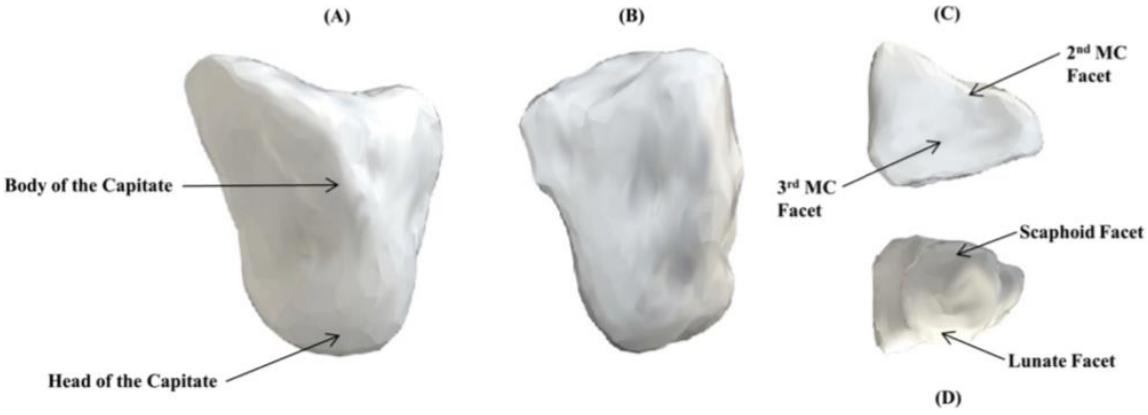

Figure 1.5: Osseous Anatomy of the Capitate. Bony anatomy of the capitate with important features highlighted. (A) Lateral View, (B) Volar View, (C) Distal Articular Surface, (D) Proximal Articular Surface.

1.2.4 Osteology of the Trapezium

The trapezium is the most radial bone within the distal carpal row and resides as the base of the thumb (**Figure** 1.6). This bone has a biconcave shape with the integration of two saddle joints in orthogonal topology. This allows for a wide range of motion of the first metacarpal and the thumb. With this bone being positioned at the most radial position of the distal carpal row, the volar, dorsal, and radial aspect of the trapezium do not articulate with other bones. These rough areas of the bone allow for the insertion of numerous stabilizing tendons and ligaments. At the ulnar distal aspect, the trapezium attaches to the second metacarpal, but little motion occurs at this joint. The ulnar aspect of this bone articulates with the trapezoid, and proximally with the scaphoid.

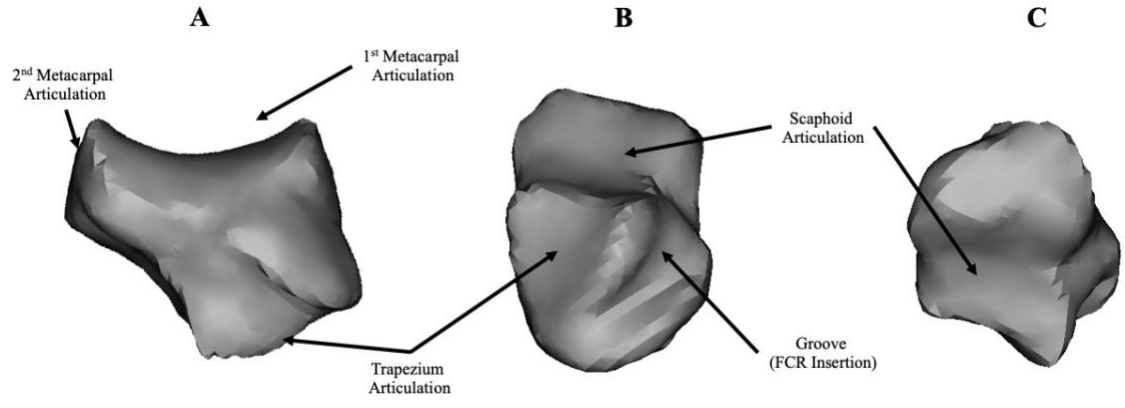

Figure 1.6: Osseous Anatomy of the Trapezium. Bony anatomy of the trapezium with important features highlighted. (A) Volar View, (B) Lateral View, (C) Proximal Articular Surface.

1.2.5 Osteology of the Trapezoid

The trapezoid is the second smallest carpal bone and resides adjacent to the trapezium (**Figure** 1.7). It has a wedge-like shape and 5 faces of articulation. On the radial aspect, the trapezoid articulates with the trapezium. Proximally, there is an articulation with the scaphoid and ulnarly, the capitate interacts with the trapezoid. Distally, there are two primary topologies. The trapezoid articulates with the second metacarpal in all cases, but in a minority of cases there is also a small distal-ulnar facet that also articulates with the third metacarpal. The trapezoid serves as a bridge between the distal carpal row and the metacarpals but is the least mobile carpal bone, contributing to a rigid and stable central aspect of the carpus.[1]

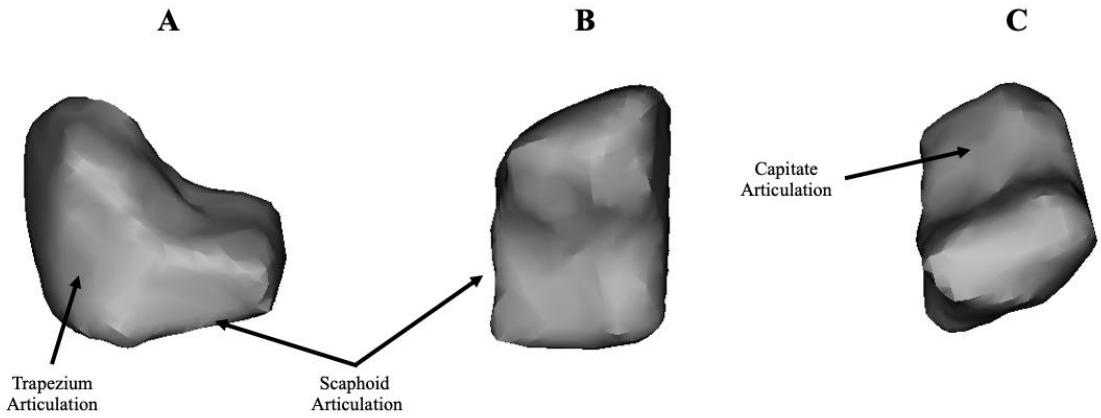

Figure 1.7: Osseous Anatomy of the Trapezoid. Bony anatomy of the trapezoid with important features highlighted. (A) Volar View, (B) Lateral View, (C) Proximal Articular Surface.

1.3 Soft Tissue Anatomy

There are numerous soft tissues of the wrist that are important for maintaining joint stability and congruency. Grossly, these tissues can be divided into two major groups: static and dynamic structures.

1.3.1 Static Stabilizers of the Wrist

The general composition of the wrist is similar to other joints with numerous ligaments contributing to its stability. In the wrist, there are 2 main groups of ligaments based on their relationship to the distal radius and ulna. Extrinsic carpal originate from the distal radius or ulna before inserting on a carpal bone, whereas intrinsic carpal ligaments originate and insert within the carpus.[3]

1.3.2 Extrinsic Carpal Ligaments

Although there is significant variation in the topology and number of extrinsic carpal ligaments[4], these structures can be subdivided into 3 main groups: palmar radiocarpal, palmar ulnocarpal, and dorsal radiocarpal (**Figure** 1.8). There are no ligaments on the dorsal ulnar aspect of the wrist as this comprised of the triangular fibrocartilage complex (TFCC).

1.3.2.1 Palmar Radiocarpal

There are 4 ligaments in this group and include the radioscaphoid ligament (RSL), radioscaphocapitate ligament (RSCL), and the long and short radiolunate ligaments (LRLL, SRLL). The RSL, RSCL, and LRLL all originate from the lateral aspect of the distal radius and are superficial. These ligaments take an oblique course ulnarly and distally to insert on the scaphoid, capitate and lunate respectively. The SRLL is deeper to the former three structures and originates from the medial aspect of the radius and travels to the lunate in a more direct path. The RSCL is a particularly important contributor to scaphoid stability; it courses over the volar aspect and serves as a fulcrum for the scaphoid to rotate. It is also worth noting that the interval between the RSCL and the LRLL, also known as the *space of Poirier*, is an area of weakness within this ligamentous system that the lunate can dislocate through in the setting of significant force.[3]

1.3.2.2 Palmar Ulnocarpal

There are typically 3 extrinsic ligaments on the ulnar-palmar aspect of the wrist although it has been shown that the majority of variation in extrinsic wrist ligaments is found at the ulnar stabilizers.[4] These can be organized into deep and superficial structures. The superficial structures include the ulnar capitate ligament (UCL) which arises from the base of the ulnar styloid. Deeper to this ligament arising from the TFCC are the ulnar triquetral (UTL) and ulnar lunate ligaments (ULL). The UCL forms a distal inverted "V", or arcuate ligament in conjunction with the RSCL, whereas the 3 collective structures (UCL, UTL, ULL) are known as the ulnar carpal ligamentous complex and form a proximal inverted "V" with the LRLL and SRLL.

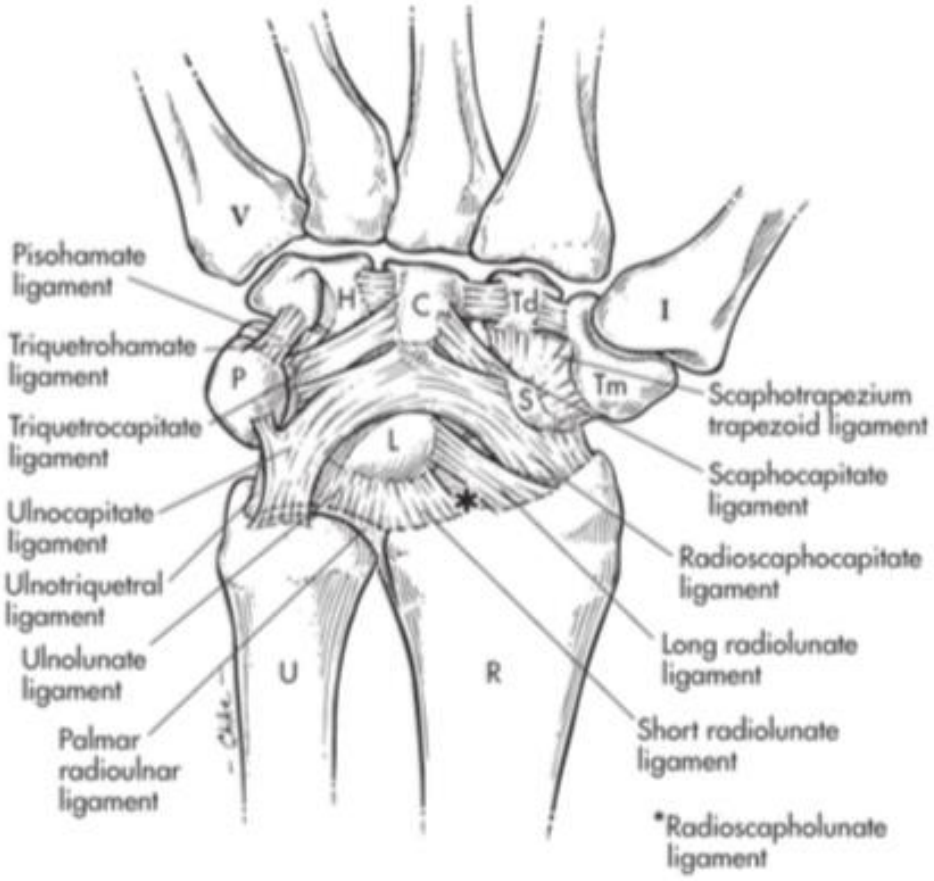

Figure 1.8: Volar Wrist Ligaments. **Pictorial representation of the ligaments present in the volar wrist.** Reprinted with permission from William P. Cooney, ed. The wrist. Diagnosis and operative treatment. Vol. 1. Ligament anatomy. St. Louis, MO: Elsevier Mosby-Year Book, 1998:79.)

1.3.2.3 Dorsal Radiocarpal

There is a single extrinsic radiocarpal ligament on the dorsal aspect of the wrist known as the dorsal radial triquetrum ligament (DRTL) (**Figure** 1.9). This is a broad ligament with numerous attachments onto the triquetrum and lunate with some variations including the scaphoid.

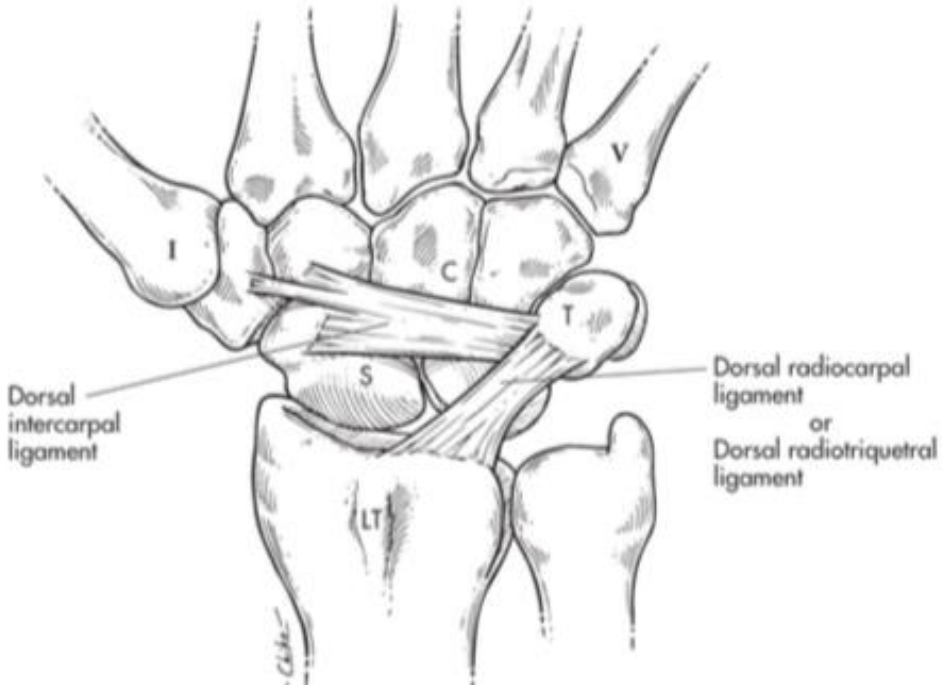

Figure 1.9: Dorsal Wrist Ligaments. **Pictorial representation of ligaments presents in the dorsal wrist.** (Reprinted with permission from William P. Cooney, ed. The wrist. Diagnosis and operative treatment. Vol. 1, Ligament anatomy. Elsevier Mosby-Year Book, 1998:88.)

1.3.3 Intrinsic Carpal Ligaments

The intrinsic carpal ligaments serve an important role in constraining the motion of each bone and ensuring intercarpal rotational forces are balanced to maintain stability. This group of soft tissue structures involves any ligament that constrains carpal bones within the same row, or between the distal and proximal row. In the proximal row, there are connections between the lunate and its neighboring triquetrum and scaphoid. In each case, there is a palmar and dorsal ligament which constrain rotational forces between carpal bones. The lunotriquetral interosseous ligaments are shorter and stronger than the scapholunate interosseous ligaments, owing to a closer relationship in the motion of the lunate and triquetrum. The scapholunate ligament is of particular importance in maintaining carpal stability as it ensures the lunate does not enter into a dorsal posture which can lead to secondary instabilities. This is a C-shaped structure with a 2-3mm thickening on the dorsal component that is thickened relative to the volar fibres.[3]

There are less interosseous ligaments in the midcarpal joint which allows for significant motion of the wrist. There is only a single dorsal ligament, the dorsal intercarpal ligament which connects the lunate to the distal scaphoid, trapezium, and trapezoid. Volarly, there are many short, strong ligaments that make various connections between the proximal and distal carpal rows. Of these, the most important in the maintenance of scaphoid position are the scaphoid capitate ligament (SCL), and the dorsolateral scaphoid-trapezium-trapezoid ligament (STTL).[1,3]

1.3.4 Dynamic Stabilizers of the Wrist

Dynamic stabilization is due to the load produced via musculature. Besides the intrinsic stabilizers of the carpus and individual carpal bones, all muscles and tendons that cross this joint also serve as dynamic stabilizers.[3,5] The wrist is capable of a wide range of motion because of relatively limited static restrictions, to facilitate this motion many muscles actively restrain the motion of the carpus to give a smooth motion path.

1.3.4.1 Volar Muscles

The volar muscles are the flexors of the digits and wrist. Anatomically, these can be subdivided into 3 layers and are summarized in **Table 1** and shown in **Figure** 1.10.[5]

1.3.4.2 Dorsal Muscles

The dorsal muscles are the extensors of the digits and wrist. Anatomically, these can be subdivided into 2 layers and are summarized in **Table 2** and shown in **Figure** 1.11.[5]

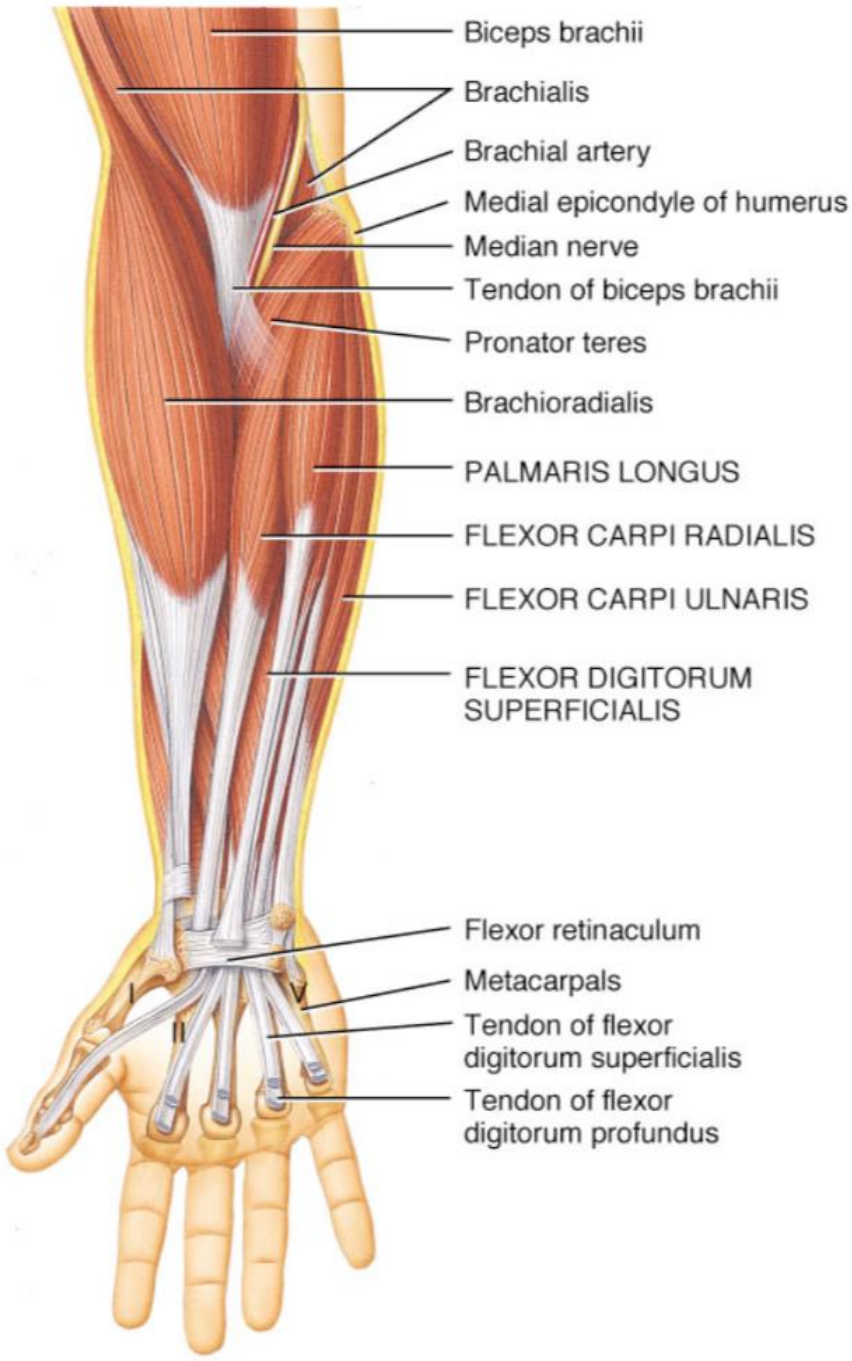

Figure 1.10: Dynamic Stabilizers of the Carpus – Volar Compartment Muscles. This figure does not contain all muscles located on the volar aspect of the forearm, as many of these contribute to flexion and motion at the elbow and do not contribute significantly to stabilization of the carpus. See description of muscles in **Table 1**.

Layer	Muscle	Origin	Insertion	Action
Superficial	Flexor Carpi Radialis (FCR)	Medial Epicondyle of Humerus	Base of 2nd and 3rd Metacarpal	Flex wrist, radially deviate wrist
	Palmaris Longus (PL)		Palmar aponeurosis	Flex wrist, tense palmar skin
	Flexor Carpi Ulnaris (FCU)		Pisiform, hook of hamate, base of 5th Metacarpal	Flex wrist, ulnarly deviate wrist
Intermediate	Flexor Digitorum Superficialis (FDS)		Base of middle phalanx of digits 2-5	Flex Fingers at Proximal Interphalangeal Joints
Deep	Flexor Digitorum Profundus (FDP)	Anterior/Medial Surface of Ulna	Base of distal phalanx of digits 2-5	Flex Fingers at Distal Interphalangeal Joints
	Flexor Pollicis Longs (FPL)	Medial Aspect of radius	Base of distal phalanx of digit 1	Flexion of the thumb
	Pronator Quadratus (PQ)	Medial anterior surface of the ulna	Lateral anterior surface of the radius	Pronation of the forearm

Table 1: Muscles on the Volar Forearm Contributing to Dynamic Carpal Stabilization. The muscles of the volar forearm can be grouped into 3 groups: superficial, intermediate, and deep. These muscles exert their forces to facilitate wrist flexion, as well as radial and ulnar deviation. As a secondary role, these muscles also stabilize the carpus during wrist extension.

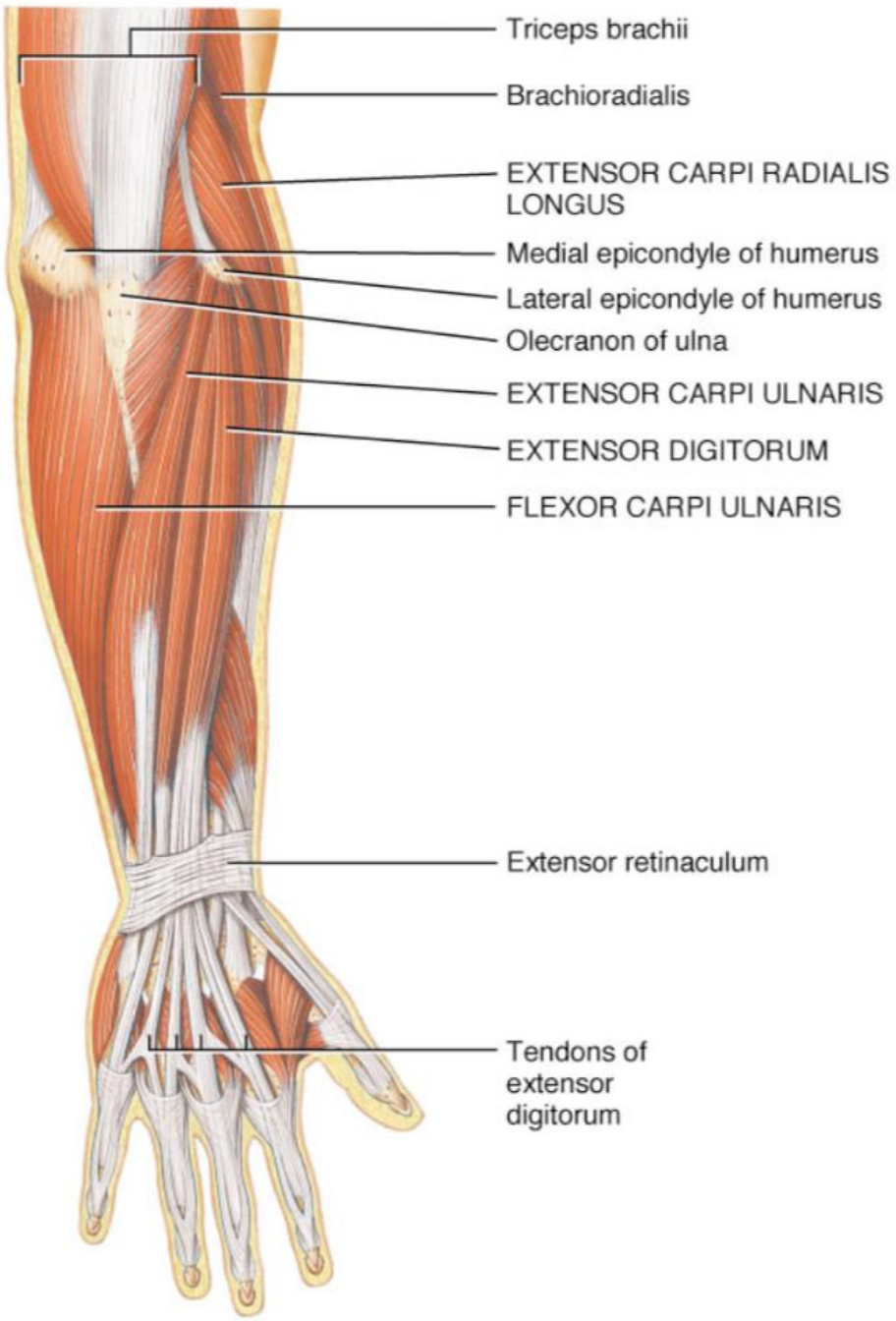

Figure 1.11: Dynamic Stabilizers of the Carpus – Dorsal Compartment. This table does not contain all muscles located on the dorsal aspect of the forearm, as many of these contribute to extension and motion at the elbow and do not contribute significantly to stabilization of the carpus. See description of muscles in **Table 2**

Layer	Muscle	Origin	Insertion	Action
Superficial	Extensor Carpi Radialis Brevis (ECRB)	Lateral Epicondyle of the Humerus	Base of the 3rd Metacarpal	Wrist extension and radial deviation
	Extensor Carpi Radialis Longus (ECRL)		Base of the 2nd Metacarpal	
	Extensor Digitorum Communis (EDC)		Base of distal phalanx of digits 2-5 & Extensor hood	Extension of the fingers
	Extensor digiti quartus (EDQ)		Base of distal phalanx of digits 5 & Extensor hood	Extension of the small finger
	Extensor Carpi Ulnaris (ECU)		Base of the 5th Metacarpal	Wrist extension and ulnar deviation
Deep	Abductor Pollicis Longus (APL)	Medial aspect of ulna and radius	Base of the 1st Metacarpal	Abduction and extension of thumb
	Extensor Pollicis Longs (EPL)	Posterior surface of ulna	Base of Distal Phalanx	Extension of thumb at IPj
	Extensor Pollicis Brevis (EPB)	Radius and interosseus membrane	Base of Proximal Phalanx	Extension of thumb at MCPj
	Extensor Indicis Proprius (EIP)	Distal third of ulna	Base of distal phalanx of digits 2 & Extensor hood	Extension of the index finger

Table 2: Muscles on the Dorsal Forearm Contributing to Dynamic Carpal Stabilization. The muscles of the dorsal forearm can be grouped into 2 groups: superficial and deep. These muscles exert their forces to facilitate wrist extension, as well as radial and ulnar deviation. As a secondary role, these muscles also stabilize the carpus during wrist flexion.

1.4 Kinematics of the Wrist

The wrist is a joint capable of wide range of motion in numerous planes including flexion-extension and radial-ulnar deviation (**Figure** 1.12**, Figure** 1.13). Rotation is also made possible through articulations of the distal radial ulnar joint (DRUJ), which adds further diversity to wrist positioning. The ranges of motion of the wrist are described with respect to neutral position, which is defined as the long axis of the third metacarpal collinear to the long axis of the radius.[6] Range of motion differs between individuals and depends on many factors including age, gender, pathology, and anatomy, among others.

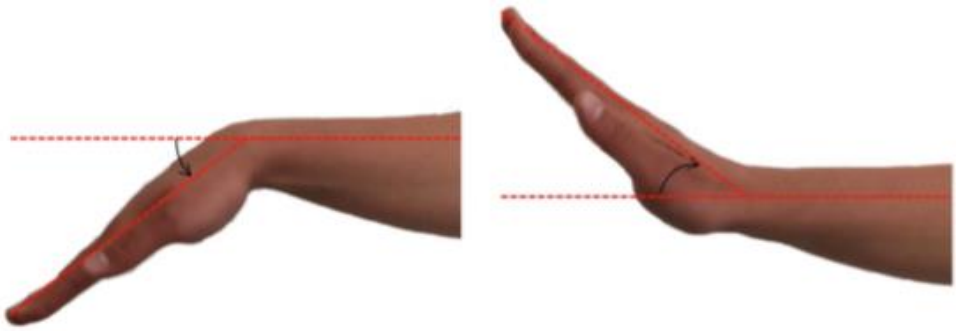

Figure 1.12: Range of Wrist Motion: Flexion-Extension. Motion of the left wrist in flexion (left) and extension (right).

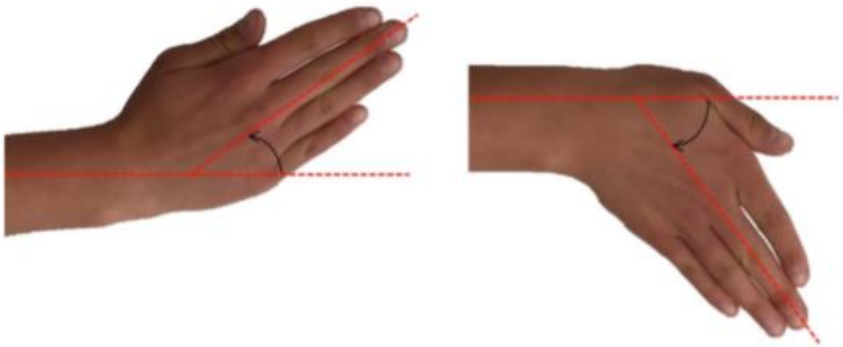

Figure 1.13: Range of Wrist Motion: Flexion-Extension. Motion of the left wrist in radial deviation (left) and ulnar deviation (right).

1.4.1 Kinematic Models of Carpal Motion

Due to the complexity of the wrist joint, there have been numerous theories developed in an effort to understand carpal motion. Despite this, there remains significant debate on the interaction between various carpal bones.[7,8] The three predominant concepts thought to govern wrist motion include: row theory, column theory, and ring theory. There have been many authors who have built upon these concepts and modified them, but these ideas remain the basis.

1.4.1.1 Row Theory

The first description of carpal motion was documented in the early 1900s by Johnston et al. In this original anatomical work, Johnston postulated that the carpal bones worked as two functional units with the distal and proximal carpal rows each moving as a separate unit.[9] Flexion and extension occurred at each joint (intercarpal and radiocarpal joint) and radial-ulnar deviation occurred at each joint, with each row pivoting around the other.

1.4.1.2 Column Theory

Over 25 years later, Navarro disputed this model and claimed the wrist worked not as 2 rows, but rather as 3 columns that each had a specific role.[10] The central column composed of the lunate, hamate, and capitate was thought to be responsible for flexion and extension, the medial column composed of the triquetrum and pisiform controlled pronation-supination, and the lateral column made up of the scaphoid, trapezium, and trapezoid functioned to regulate load transfer across the wrist. This model was later modified by Taleisnik in the late 1970s who hypothesized that the distal row interacted with the lunate to facilitate flexion and extension. The pisiform was removed from the model as it is a sesamoid bone and does not have any true articulations. The triquetrum and scaphoid were thought to control radial and ulnar deviation through rotation about the central column.[11]

1.4.1.3 Ring Theory

The next theory modelling the motion of the wrist and carpal stability was introduced by Lichtman et al. in 1980. Similar to the row theory, it was hypothesized that the distal row acted a single unit, but it also influenced motion of the proximal row motion, and more specifically, the lunate. Connections through the capitate, scaphoid, and triquetrum influence the rotational position of the lunate which has implications in wrist stability.[12]

There have been many other theories related to carpal motion and understanding the interactions that occur between carpal bones to facilitate motion yet maintain stability, but the row, column, and ring theory serve as the basis in each of these variations. As an example, Craigen and Stanley carried out a study examining radiographs of various types of wrists and determined that motion of the carpal bones differs between various types of wrists and some exhibit motion behaviour that is best explained by the row theory of carpal motion, whereas others behave in a manner explained by column theory.[7]

1.4.2 Current State of Knowledge Regarding Laboratory-Based Assessments of Wrist Kinematics

Historically, the majority of wrist motion studies have been carried out by examining a series of static images as a healthy subject moved their wrist through various planes of motion. Although these methods have the benefit of understanding *in-vivo* motion, they are limited in the fact that tendon forces cannot be measured, and it is not possible to evaluate how injuries or surgical repairs of various structures impact total carpal motion. For this reason, investigations into understanding carpal motion generally takes place in an *in-vitro* environment using cadaveric specimens. Carpal motion simulators can be categorized as passive or active based on how motion is accomplished, with active representing applying forces using physiological structures to exert force on the wrist, whereas passive simulators rely on external application of forces. Each of these methods has benefits and drawbacks.

1.4.2.1 Passive Motion Simulators

The benefit of this setup is based in its simplicity and reproducibility, and the minimal dissection required which maintains all soft tissue structures. The drawbacks of this setup are that although motion may attain a similar arc, the loading through the carpus is drastically different than what would be expected *in-vivo* and as such, the motion and articulations of the carpal bones are potentially different. A method to overcome this flaw is to attach tendons of interest and apply tone loads to each tendon. This in theory loads the wrist but results are still subject to error and variability.

An example of a simulator of this type was created by Nishiwaki et al. (**Figure** 1.14). This apparatus was capable of producing planar wrist flexion and extension. Cadaveric specimens amputated at the mid-humerus were rigidly attached to the base of the simulator and actuators affixed to ECU, ECRL, FCU, PT, and BB. Optical trackers were inserted into bones of interest and motion was simulated by an investigator moving a pin within a constrained tract that was inserted into the specimens third metacarpal.

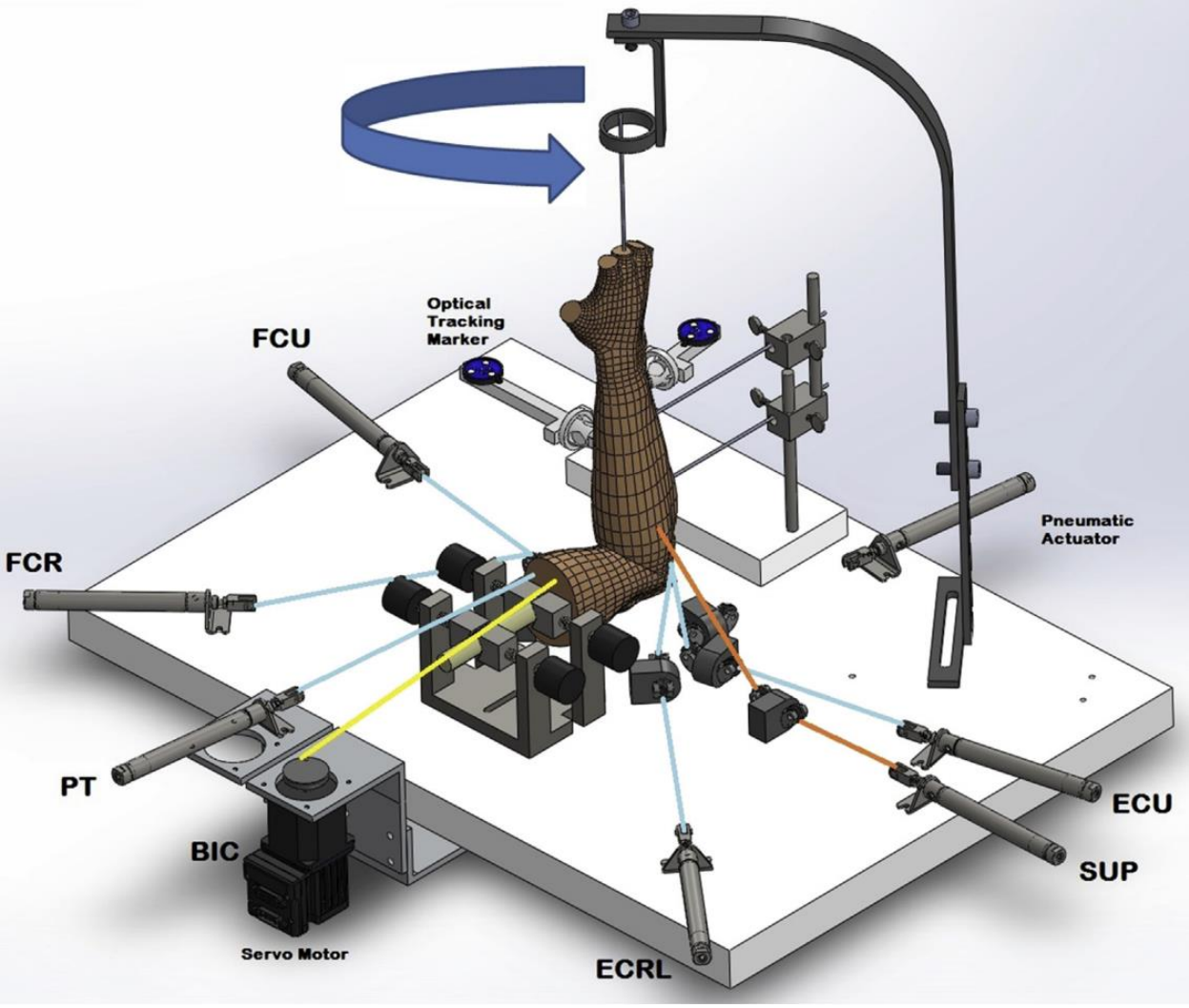

Figure 1.14: Passive Motion Simulator from Nishiwaki et al. This simulator was used to study the effect of dorsal radial angulation deformities on DRUJ kinematics.

1.4.2.2 Active Motion Simulators

In active motion simulators tendons of interest are attached to mechanical actuators and the force through each tendon is measured. The force and position of each tendon is monitored in an effort to apply an antagonistic force to stabilize wrist motion. Synergistic muscles apply a force to produce an angular motion, while the antagonistic group applies a force to maintain tone loads within their tendons in a method that approaches physiologic motion. This methodology is much more complicated but produces motion that more closely mirrors that of an *in-vivo* wrist.

An example of such a device was reported by Dunning et al. whom created an apparatus capable of generating wrist and finger motion using pneumatic actuators attached to 9 muscles (**Figure** 1.15**).**[13] A cadaveric specimen amputated at the mid humerus is mounted in the device and cables are sutured to the musculotendinous junction of FCU, FCR, FDP, FPL, ECU, ECRL, ECRB, PT, and BB. Electromagnetic receivers were inserted into the bones of interest and planar motion was simulated. Although this topology produces motion that is much more physiologic than that created by passive simulators, this instance did not employ closed loop feedback and as such, motion paths could differ dramatically if careful tuning of the machine was not carried out. This resulted in variations between specimens and made it difficult to repeat trials.

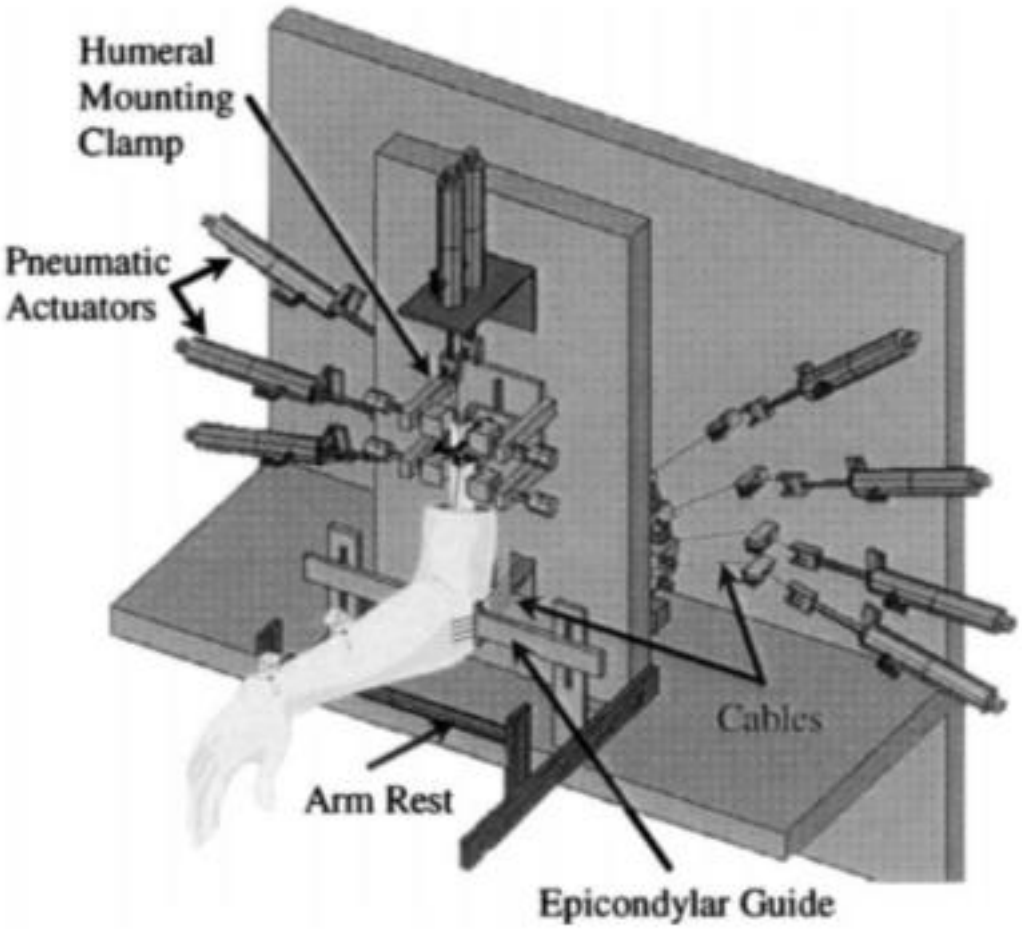

Figure 1.15: Active Motion Simulator from Dunning et al. Active motion wrist simulator capable of producing wrist flexion-extension, as well as finger flexion-extension.

A further refinement of this methodology with the implementation of a closed loop feedback system was created by Werner et al. (**Figure** 1.16).[14] This simulator used specimens that were amputated at the elbow and denuded of all soft tissues except for ligaments and tendons. The ECU, ECRL, ECRB, FCU, FCR, and APL were attached to a servo-hydraulic system and electromagnetic trackers were placed in the ulna, third metacarpal and lunate. These trackers supplied real time feedback that enabled dynamic optimization of tendon loads to maintain motion paths and create reproducible motion between trials, as well as specimens. The obvious drawback of this implementation is the stripping of all soft tissues that may act as static stabilizers of the wrist and carpus during wrist motion.

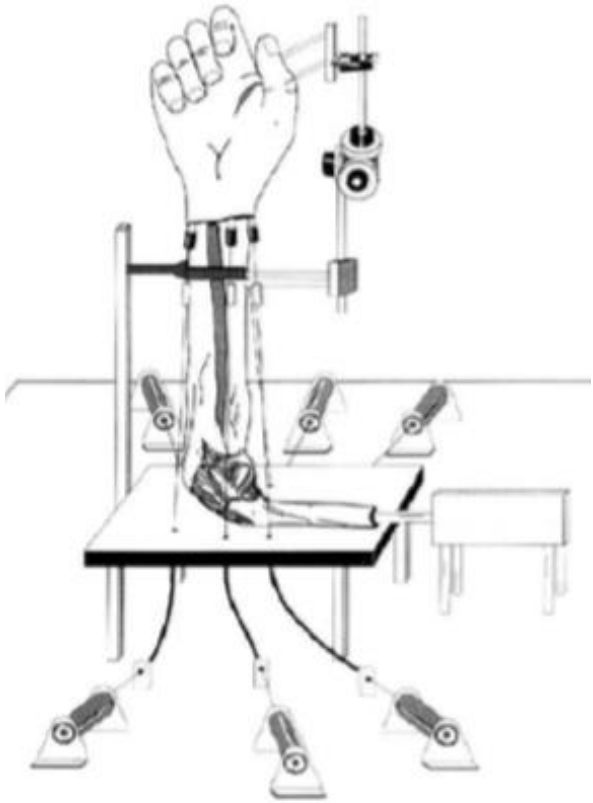

Figure 1.16: Active Motion Simulator from Werner et al. Demonstrated is an active motion wrist simulator with electromagnetic feedback facilitating closed-loop control and reproducible motion of the wrist. (Reprinted with Permission from John Wiley and Sons: Wrist Joint Motion Simulator).

Most recently, Iglesias et al. developed an active wrist motion simulator capable of performing active motion in a variety of gravity loaded positions that preserved soft tissue attachments (**Figure** 1.17).[15] By attaching 7 tendons of interest (ECU, ECRL, ECRB, FCU, FCR, PT, BB) to electric servomotors mounted on a strain gauge, muscle feedback is monitored throughout testing. This facilitates the maintenance of tone loads on antagonistic muscles throughout motion trials. Optical trackers are placed on bones of interest as well as the third metacarpal, radius, and ulna. Information from the latter 3 sensors facilitates a closed loop feedback control via real time feedback.

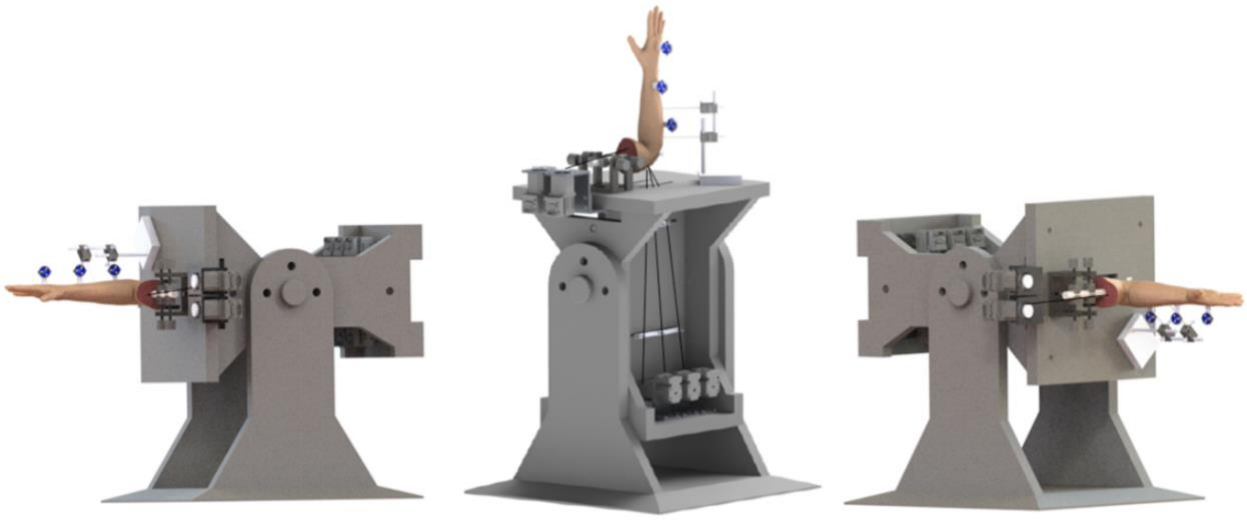

Figure 1.17 Active Motion Simulator from Iglesias et al. Demonstrated is an advanced motion simulator capable of active motion wrist simulator with optical closed-loop control in numerous gravity loaded positions. [15]

1.4.3 Current State of Knowledge Regarding Laboratory-Based Assessments of Wrist Loading

Wrist kinetics refers to the ability of the wrist to maintain stability with axial loading in order to transmit force from the hand to the forearm. The primary purpose of the wrist is to provide a stable platform for gripping in a variety of positions. Many studies have demonstrated the large amount of force transferred across the carpal joints, in some instances, this can be in excess of 500kg for the average male.[16] The evolution of the understanding of wrist kinetics has evolved in synchrony with the knowledge about carpal motion.

Gilford was one of the first to propose a theory explaining wrist mechanics was based on the scaphoid bridging the proximal and distal carpal rows and acting to prevent collapse when the wrist was loaded.[17] This deformity was further investigated in later years with Landsmeer describing a zig-zag wrist deformity,[18] which was later refined by Fisk who called it the concertina deformity.[19] In each case, if the linkage of the scaphoid or its soft tissue attachments was lost, the wrist would collapse when loaded.[8,20]

There are multiple explanations describing how the scaphoid contributes to the maintenance of carpal alignment. Linsheid et al postulated that the scaphoid acts as a 3-point slider crank due to its oblique positioning between the radius and distal row. Kauer noted that when the scaphoid was loaded, it tended to flex whereas the lunate tended to extend because of its wedge shape. If all soft tissue attachments are intact, particularly the SL ligament, the proximal row achieves rotational stability. This concept of rotational stability was further expanded by Weber who noted that the shape of the hamate-triquetral joint imposed an extension moment to the triquetrum. With the LT ligament intact, the extension movement of the lunate is further supported by the motion of the triquetrum.

Regardless of the model used to conceptualize wrist biomechanics, each emphasizes the importance of the scaphoid to position the proximal row in a manner that the radio-lunate joint is collinear with the luno-capitate joint. This facilitates load to be transferred across

these joints in a fashion that ensures stability. It is worth noting however that the load transfer across the wrist is heavily dependent on the position of the wrist and much work has demonstrated that forces are not always transferred in the same matter. In the situation of an extremely radially deviated wrist, the majority of force transmits through the scaphoid, and it is only with ulnar deviation that the lunate begins to play a larger role.

1.4.4 Current Laboratory Methods of assessing Joint Loading

The study of joint kinetics is difficult as the measurement of contact between two bones inherently alters the normal interaction that would occur between these structures. These technical difficulties are further complicated by the small size of the wrist and the numerous articulations between carpal bones. The two approaches to quantify interactions between joints include direct and indirect methods. Many direct methods are historical because their invasive nature may alter joint kinetics.

1.4.4.1 Direct Methods of Assessing Joint Kinetics

1.4.4.1.1 Casting

Casting is a technique whereby cement is injected within the articular surface and the resultant thickness studied after the cement sets. An area lacking cement represents direct joint contact (**Figure** 1.18).[21] Although simple, this method has many limitations. It is destructive as the joint capsule must be violated for the injection of the cement and it can only assess contact in a single position and successive castings may be altered from the removal of prior castings. This method is also time consuming as it requires the injection and setting time of the selected cement.

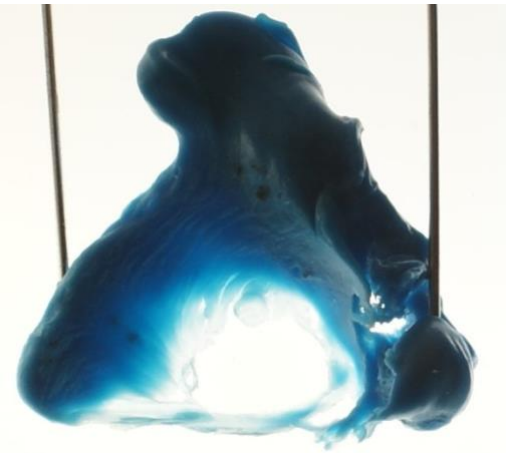

Figure 1.18: Casting of Distal Radius.: A cement casting of a DRUJ with a central area lacking cement representing the area of joint contact in this position. Areas of thicker cement represent open joint space

1.4.4.1.2 Pressure Sensitive Films

Another common method of measuring joint contact directly is the use of pressure sensitive films. These films are placed into the joint of interest and the joint is loaded. Areas of varying degrees of contact are represented by different colors within the film which is calibrated for various pressures.[22] The advantages of this strategy involve ease of placement and the possibility for measurements in numerous different wrist locations. Drawbacks include the required dissection of soft tissues to place the film within the joint, as well as aberrant pressure recordings that result from the folding or sliding of the film while it is placed within the joint. The thickness of this film when placed within the joint may also alter subtle joint kinetics.

A higher fidelity dynamic film has also been used with the most common type being Tekscan (Tekscan Inc, South Boston, MA). This is a thin film that outputs live contact data and is reusable between trials.[23] The advantages of this method include the need to only place it once within the joint to acquire recordings in numerous loaded positions. Drawbacks are similar to conventional film and are related to the inherent thickness of the film (0.1mm) altering joint kinetics, as well as the semi-destructive nature of placing the film within the joint.

1.4.4.2 Indirect Methods of Assessing Joint Kinetics

Indirect methods of assessing loading are heavily dependent on imaging or computational modelling of carpal bones and infer joint contact. In general, these image-based methods create models from CT or MRI data and the distance between bones of interest are calculated.[24,25] The joint can be loaded in a static position and the resultant images used to determine areas of contact.

This methodology is often applied in synchrony with joint motion simulation as discussed in **Section 1.4**. Motion data is collected using optical, electromagnetic, or live radiography and later coupled with the joint contact data by registering the acquired images with the motion data. This then allows for proximity maps to be generated and the distance between resultant volumes at a given position determined using computational processes.

1.5 Clinical Aspects of Scaphoid Injuries

1.5.1 Fractures

One of the most common injuries that alters carpal morphology and impact motion are fractures. The scaphoid is the most commonly fractured carpal bone, accounting for over two-thirds of carpal bone fractures.[26] It is the second most common fracture of the upper limb after distal radius fractures. Anatomically, scaphoid fractures most often occur at the anatomic waist due to compression, torsion, and distraction forces that are transmitted through this narrowing of the bone at this level.

1.5.2 Fracture Classification

Many authors have established different classification systems to characterize scaphoid fractures based on fracture stability (Herbert) [27], fracture location (Mayo)[28] , or fracture orientation (Russe).[29]

1.5.2.1 Herbert Fracture Classification

Herbert categorized fractures as stable or unstable. In this scheme, there are 2 types of stable acute fractures: A1 – A fracture of the distal tubercle, or A2- an incomplete fracture through the waist. There are 4 types of unstable fractures in this classification: B1 – distal oblique fracture, B2 – complete waist fracture, B3 – proximal pole fracture, B4 – trans-scaphoid perilunate fracture dislocation.

1.5.2.2 Mayo Fracture Classification

Cooney et al. classified scaphoid fractures based on anatomic location as well as stability. Factors that made a scaphoid fracture unstable included: displacement of the fracture >1mm, comminuted fracture, perilunate fractures, as well as secondary carpal malalignments such as a DISI deformity or increase in lateral intrascaphoid angle (LISA).[30] Following the determination of stability, the fracture could be classified based on fracture location into 5 different categories: 1 – distal tubercle, 2 – distal intraarticular surface, 3 – distal third, 4 – waist, 5 – proximal pole.[31]

1.5.2.3 Russe Fracture Classification

Russe examined fracture union rates based on the plane of fracture orientation and classified fractures as horizontal oblique (HO), transverse, or vertical oblique (**Figure** 1.19**)**. He found that the union rate in these types of fractures when treated conservatively was 30%, 60%, and 5% respectively.[29]

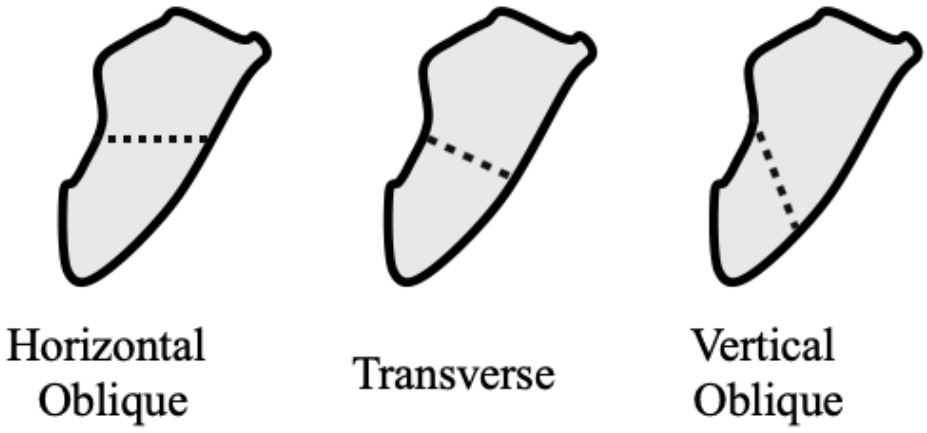

Figure 1.19: Russe Classification of Scaphoid Fractures. Russe classified fractures based on fracture plane orientation into horizontal oblique (HO), transverse (T), and vertical oblique.[32]

1.5.3 Etiology and Demographics

The most common mechanism resulting in fractures and soft tissue injuries of the carpus is axial loading from a fall on outstretched hand (FOOSH).[26] The majority of these injuries are low energy such as a fall from standing height although a minority of injuries occur in high impact trauma such as motor vehicle collisions. The former mechanism primarily effects the elderly with issues ambulating, whereas the latter mechanism is seen in young otherwise healthy individuals Given this second group, many young, otherwise individuals suffer these injuries while playing sports, but the distribution is bimodal with elderly populations suffering from more frequent falls.

1.5.3.1 Diagnosis and Treatment

The diagnosis of scaphoid fracture like many other injuries to the upper limb is dependent on clinical exam as well as imaging investigations. Patients often present with pain in the anatomical snuff box following axial loading to the wrist. This pain is reproducible on palpation and an element of soft tissue swelling may be present. Imaging in the form of plain film radiographs can be difficult to interpret and has a low sensitivity. For this reason, if there is a high clinical suspicion and a convincing clinical exam, the patient will require further investigations typically using computed tomography scanning.[3]

1.5.3.2 Radiographic Definitions

The scaphoid has a very complicated three-dimensional shape which makes it difficult to quantify changes resulting from injury. There have been numerous attempts to make metrics to assess scaphoid deformity based on radiographs that are consistent, reproducible, and accurately representative of scaphoid malunion severity. The 3 most common methods include height-to-length ratio (H/L), dorsal cortical angle (DCA), and lateral intrascaphoid angle (LISA). These radiographic measurements are each demonstrated in **Figure** 1.20.

Each of these metrics is calculated from a central sagittal CT image of the scaphoid typically from dedicated scaphoid views. The height-to-length ratio was determined as previously described by Bain et al. [27] A line is drawn parallel to the long axis of the scaphoid on the volar

aspect that is tangent to the distal and proximal pole. The length of the scaphoid is then measured along this line. The maximal height is then determined perpendicular to this line extending towards the dorsal cortex and the height-to-length ratio is determined. Using this metric, a scaphoid with a H/L >0.6 is considered to be malunited.[33,34] To measure LISA, a parallel line is drawn to the proximal and distal articular surface. A second line is drawn perpendicular to this line in the central aspect of each scaphoid pole and the resultant angle between these two is measured.[35] A normal LISA is defined as less than 35°, and a malunited scaphoid is defined as a LISA ≥35° [35], although many other authors have used LISA >45°.[36] Dorsal cortical angle is similarly measured using a central sagittal CT slice. In this case, a line is drawn parallel to the dorsal cortex of the proximal and distal pole of the scaphoid and the angle between these resultant lines measured. The normal range of DCA is not well established and this metric is not widely used in the literature.[37]

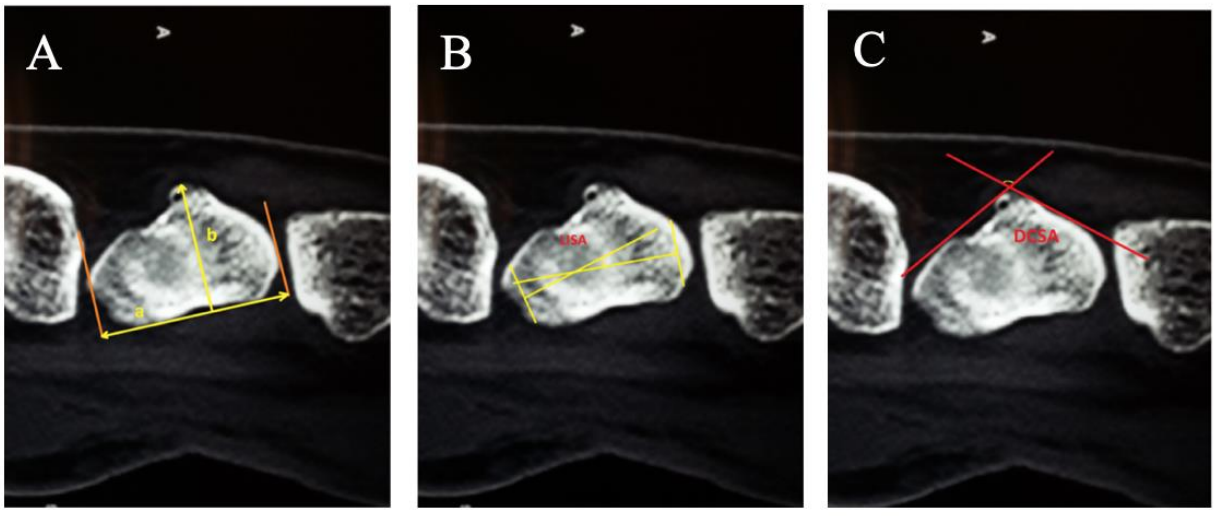

Figure 1.20: Radiographic Measurements of Scaphoid Malunion. Schematic representations of the calculation of various radiographic measurements of scaphoid malunion; (**A**) height-to-length ratio, (**B**), and (**C**) dorsal cortical scaphoid angle.

When evaluating the efficacy of each of these measurements, there are numerous pitfalls that lead to inconsistent measurement as well as a variable definition of malunion. These issues can be categorized as problems when comparing measurement tools as well as deficits intrinsic to the measurement. First, because there is no standardized method, practitioners are free to use any system which leads to inconsistencies in publication making it difficult to compare patient populations. A second issue is the reliability of these measurements between practitioners, which has been demonstrated to be quite variable.[15-17] Bain et al examined the inter, and intra-rater reliability of these metrics and found that H/L was the most consistent between measurements followed by DCA and LISA.[37] This is likely a direct result from the simplicity of this measurement, although it can be argued that this increased reproducibility comes at the cost of specificity.

A third issue becomes apparent when evaluating the definition of malunion for each specific measurement. In the case of both H/L and LISA, this baseline was created from a single study and referenced throughout literature without further validation. The normal LISA of <35° was established by Amadio et al.[35] in which 8 examiners evaluated 10 normal scaphoid radiographs. A normal H/L of 0.6 was defined by Forward et al in 2009 and was arbitrarily chosen because this was the mean H/L of their entire patient population and divided the total population into two equal sized groups (42 patients with scaphoid malunion treated non-operatively).[38] This benchmark was also reported by Meagrle, who noted normal scaphoids had a H/L of 0.61 and reported that H/L>0.7 had a risk of DISI deformity.[39]

1.5.4 Current Understanding of Scaphoid Malunion

The clinical and biomechanical understanding of scaphoid malunion remains limited as there are very few studies currently published. A single basic science study by Burgess et al. explored the implications of scaphoid malunion on carpal motion in 4 embalmed cadaveric specimens.[40] This work demonstrated that wrist motion was inversely proportional to the severity of angular deformity with total wrist extension loss with an angular scaphoid deformity of 30°.

Regarding clinical work on scaphoid malunion, the literature paints a mixed picture. Amadio first reported a relationship between LISA and clinical outcomes in 1989. He reported on a cohort of 46 fractures and found that only 27% of patients with a LISA > 45 degrees had satisfactory clinical outcomes compared to 83% of patients whom had normal scaphoid anatomy (LISA < 35 degrees).[35] Birchard and Pichora, Nakamura, as well as Linscheid and Lynch bolstered these findings with case reports of 2,7, and 5 patients respectively who had symptomatic scaphoid malunions that improved following reconstructive surgery. [41–43] More recently Fernandez, as well as El-Karef reported on a total of 16 patients whom underwent corrective bone grafting with similar presentations to earlier studies and each patient improved clinically. [44,45]

Conversely, other authors have published works that refute the importance of scaphoid malunion. Jiranek et al followed a cohort of 26 fractures whom underwent Russe anterior corticocancellous bone grafting for symptomatic non-union with a mean follow up of 11 years. Using lateral intrascaphoid angle (LISA) as a radiologic measurement and a threshold of LISA >45 degrees, these patients were classified as anatomically normal or malunited. There were statistically significant findings in objective measurements such as strength and range of motion but subjective patient outcomes were not significantly different. Forward et al reported similar results in 42 patients whom had united scaphoid fractures after cast immobilization. He was unable to find an association between any radiographic measure of scaphoid topology and functional outcome as graded by patient rated scores. Ashfar and Lee examined the relationship between functional outcomes and scaphoid height-to-length ratio in 17 and 25 patients, respectively without any positive association reported. Meagrle attempted to correlate radiographic measures of scaphoid morphology as well as of carpal alignment with patient rated

outcomes. Radiologic measurements included scapholunate angle (SLA) angle, radiolunate angle (RLA), LISA, dorsal cortical angle (DCA) and height-to-length ratio. Only RLA demonstrated a significant association with outcome measures. Gillete and Amadio evaluated a group of 17 patients and investigated outcomes with regards to the management they received for malunion.[46] Six patients were treated non-operatively, 4 patients received corrective osteotomy and bone grafting, 7 patients underwent salvage procedures such as radial styloidectomy. At an average of 30 years follow up, the functional outcomes of all groups were similar.

1.6 Thesis Rationale

The wrist is an important joint as it allows for the positioning of the hand, which is the primary method in which patients interact with the world. Its range of motion is so great that any deficit is easily perceivable. The wrist and the carpus are also at significant risk of injury and as such, there has been significant effort to understand the mechanics of the wrist in order to improve clinical assessment and outcomes. Researchers have investigated normal carpal mechanics but due to the complexity of this system, there still has yet to be a unified understanding. The one common theme in each theory of wrist kinematics or kinetics is based on the scaphoid coordinating motion and preventing the carpus from collapse. Surprisingly, the biomechanics of common pathologies such as scaphoid malunion remain largely unstudied. Based on a brief review of the literature there are many reports on patients presenting with scaphoid malunion following fracture that have limited range of motion and pain. These patients were successfully treated with corrective surgery. On the contrary, there are also other case series and retrospective reviews demonstrating patients with malunions that are clinically asymptomatic. This incongruence in the literature makes it difficult to evaluate patients, and surgeons are forced to manage this population expectantly. Once wrist arthrosis begins, procedures are limited and based on varying arthrodesis techniques. With scaphoid fractures occurring primarily in a young population, the potential for lost work and quality of life is significant.

It is not possible to compare the available clinical studies directly due to the variety of scaphoid malunion measurements as well as the variety of outcome measurements. That being said, appraising the literature implies that some patients may be at risk of a symptomatic malunion whereas others may not. By understanding how scaphoid malunion affects wrist kinetics and kinematics, future studies may be better targeted at identifying these patients and offering prophylactic intervention prior to the manifestation of symptoms.

1.6.1 Objectives and Hypothesis

There are two (2) primary objectives of this work:

1. Characterize how wrist contact is altered with progressive scaphoid malunion
2. Characterize how progressive scaphoid malunion affects the radial sided carpal bones.

We hypothesize that increasing scaphoid malunion severity will result in increased joint contact at the radioscaphoid joint, as well as increasingly pathologic motion of the scaphoid and lunate.

1.6.2 Overview

Chapter 2: This study investigates carpal kinetics employing a previously validated computational model of the carpus will be presented

Chapter 3: This study examines carpal kinematics using progressive scaphoid malunion during unconstrained flexion-extension, as well as radial ulnar deviation motion

Chapter 4: This chapter provides a general discussion, summary, and potential future directions of work.

1.7 References

1. Hirt B, Seyhan H, Wagner and M. *Hand and Wrist Anatomy and Biomechanics : A Comprehensive Guide*.; 2016. doi:4718699

2. Gray H. Anatomy of the Human Body. *Am J Med Sci*. 1919;157(5):704. doi:10.1097/00000441-191905000-00011

3. Wolfe SW (Weill MCU, Hotchkiss RN (Weill MCU, Pederson WC (University of THSCSATHC of SA, Kozin SH (Shriners H for CTUS of M. *Green's Operative Hand Surgery*. 6th ed. (Green DP, ed.). Philadelphia, PA: Elsevier; 2011.

4. Feipel V, Rooze M. The capsular ligaments of the wrist: Morphology, morphometry and clinical applications. *Surg Radiol Anat*. 1999;21(3):175-180. doi:10.1007/BF01630897

5. Hanse J, Saunders JB. *Netters Clinical Anatomy*. 2nd ed.; 2010.

6. Wu G, Van Der Helm FCT, Veeger HEJ, et al. ISB recommendation on definitions of joint coordinate systems of various joints for the reporting of human joint motion - Part II: Shoulder, elbow, wrist and hand. *J Biomech*. 2005;38(5):981-992. doi:10.1016/j.jbiomech.2004.05.042

7. Craigen MAC, Stanley JK. WRIST Row , column or both ? *J Hand Surg Br Eur Vol*. 1995;20(Fig 2):165-170.

8. Garcia-Elias M. Understanding Wrist Mechanics: A Long and Winding Road. *J Wrist Surg*. 2013;02(01):005-012. doi:10.1055/s-0032-1333429

9. Johnston H. Varying positions of the carpal bones in the different movements al the wrist PART II. *J Anat Physiol*. 1907;4:280-292.

10. Navarro A. Anatomy and physiology of the carpus [in Spanish]. *Imprenta Artist Dornaleche Hnos*. 1935:166-189.

11. Taleisnik J. The Ligaments of the Wrist. *J Hand Surg Am*. 1976;1(2):110-118.

12. Lichtman DM, Schneider JR, Swafford AR, Mack GR. Ulnar midcarpal instability—Clinical and laboratory analysis. *J Hand Surg Am*. 1981;6(5):515-523. doi:10.1016/S0363-5023(81)80115-3

13. Dunning C, CS L, RT B, PattersonSD, JA J, GJ K. Supplemental pinning improves the stability of external fixation in distal radius fractures during simulated finger and forearm motion. *J Hand Surg Am*. 1999;24(5):992-1000.

14. Werner FW, Palmer AK, Somerset JH, et al. Wrist Joint Motion Simulator. *J Bone Jt Surg*. 1996;14(6):639-646.

15. Iglesias DJ. Development of an in-vitro passive and active motion Simulator for the investigation of wrist function and Kinematics. 2015.

16. Rikli DA, Honigmann P, Babst R, Cristalli A, Morlock MM, Mittlmeier T. Intra-Articular Pressure Measurement in the Radioulnocarpal Joint Using a Novel Sensor: In Vitro and In Vivo Results. *J Hand Surg Am*. 2007;32(1):67-75. doi:10.1016/j.jhsa.2006.10.007

17. W GW, H BR, C. L. Mechanism of wrist joint with special reference to fractures of the scaphoid. *Guys Hosp Rep*. 1943;92:52–59.

18. Landsmeer J. Studies in the anatomy of articulation. I. The equilibrium of the "intercalated" bone. *Acta Morphol Neerl Scand*. 1961;3:287-303.

19. Fisk G. The wrist. Review article. *J Bone Joint Surg Br*. 1984:396-407.

20. JM K. The interdependence of carpal articulation chains. *Acta Anat*. 1974;88:481-501.

21. Stormont TJ, An KN, Morrey BF, Chao EY. Elbow joint contact study: Comparison of techniques. *J Biomech*. 1985;18(5):329-336. doi:10.1016/0021-9290(85)90288-X

22. Pogue DJ, SF V, RM P, et al. Effects of distal radius fracture malunion on wrist joint mechanics. *J Hand Surg Am*. 1990;15(5):721-727.

23. Nishiwaki M, T N, T N, Y T, Ikegami H. Ulnar-shortening effect on distal radioulnar joint pressure: a biomechanical study. *J Hand Surg Am*. 2008;33(2):198-205.

24. Wan L, Deasla R, Rubash H, Li G. Determination of in-vivo articular cartilage contact areas of human talocrural joint under weightbearing conditions. *Osteoarthr Cartil*. 2006;14(12):1294-1301.

25. GE M, DH L, C D, S A, CM G, Crisco JJ. Estimating Joint Contact Areas and Ligament Lengths From Bone Kinematics and Surfaces. *IEEE Trans Biomed Eng*. 2004;51(5):770-779.

26. Sendher R, Ladd AL. The Scaphoid. *Orthop Clin North Am*. 2013;44(1):107-120. doi:10.1016/j.ocl.2012.09.003

27. Herbert J, Fisher E. Management of the fractured scaphoid using a new bone screw. *J Bone Jt Surg*. 1984;66(1):114-123.

28. Cooney W, Dobyns J, Linscheid R. Fractures of the scaphoid: a rational approach to management. *Clin Orthop*. 1980;149(149):90-97.

29. Russe O. Fractures of the Carpal Navicular. *J Bone Jt Surg*. 1960;42(5):759-768.

30. Ten Berg P, Drijkoningen T, Strackee S, Buijze G. Classifications of Acute Scaphoid Fractures: A Systematic Literature Review. *J Wrist Surg*. 2016;05(02):152-159. doi:10.1055/s-0036-1571280

31. Cooney WP. *The Wrist: Diagnosis and Operative Technique*. St.Louis; 1998.

32. Russe O. Fracture of the Carpal Navicular: Diagnosis, Non-operative Treatment, and Operative Treatment. *J Bone Jt Surg*. 1960;42(5):759–768.

33. Forward DP, Singh HP, Dawson S, Davis TRC. the Clinical Outcome of Scaphoid Fracture Mal Union At 1 Year. *Hand, The*. 2009:40-46.

34. Lee CH, Lee KH, Lee BG, Kim DY, Choi WS. Clinical outcome of scaphoid malunion as a result of scaphoid fracture nonunion surgical treatment: A 5-year minimum follow-up study. *Orthop Traumatol Surg Res*. 2015;101(3):359-363. doi:10.1016/j.otsr.2014.09.026

35. Amadio PC, Berquist TH, Smith DK, Ilstrup DM, Cooney WP, Linscheid RL. Scaphoid

malunion. *J Hand Surg Am*. 1989;14(4):679-687. doi:10.1016/0363-5023(89)90191-3

36. Jiranek WA, Ruby LK, Millender LB, Bankoff MS, Newberg AH. Long-term results after Russe bone-grafting: The effect of malunion of the scaphoid. *J Bone Jt Surg - Ser A*. 1992;74(8):1217-1228. doi:10.2106/00004623-199274080-00012

37. Bain GI, Bennett JD, MacDermid JC, Slethaug GP, Richards RS, Roth JH. Measurement of the scaphoid humpback deformity using longitudinal computed tomography: Intra- and interobserver variability using various measurement techniques. *J Hand Surg Am*. 1998;23(1):76-81. doi:10.1016/S0363-5023(98)80093-2

38. Singh HP, Forward D, Davis TRC, Dawson JS, Oni JA, Downing ND. Partial union of acute scaphoid fractures. *J Hand Surg Am*. 2005;30(5):440-445. doi:10.1016/j.jhsb.2005.05.007

39. Mathoulin CL, Arianni M. Treatment of the scaphoid humpback deformity – is correction of the dorsal intercalated segment instability deformity critical? *J Hand Surg Eur Vol*. 2018;43(1):13-23. doi:10.1177/1753193417739526

40. Burgess RC. The effect of a simulated scaphoid malunion on wrist motion. *J Hand Surg Am*. 1987;12(5):774-776. doi:10.1016/S0363-5023(87)80067-9

41. Birchard D, Pichora D. Experimental corrective scaphoid osteotomy for scaphoid malunion with abnormal wrist mechanics. *J Hand Surg Am*. 1990;15(6):863-868. doi:10.1016/0363-5023(90)90004-B

42. Lynch NM, Linscheid RL. Corrective osteotomy for scaphoid malunion: technique and long-term follow-up evaluation. *J Hand Surg Am*. 1997;22(1):35-43. doi:10.1016/S0363-5023(05)80177-7

43. T N. Scaphoid Malunion. *J Bone Jt Surg*. 1991;73(1):134-137.

44. Fernandez DL. A technique for anterior wedge-shaped grafts for scaphoid nonunions with carpal instability. *J Hand Surg Am*. 1984;9(5):733-737. doi:10.1016/S0363-5023(84)80025-8

45. El-Karef EA. Corrective osteotomy for symptomatic scaphoid malunion. *Injury*. 2005;36(12):1440-1448. doi:10.1016/j.injury.2005.09.003

46. Gillette BP, Amadio PC, Kakar S. Long-Term Outcomes of Scaphoid Malunion. *Hand*. 2017;12(1):26-30. doi:10.1177/1558944716643295

47. Inoue G, Sakuma M. The natural history of scaphoid non-union Radiographical and clinical analysis in 102 cases. *Arch Orthop Trauma Surg*. 1996;115(1):1-4. doi:10.1007/BF00453208

48. Buijze GA, Goslings JC, Rhemrev SJ, et al. Cast immobilization with and without immobilization of the thumb for nondisplaced and minimally displaced scaphoid waist fractures: A multicenter, randomized, controlled trial. *J Hand Surg Am*. 2014;39(4):621-627. doi:10.1016/j.jhsa.2013.12.039

49. Megerle K, Harenberg PS, Germann G, Hellmich S. Scaphoid morphology and clinical outcomes in scaphoid reconstructions. *Injury*. 2012;43(3):306-310. doi:10.1016/j.injury.2011.08.015

50. Afshar A, Mohammadi A, Zohrabi K, Navaeifar N, Sami SH, Taleb H. Correlation of Reconstructed Scaphoid Morphology with Clinical Outcomes. *Arch bone Jt Surg*. 2015;3(4):244-249. http://www.pubmedcentral.nih.gov/articlerender.fcgi?artid=4628629&tool=pmcentrez&rendertype=abstract.

51. Lalone EA, Willing RT, Shannon HL, King GJW, Johnson JA. Accuracy assessment of 3D bone reconstructions using CT: An intro comparison. *Med Eng Phys*. 2015;37(8):729-738. doi:10.1016/j.medengphy.2015.04.010

52. Lalone EA, Grewal R, King GW, MacDermid JC. Evaluation of an Image-Based Tool to Examine the Effect of Fracture Alignment and Joint Congruency on Outcomes after Wrist Fracture. *Open Orthop J*. 2015;9:168-178. doi:10.2174/1874325001509010168

53. Gammon BM. Arthrokinematics of the Distal Radioulnar Joint in the Normal Wrist and Following Distal Radius Malunion Graduate Program in Medical Biophysics.

2016;(April):166. http://ir.lib.uwo.ca/etd.

54. Wu K, Padmore C, Lalone E, Suh N. An Anthropometric Assessment of the Proximal Hamate Autograft for Scaphoid Proximal Pole Reconstruction. *J Hand Surg Am*. 2018:1-8. doi:10.1016/j.jhsa.2018.04.021

55. Stoesser HL. A Biomechanical Investigation of Scaphoid and Lunate Kinematics During Wrist Motion. 2017;(January).

56. Kim JH, Lee KH, Lee BG, Lee CH, Kim SJ, Choi WS. Dorsal intercalated segmental instability associated with malunion of a reconstructed scaphoid. *J Hand Surg Eur Vol*. 2017;42(3):240-245. doi:10.1177/1753193416680133

57. Berger R, Bishop A, Bettingger P. New dorsal capsulotomy for the surgical exposure of the wrist. *Ann Plast Surg*. 1995;35(1):54-59.

Chapter 2

2 The Impact of Scaphoid Malunion on Radioscaphoid Joint Contact: An *In-Silico* Analysis

The biomechanical significance of scaphoid malunion remains largely unstudied. The intent of this chapter is to explore the impact of scaphoid malunion on joint kinetics at the radioscaphoid joint using an in-silico model derived from previously validated methods.

A version of this work has been submitted to the Journal of Hand Surgery for publication, as well as presented at the 2019 Annual Meeting of the American Association for Hand Surgery (AAHS), the 2019 Western Department of Surgery Research Day, and the 2018 Department of Plastic & Reconstructive Surgery Research Day.

2.1 Introduction

As highlighted in **Chapter 1** (**Section 1.2**), the wrist is a complex joint that relies on the intimate anatomical relationships of numerous carpal bones to facilitate motion. The scaphoid has been implicated in many theories explaining carpal motion as discussed in **Chapter 1** (**Section 1.4**). It is believed that it plays a critical role in synchronizing wrist motion and coordinating stability due to its position bridging the proximal and distal carpal rows. This position also places the scaphoid at high risk of fracture that can result in alterations to scaphoid morphology.[39,47] The vast majority of these fractures are treated with cast immobilization and heal uneventfully but a proportion go on to have pathologic healing resulting in non-union or malunion.[48] The consequences of scaphoid non-union is predictable and involves secondary alterations to carpal mechanics related to a disassociation between the proximal and distal carpal rows.[26] This leads to abnormal joint contact and eventual arthrosis.

The natural history of scaphoid malunion is less clear. It has been hypothesized that alterations to scaphoid shape may result in altered carpal mechanics leading to painful, limited wrist motion.[39] This has been reported clinically by many authors whom successfully treated symptomatic patients with operative reconstruction of the scaphoid. [34,41,42,44,45]. Conversely, other authors have attempted to correlate radiographic measures of scaphoid malunion with patient functional status and failed to elucidate a relationship.[33,36,46,49,50] This inconsistency within the literature limits the development of clinical guidelines for the treatment of patients with asymptomatic scaphoid malunion and surgeons are forced to wait for the manifestation of symptoms prior to intervention. Due to the limitations in the understanding of the impact of scaphoid malunion on carpal bone biomechanics, it remains unclear if these symptoms may correlate with irreversible changes, as is seen in pathologies such as scaphoid non-union advanced collapse traumatic arthritis.

393. The objective of this study was to examine and characterize how wrist contact is altered with progressive scaphoid malunion using a previously validated computational method [51–54].

2.2 Methods

Six (6) computational carpal models were created from previously acquired motion and imaging data within a departmental database. These specimens were all male, with an average age of 68.1 (range: 54-82). An overview of the total methodology is demonstrated in Figure 2.1 Overview of Computational Model Creation Methodology: A schematic overview demonstrating a simplified stepwise approach used within the creation of this computational model

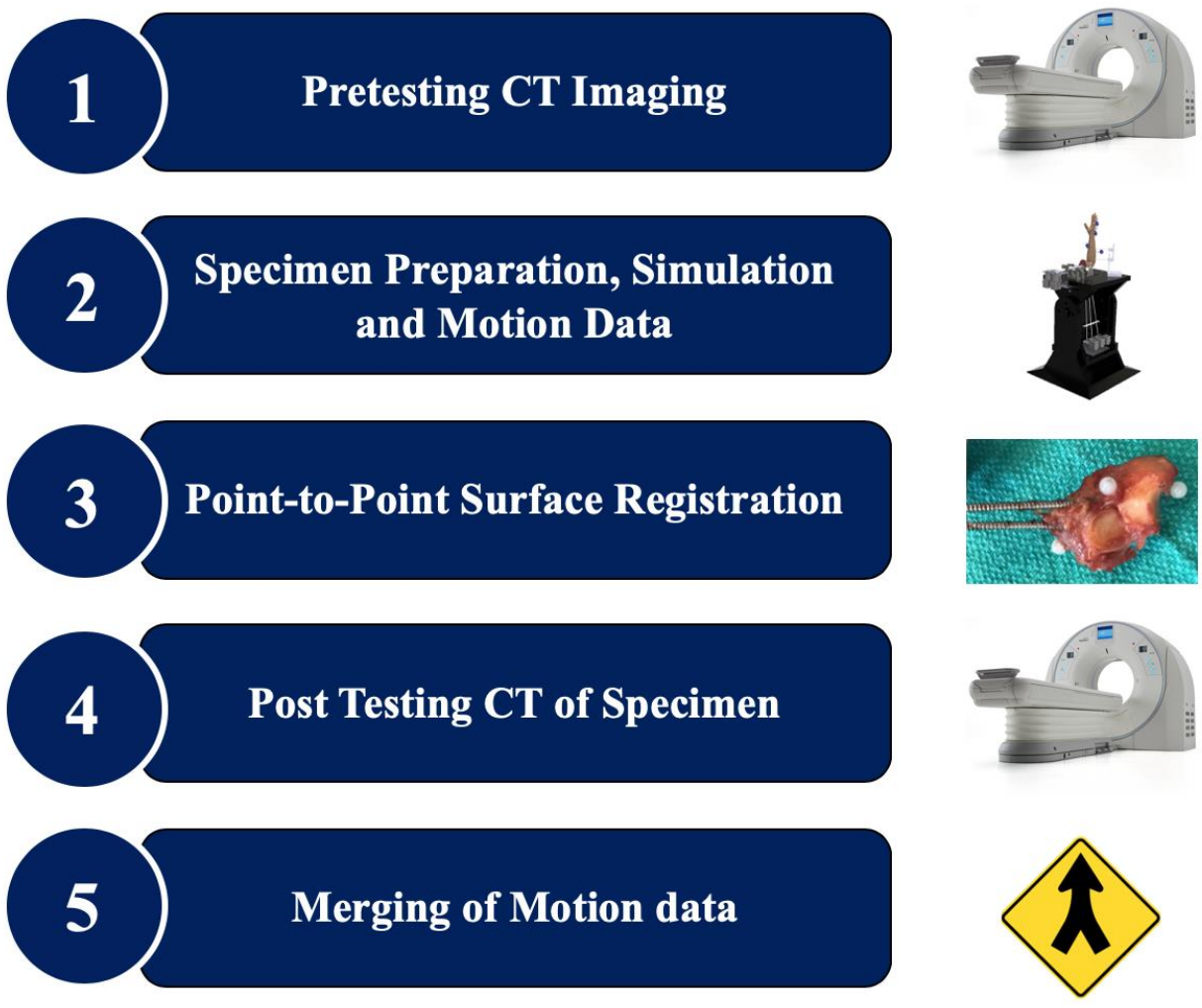

Figure 2.1 Overview of Computational Model Creation Methodology: A schematic overview demonstrating a simplified stepwise approach used within the creation of this computational model

2.2.1 Specimen Preparation

2.2.1.1 Pretesting Validation

Six (6) male fresh frozen cadaveric upper-limb specimens amputated at the upper humerus were included in this cohort. Prior to inclusion for testing each upper limb underwent radiographic analysis using computed tomography (CT) scans to ensure they were free from osseous pathology. Once verified all specimens were thawed for 18 hours prior to commencement of biomechanics testing. These upper limbs were then analyzed using fluoroscopy under passive range of motion to interrogate for evidence of previous soft tissue injuries. All specimens were verified to be free of disease prior to proceeding.

2.2.1.2 Placement of Carpal Bone Optical Trackers

Tracking screws were then placed in carpal bones of interest under fluoroscopic guidance (**Figure** 2.2). Although biomechanical treatment protocols differed between specimens, each wrist underwent a similar surgical methodology and all specimens had motion data collected from the scaphoid, radius, ulna, and capitate. In order to access the carpus from the volar aspect, an extended carpal tunnel incision was designed, taking care to preserve soft tissues. The wrist was approached through a standard capsulotomy and screw placement was verified with fluoroscopy. Similarly, carpal bones were approached dorsally using a midline incision. The wrist joint was approached between the interval of the third and fourth extensor compartments. A capsulotomy was made and once again screws were placed into carpal bones of interest and placement verified using fluoroscopy

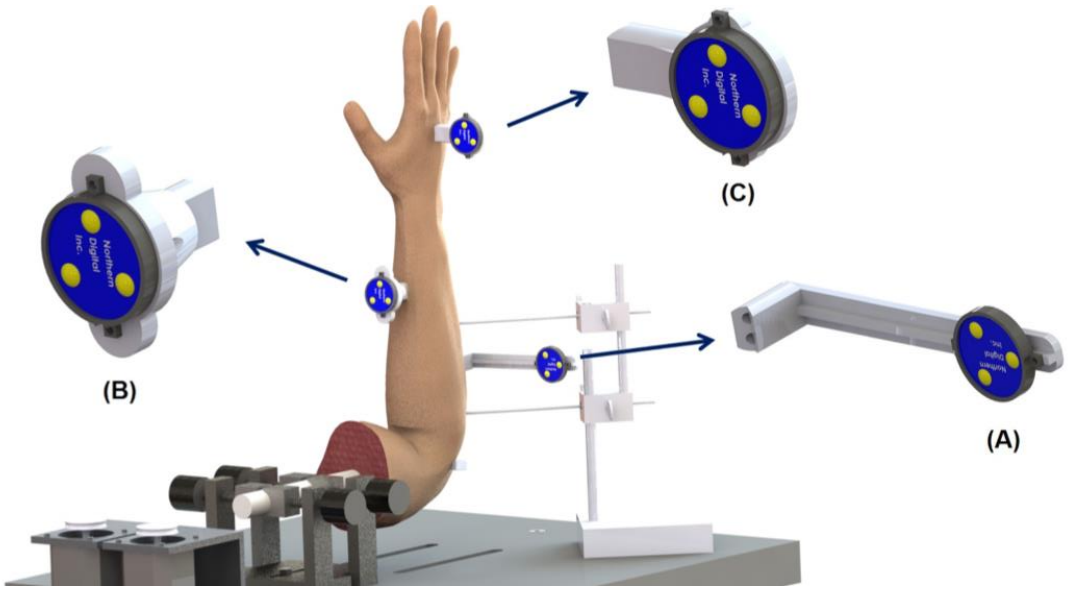

Figure 2.2 Optical Trackers in Cadaveric Specimen: This schematic demonstrates the typical placement of optical trackers into a cadaveric specimen. (**A**) Ulna tracker, (**B**) Radial Tracker, (**C)** Third Metacarpal Tracker. Not pictured in this schematic is the scaphoid optical tracker, which is placed volarly.

2.2.1.3 Soft Tissue Repairs and Tendon Preparation

With all bone trackers placed, the tendons of interest were identified and sutured for later connection to the live motion simulator. Extensor tendons of interest included extensor carpi ulnaris (ECU), extensor carpi radialis longus (ECRL), extensor carpi radialis brevis (ECRB). Flexors included flexor carpi ulnaris (FCU) and flexor carpi radialis (FCR). Additionally, biceps brachii (BB) and pronator teres (PT) were also tagged in order to allow for rotational control of the forearm. Once these tendons were identified, a running Krackow stich was placed at the musculotendinous junction taking care to minimize disruption of soft tissue attachments (**Figure** 2.3*)*. The proximal end of these tendons were then passed subcutaneously and secured through epicondylar blocks at the elbow (**Figure** 2.4).

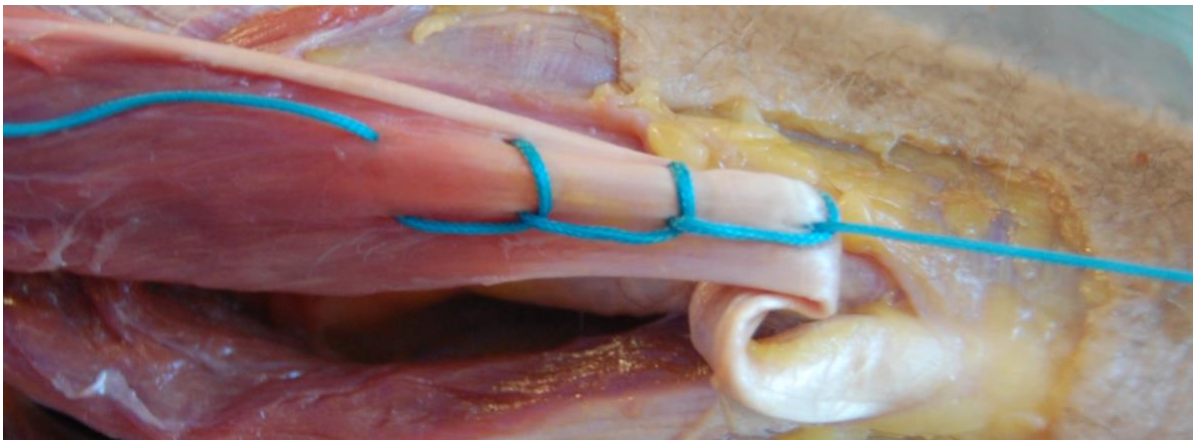

Figure 2.3: Running Krakow Stitch. Each tendon of interest is attached to its respected servo motor using high-tensile strength fishing line in the above topology.

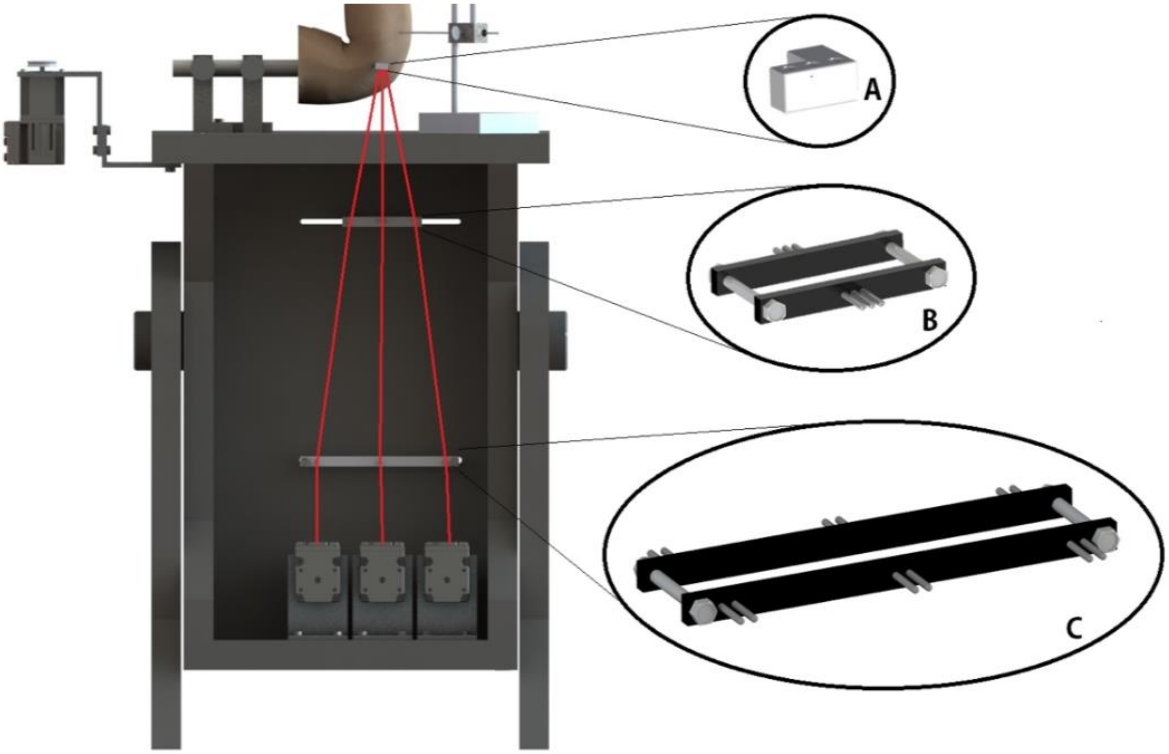

Figure 2.4: Epicondyle Blocks and Cable Stabilization Guide. After the tendons of interests are identified, the suture line is threaded through an epicondyle block to ensure the line of pull exerted by the SmartMotors is in a physiologic direction.

The entire construct was then loaded into a custom wrist simulator jig via a humeral clamp and threaded pins were used to secure the ulna to the simulator and the elbow as placed at 90° flexion (**Figure** 2.5**, Figure** 2.6).

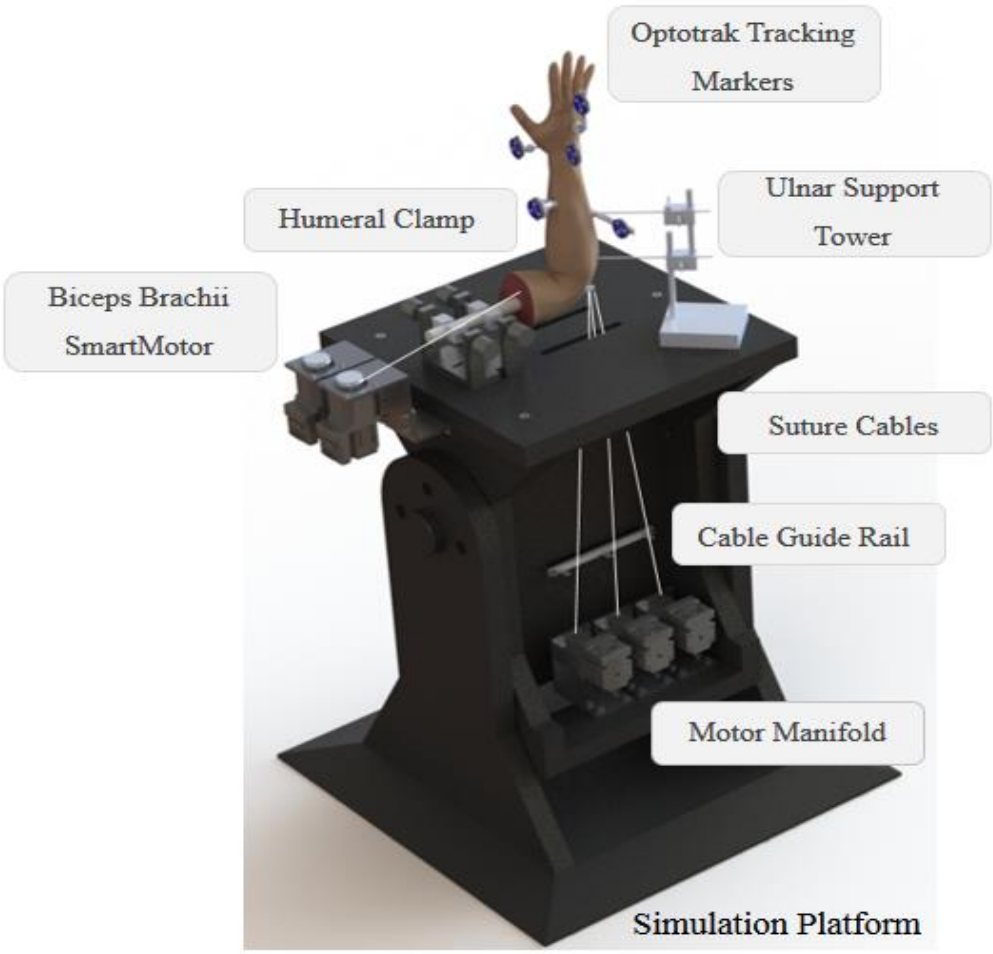

Figure 2.5: Live Motion Wrist Simulator. With specimens secured in the simulator using the humeral clamp and ulnar support tower, the previously sutured tendons can be attached to their respective smart motors. The optical trackers are then placed, and simulation can commence.

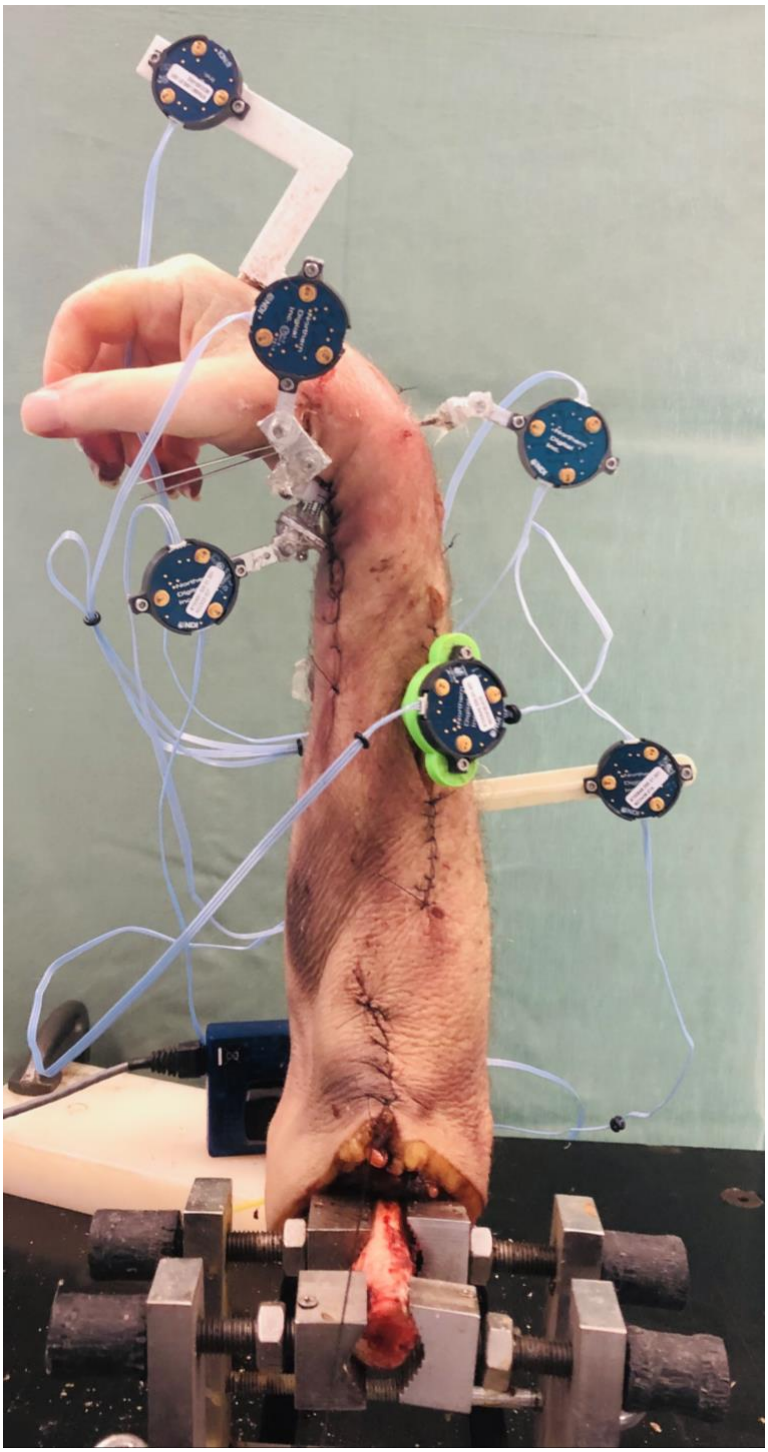

Figure 2.6: Cadaveric Specimen Loaded in Simulator. Once loaded in the simulator and all optical markers are confirmed to be visible, simulation occurs using optical feedback with variable forces translated through the tendons of interested to create the desired motion path.

2.2.1.4 Testing Protocol

Although the ultimate testing protocol differed for each specimen included in this study, it is the standard practice of our laboratory to acquire baseline motion data of the native carpus prior to the initiation of any biomechanical investigations or modifications. The motion data acquired during these runs is used in the creation of the computational models used in this study. Motion data collected included the following motion paths: flexion-extension, dart-throw, and radial-ulnar deviation.

Following the testing protocol, each specimen was disarticulated and denuded. Soft tissues are dissected away from each bone, taking care not to disrupt the optical trackers. Fiducial markers are then placed over prominent anatomic landmarks and these are used in conjunction with the optical tracking device to create 3D models of the bones of interest (**Figure** 2.7). This was accomplished using optical tracking to create a point-to-point representation of each bone of interest. These bones were then imaged using computational tomography in air in order to delineate cartilage which was identified using a semi-automated thresholding algorithm. This allows for the association of the motion data that was previously acquired with the model of each bone in later analysis.

Figure 2.7 Fiducial Markers in Carpal Bone. Fiducial markers placed over prominent carpal bone landmarks for the purpose of digitization and cluster point registration within computational model.

2.2.1.5 Digitization

CT visualization software (Mimics Research 17.0, Materialise, Ann Arbor, MI) was then used to generate the computational models that included the carpal bones, radius, and ulna. Each bone of interest was isolated using a threshold-based semiautomated segmentation technique. Subsequently, 3D reconstruction models of the bones of interest were created, exported as stereolithography (STL) files, and re-meshed to create an optimized uniform triangulated surface mesh (**Figure** 2.8). The motion data acquired from the native testing protocol was then associated with these models to reconstruct the *in-vivo* motion with this *in-silico* model.

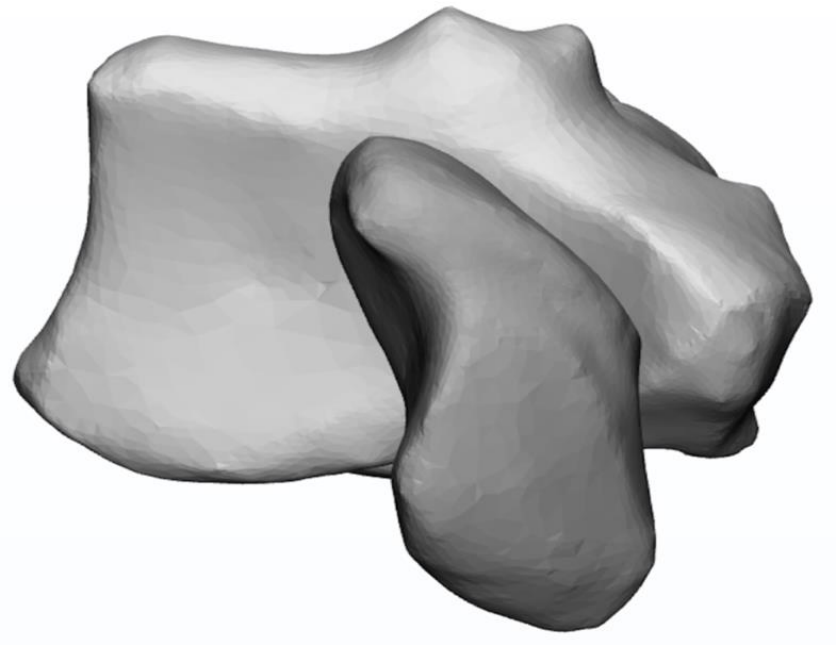

Figure 2.8: STL Computational Reconstruction of Distal Radius and Scaphoid. Using computational software CT scans are transformed to stereolithography files and volume rendered to be simulated for determination of radioscaphoid joint contact for various scaphoid malunion models.

2.2.1.6 Computational Malunion Model

Scaphoid malunion models were then generated computationally by using 3D modeling software (3-Matic 11.0, Materialise, Ann Arbor, MI) (**Figure** 2.9). The native scaphoid was placed in a sagittal orientation and the total length from the proximal to the distal pole was measured. The midpoint was marked, and a simulated osteotomy was carried out perpendicular to the axis of length measurement. An additional 2 osteotomies were simulated at a distance of 1mm symmetrically around this midpoint, removing a total of 2 mm of the waist of the scaphoid to imitate bony loss and comminution associated with a fracture. The distal pole was then translated proximally until it contacted the proximal pole. To simulate malunion the distal pole was then angulated relative to the proximal pole to simulate a humpback deformity. The center of rotation was selected at the volar most point of contact of the proximal and distal poles at the midline. The distal pole was then rotated about this center at predefined angles (0°, 15°, 25°, 35°, 45°, 55°). After each angulation of the distal pole, the resultant space between the two fragments was filled by extrapolating the face of the osteotomy of the distal pole to the proximal interface around the same arc of rotation that the malunion was created. This malunion model was then inserted back into its native wrist model in 3 different positions of 45° extension, neutral position, and 45° flexion and the resultant contact was recorded. Contact data was assessed as squared millimeters with each native state serving as its own reference point as there is significant variability in the size of specimen.

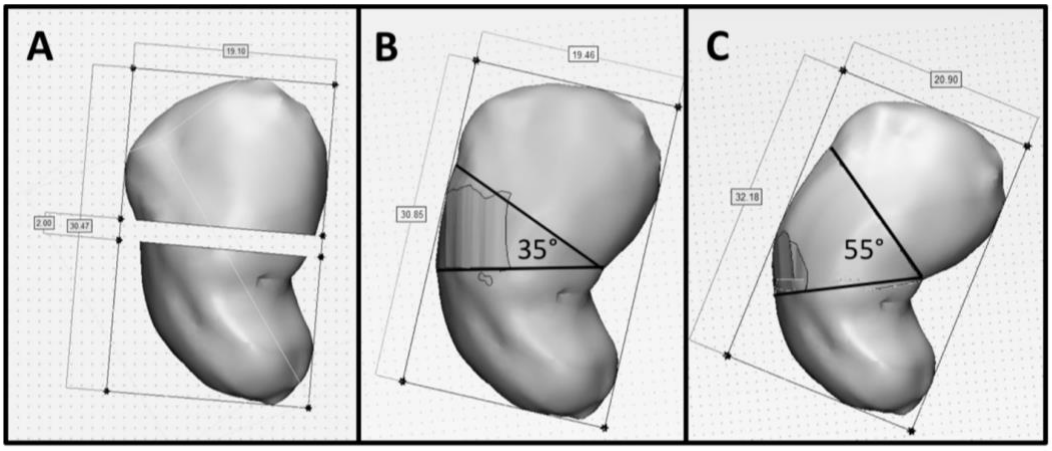

Figure 2.9: Malunion Creation Process. (**A**) 2mm section of bone was taken from the middle aspect of the scaphoid to represent comminution and bony loss (**B**) Simulated 35° malunion where the distal pole was rotated about a point where the volar cortex of the proximal and distal poles interact and the remaining space was interpolated (**C**) Simulated 55° malunion prepared in similar fashion.

2.2.1.7 Outcome Variables and Data Analysis

The joint congruency of each model was assessed with their respective radius using a previously validated, custom, inter-bone distance algorithm with the wrist in 3 different positions (40° extended, neutral, 40° flexed).[51,53] This process produced color maps of the radioscaphoid joint representing the distance between the two surfaces (**Figure** 2.10). Contact was defined as any location where the distance between the two surfaces was 0mm or less, implying an overlap of the cartilage. A 2-dimensional average of this contact area (centroid) was calculated for each scaphoid malunion model. A local two-dimension coordinate system was generated on the distal radius for each specimen to normalize the centroid values between specimens and to account for size discrepancies. The origin of the coordinate system was located at the intersection between the midpoint of the volar midridge and the dorsal midridge and the midpoint of the radial styloid and the distal radioulnar joint. Any point radial to this position was defined using a positive "x" coordinate, and any point ulnar defined as a negative "x" coordinate. Similarly, a point dorsal and volar were defined as positive and negative respectively in the y-dimension.

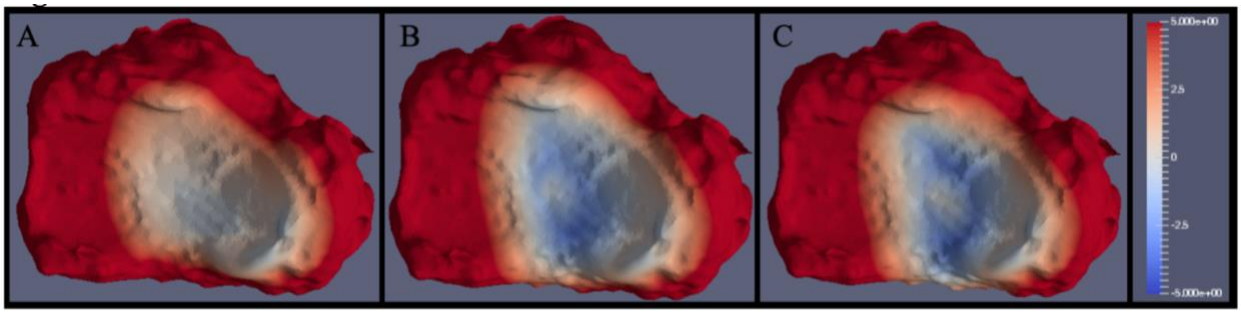

Figure 2.10: Representative Radio Scaphoid Contact Map (Specimen 13-05027R). Joint contact for malunion severity of 0° (A), 35° (B) and 55° (C). Warm colors imply a positive distance between the scaphoid and radioscaphoid fossa, whereas cool colors represent areas of interaction or overlap.

2.2.1.8 Statistical Analysis

An a priori power study demonstrated that a sample size of 6 specimens was sufficient to have greater than 80% power with 95% confidence for each comparison that was tested.[55] To detect statistical differences in radioscaphoid joint contact area between malunion states (0°, 15°, 25°, 35°, 45°, 55°) a two-way repeated-measures analysis of variance (RM-ANOVA) was performed with Bonferroni correction factor for multiple comparisons. The factors included scaphoid malunion angle (0°, 15°, 25°, 35°, 45°, 55°) and wrist position (40° extended, neutral, 40° flexed). Additionally, a three-way RM-ANOVA with Bonferroni correction factor was performed to examine joint contact centroid location in the radial-ulnar and dorsal-volar directions. The factors included scaphoid malunion angle (0°, 15°, 25°, 35°, 45°, 55°), wrist position (40° extended, neutral, 40° flexed), and centroid location direction (radial-ulnar, dorsal-volar). Statistical significance was set at $p<0.05$.

2.3 Results

2.3.1 Description of Specimens

The average native scaphoid height was 20.1 ± 2.0mm, and the average native scaphoid width was 33.7 ± 2.3mm.

2.3.2 Extended Wrist Results

There was a significant association between scaphoid malunion angle severity and an increase in average joint contact area ($p<0.05$) (**Figure** 2.11). The mean increase in joint contact area with the wrist in its extended position compared to intact are as follows; 15° = 90.5 mm^2, 25° = 128.4 mm^2, 35° = 140.0 mm^2, 45° = 140.5 mm^2, 55° = 143.4 mm^2, with $p<0.05$ for all tested malunion angles compared to intact. However, there were not significant increases in contact area following 35° of malunion ($p>0.05$). There was a statistically significant translation of the average centroid position in the ulnar and volar direction for all malunion angle severities ($p<0.05$, $p<0.05$), when compared to the intact state (**Figure** 2.12).

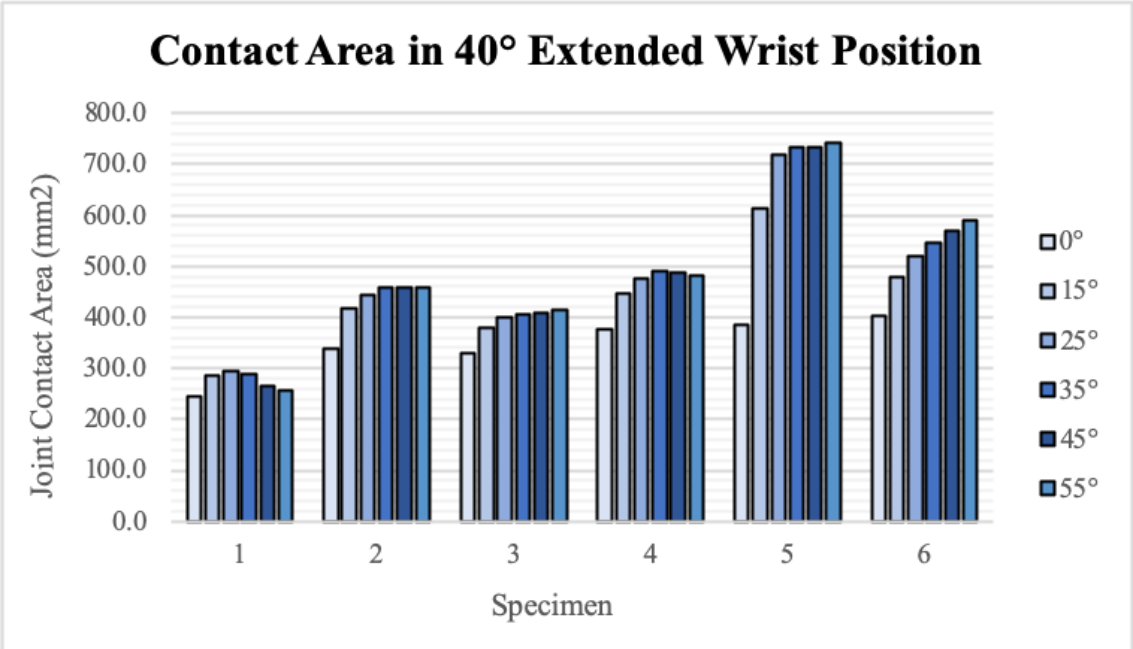

Figure 2.11: Contact area for 40° extended wrist position. The increase in joint contact was less linear with increasing angulation of the proximal and distal scaphoid fragment in the extended wrist position. The largest differences are observed through the angulation angles of 0°-25° with a plateau thereafter. The data represents the results of 6 specimens. Standard deviations are removed for clarity but ranged from 57-164 mm2.

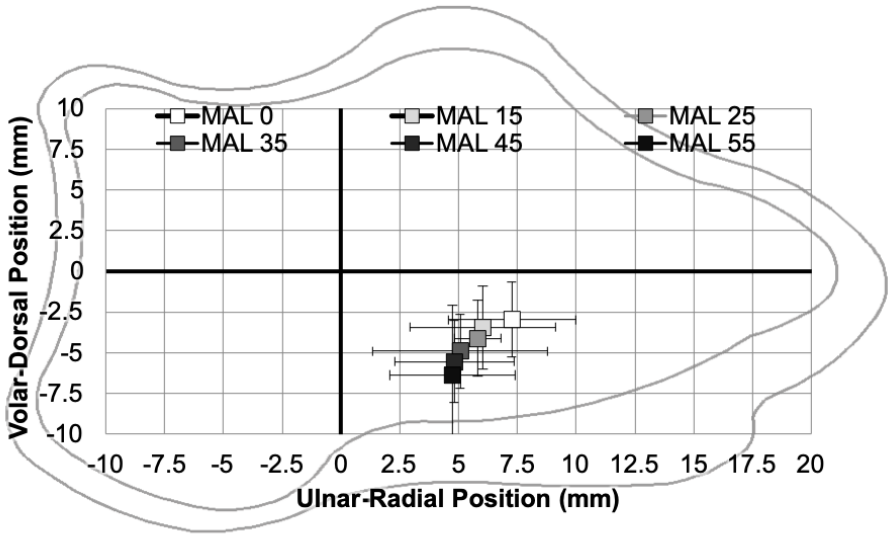

Figure 2.12: Mean ±1 SD of centroid location for 40° extended wrist position. This figure is a pictorial demonstration of the distal radioscaphoid joint with the upper aspect representing the dorsum and left portion representing the ulnar aspect. The average joint contact location moves ulnarly and volarly with increasing malunion severity.

2.3.3 Neutral Wrist Results

There was a significant association between scaphoid malunion angle severity and an increase average joint contact area ($p<0.05$) (**Figure** 2.13). The mean increase in joint contact area at neutral wrist position compared to intact are as follows; 15° = 81.5 mm^2, 25° = 129.6 mm^2, 35° = 179.3 mm^2, 45° = 201.8 mm^2, 55° = 249.6 mm^2, with $p<0.05$ for all tested malunion angles compared to intact. Scaphoid malunion severity of 0° - 35° were all statistically different from each other ($p<0.05$); however, there were not significant increases in contact area past 35° of malunion severity ($p>0.05$). There was a statistically significant translation of the average centroid position in the ulnar direction ($p<0.05$) when compared to the intact state (**Figure** 2.14).

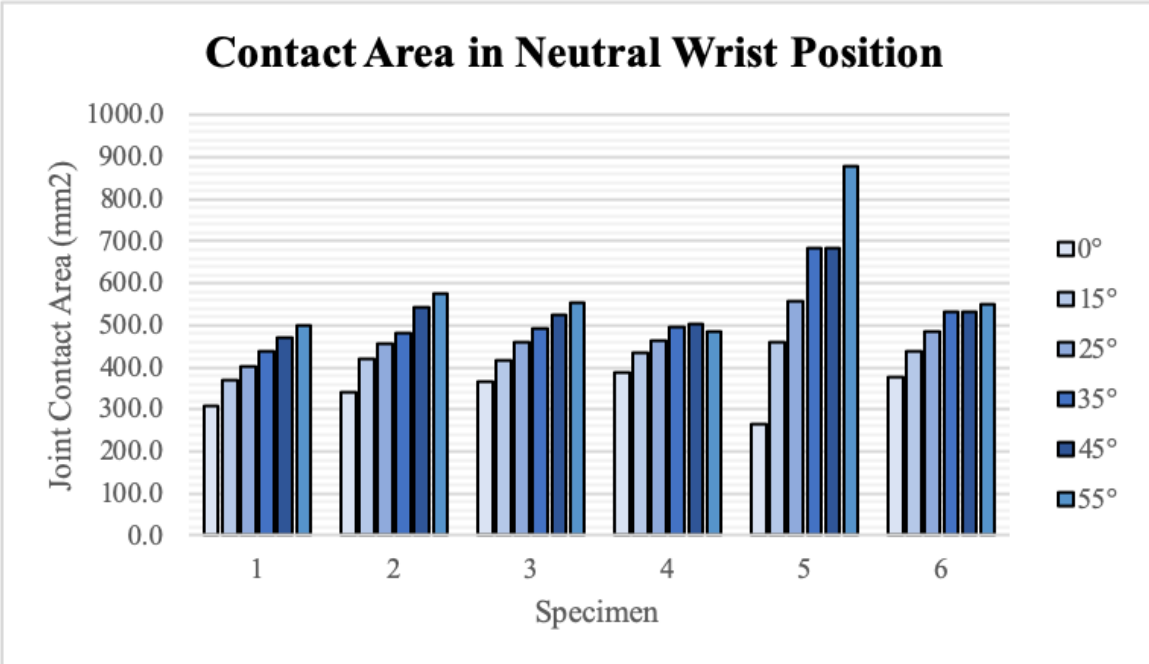

Figure 2.13: Contact area for neutral wrist position. With increasing angulation between the distal and proximal scaphoid fragments there was increased contact between the scaphoid and radius with the wrist in neutral position. All specimens follow a similar pattern of increasing joint contact with the exception of specimen 5, which has a very prominent ridge between the radioscaphoid and radiolunate fossa resulting in a different pattern of interaction. The data represents the results of 6 specimens. Standard deviations are removed for clarity but ranged from 45-145 mm2.

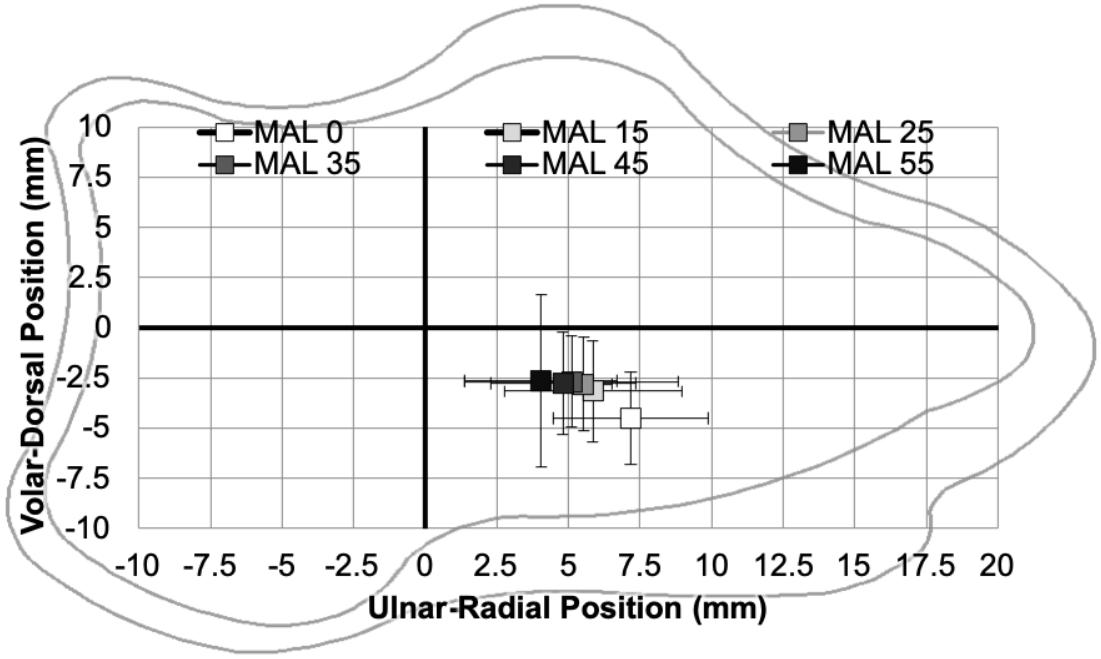

Figure 2.14: Mean ± 1 SD of centroid location for neutral wrist position. The average joint contact location moves ulnarly with increasing malunion severity but does not differ significantly in terms of volar-dorsal position.

2.3.4 Flexed Wrist Results

There was a significant association between scaphoid malunion angle severity and an increase in average joint contact area ($p<0.05$) (**Figure** 2.15). The mean increase in joint contact area in the wrist flexion position compared to intact are as follows: 15° = 76.0 mm^2, 25° = 112.0 mm^2, 35° = 144.6 mm^2, 45° = 171.0 mm^2, 55° = 241.8 mm^2, with $p<0.05$ for all tested malunion angles compared to intact. Additionally, all malunion severities were statically different from each other with the exception of 35° and 45° ($p>0.05$). There was a statistically significant translation of the average centroid position in the ulnar direction ($p<0.05$), when compared to the intact state. (**Figure** 2.16).

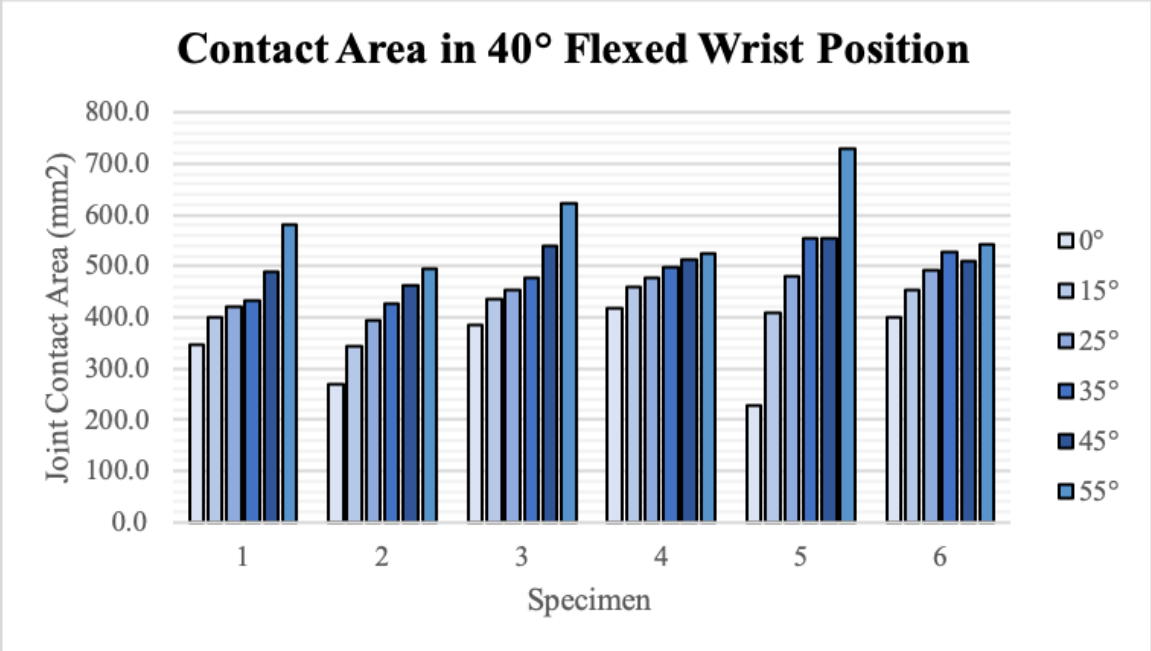

Figure 2.15: Contact area for 40° flexed wrist position. As the angulation between the distal and proximal scaphoid fragment increases there was an increase in contact with the radius. This increase was linear for most specimens, with the exception of specimen 5 which had a dramatic increase in joint contact at 55° angulation. The data represents the results of 6 specimens. Standard deviations are removed for clarity but ranged from 33-85 mm2.

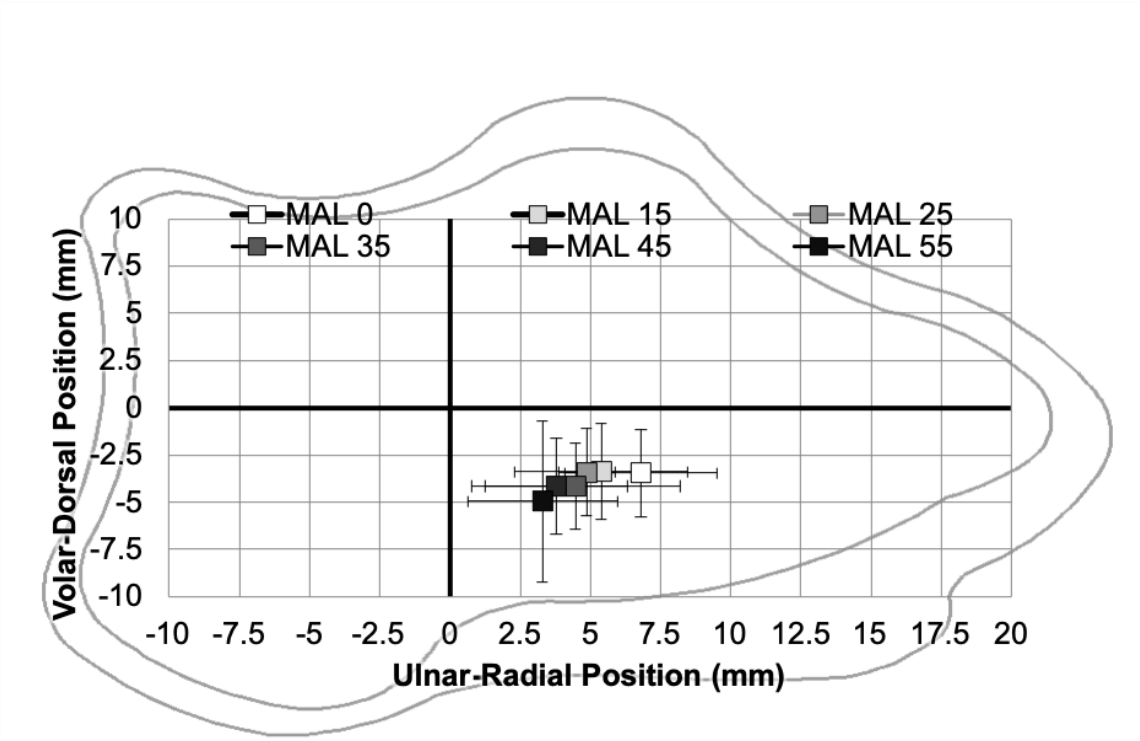

Figure 2.16: Mean ± 1 SD of centroid location for flexed wrist position. Similar to the neutral wrist position, the average joint contact location moves ulnarly with increasing malunion severity but does not differ significantly in terms of volar-dorsal position.

2.4 Discussion

Scaphoid malunion is a well-recognized complication of scaphoid fracture following both conservative and operative therapy. The importance of this alteration to native scaphoid geometry is debated. Amadio et al. first investigated the importance of scaphoid malunion by correlating lateral intrascaphoid angles (LISA) with patient-rated outcomes and reported that a LISA > 45° was associated increased pain, decreased range of motion, and decreased grip strenth compared to radiographically normal patients. Similar results were obtained by many other authors.[41,42,45,56] The measurement of scaphoid malunion, as well as the tools to evaluate outcomes differed amongst these papers but in each of these studies, symptomatic malunions were successfully treated with operative intervention that improved functional status. Conversely, many retrospective cohort studies have shown that patients outcomes are not correlated with the degree of scaphoid deformity.[33,36,46,49,50] Once again, there was a broad range of approaches in quantifying both malunion severity and patient outcomes within these studies. The diversity of methodologies amongst both the positive and negative studies limits the ability to appraise the literature as a whole. This is also limited by a restricted understanding of the underlying natural history of scaphoid malunion, as only a single study to date has attempted to elucidate the pathologic mechanics associated with this injury.[40]

In this computational study, there was a statistically significant relationship between malunion severity and increased joint contact. Although there was variation in bony anatomy amongst the specimens, all cases demonstrated a similar pattern of joint contact. This could imply that scaphoid malunion may have a common biomechanical pathology. As the distal pole of the scaphoid progresses into a humpback deformity, the scaphoid begins to interact with the ulnar aspect of the radioscaphoid fossa. This is demonstrated in the ulnar shift of the centroid that occurred in all wrist positions. This pattern of joint contact appears to be in contrast to that of scaphoid non-union in which the radial styloid experiences the first signs of degenerative changes in this process. The ulnar aspect of the radial articular surface is sufficiently covered with cartilage, possibly making this change tolerable and explaining why many studies have failed to demonstrate clinical symptoms associated with this change.

Within our study cohort, there was one specimen (14-06011R) that demonstrated a dramatic increase in joint contact with increasing malunion severity. This specimen had well-defined scaphoid and lunate fossae with a prominent inter-fossa ridge. The significance of wrist topology in the understanding of injuries to the carpus is not well documented. Although authors have documented various different systems to classify particular carpal bones, it is not common to examine an injury in the context of subtle anatomic variations. Based on the studies that reported patients with symptomatic malunion, potentially these patients had particular radioscaphoid topologies that were susceptible to alterations in scaphoid topology leading to secondary changes in wrist mechanics and painful motion.

This study has limitations related to small sample size, age of specimens used, and its computational nature. Six specimens were used given the availability of high-quality computational models. Within this subset, there was significant variability in radius and scaphoid topology. The average age of the included specimens was 68 years and although each limb was screened for evidence of underlying pathology, age-related degenerative changes are common in this age group. The model of scaphoid malunion was intentionally simplistic to maximize consistency between specimens. In reality, a fractured scaphoid undergoes a complex, multi-dimensional, change in orientation resulting in a humpback deformity. Finally, although it can be inferred that increasing joint contact may represent increased bone-to-bone interaction within a normal wrist, the carpus bones are a dynamic system. The exact impact of scaphoid topology *in-vivo* may be compensated by other mechanisms.

2.5 Conclusion

Increasing scaphoid malunion deformity resulted in an increase in the amount of joint contact in this computational simulation. This serves as a hypothesis generating experiment and gives insight into potential pathologic mechanisms associated with scaphoid malunion. Future work would include validating this hypothesis in biomechanical studies or analyzing the radioscaphoid joint using finite element studies to better understand the stresses experienced by the scaphoid and radius with increasing severity of malunion.

2.6 References

1. Hirt B, Seyhan H, Wagner and M. *Hand and Wrist Anatomy and Biomechanics : A Comprehensive Guide*.; 2016. doi:4718699

2. Gray H. Anatomy of the Human Body. *Am J Med Sci*. 1919;157(5):704. doi:10.1097/00000441-191905000-00011

3. Wolfe SW (Weill MCU, Hotchkiss RN (Weill MCU, Pederson WC (University of THSCSATHC of SA, Kozin SH (Shriners H for CTUS of M. *Green's Operative Hand Surgery*. 6th ed. (Green DP, ed.). Philadelphia, PA: Elsevier; 2011.

4. Feipel V, Rooze M. The capsular ligaments of the wrist: Morphology, morphometry and clinical applications. *Surg Radiol Anat*. 1999;21(3):175-180. doi:10.1007/BF01630897

5. Hanse J, Saunders JB. *Netters Clinical Anatomy*. 2nd ed.; 2010.

6. Wu G, Van Der Helm FCT, Veeger HEJ, et al. ISB recommendation on definitions of joint coordinate systems of various joints for the reporting of human joint motion - Part II: Shoulder, elbow, wrist and hand. *J Biomech*. 2005;38(5):981-992. doi:10.1016/j.jbiomech.2004.05.042

7. Craigen MAC, Stanley JK. WRIST Row , column or both ? *J Hand Surg Br Eur Vol*. 1995;20(Fig 2):165-170.

8. Garcia-Elias M. Understanding Wrist Mechanics: A Long and Winding Road. *J Wrist Surg*. 2013;02(01):005-012. doi:10.1055/s-0032-1333429

9. Johnston H. Varying positions of the carpal bones in the different movements al the wrist PART II. *J Anat Physiol*. 1907;4:280-292.

10. Navarro A. Anatomy and physiology of the carpus [in Spanish]. *Imprenta Artist Dornaleche Hnos*. 1935:166-189.

11. Taleisnik J. The Ligaments of the Wrist. *J Hand Surg Am*. 1976;1(2):110-118.

12. Lichtman DM, Schneider JR, Swafford AR, Mack GR. Ulnar midcarpal instability—Clinical and laboratory analysis. *J Hand Surg Am*. 1981;6(5):515-523. doi:10.1016/S0363-5023(81)80115-3

13. Dunning C, CS L, RT B, PattersonSD, JA J, GJ K. Supplemental pinning improves the stability of external fixation in distal radius fractures during simulated finger and forearm motion. *J Hand Surg Am*. 1999;24(5):992-1000.

14. Werner FW, Palmer AK, Somerset JH, et al. Wrist Joint Motion Simulator. *J Bone Jt Surg*. 1996;14(6):639-646.

15. Iglesias DJ. Development of an in-vitro passive and active motion Simulator for the investigation of wrist function and Kinematics. 2015.

16. Rikli DA, Honigmann P, Babst R, Cristalli A, Morlock MM, Mittlmeier T. Intra-Articular Pressure Measurement in the Radioulnocarpal Joint Using a Novel Sensor: In Vitro and In Vivo Results. *J Hand Surg Am*. 2007;32(1):67-75. doi:10.1016/j.jhsa.2006.10.007

17. W GW, H BR, C. L. Mechanism of wrist joint with special reference to fractures of the scaphoid. *Guys Hosp Rep*. 1943;92:52–59.

18. Landsmeer J. Studies in the anatomy of articulation. I. The equilibrium of the "intercalated" bone. *Acta Morphol Neerl Scand*. 1961;3:287-303.

19. Fisk G. The wrist. Review article. *J Bone Joint Surg Br*. 1984:396-407.

20. JM K. The interdependence of carpal articulation chains. *Acta Anat*. 1974;88:481-501.

21. Stormont TJ, An KN, Morrey BF, Chao EY. Elbow joint contact study: Comparison of techniques. *J Biomech*. 1985;18(5):329-336. doi:10.1016/0021-9290(85)90288-X

22. Pogue DJ, SF V, RM P, et al. Effects of distal radius fracture malunion on wrist joint mechanics. *J Hand Surg Am*. 1990;15(5):721-727.

23. Nishiwaki M, T N, T N, Y T, Ikegami H. Ulnar-shortening effect on distal radioulnar joint pressure: a biomechanical study. *J Hand Surg Am*. 2008;33(2):198-205.

24. Wan L, Deasla R, Rubash H, Li G. Determination of in-vivo articular cartilage contact areas of human talocrural joint under weightbearing conditions. *Osteoarthr Cartil*. 2006;14(12):1294-1301.

25. GE M, DH L, C D, S A, CM G, Crisco JJ. Estimating Joint Contact Areas and Ligament Lengths From Bone Kinematics and Surfaces. *IEEE Trans Biomed Eng*. 2004;51(5):770-779.

26. Sendher R, Ladd AL. The Scaphoid. *Orthop Clin North Am*. 2013;44(1):107-120. doi:10.1016/j.ocl.2012.09.003

27. Herbert J, Fisher E. Management of the fractured scaphoid using a new bone screw. *J Bone Jt Surg*. 1984;66(1):114-123.

28. Cooney W, Dobyns J, Linscheid R. Fractures of the scaphoid: a rational approach to management. *Clin Orthop*. 1980;149(149):90-97.

29. Russe O. Fractures of the Carpal Navicular. *J Bone Jt Surg*. 1960;42(5):759-768.

30. Ten Berg P, Drijkoningen T, Strackee S, Buijze G. Classifications of Acute Scaphoid Fractures: A Systematic Literature Review. *J Wrist Surg*. 2016;05(02):152-159. doi:10.1055/s-0036-1571280

31. Cooney WP. *The Wrist: Diagnosis and Operative Technique*. St.Louis; 1998.

32. Russe O. Fracture of the Carpal Navicular: Diagnosis, Non-operative Treatment, and Operative Treatment. *J Bone Jt Surg*. 1960;42(5):759–768.

33. Forward DP, Singh HP, Dawson S, Davis TRC. the Clinical Outcome of Scaphoid Fracture Mal Union At 1 Year. *Hand, The*. 2009:40-46.

34. Lee CH, Lee KH, Lee BG, Kim DY, Choi WS. Clinical outcome of scaphoid malunion as a result of scaphoid fracture nonunion surgical treatment: A 5-year minimum follow-up study. *Orthop Traumatol Surg Res*. 2015;101(3):359-363. doi:10.1016/j.otsr.2014.09.026

35. Amadio PC, Berquist TH, Smith DK, Ilstrup DM, Cooney WP, Linscheid RL. Scaphoid

malunion. *J Hand Surg Am*. 1989;14(4):679-687. doi:10.1016/0363-5023(89)90191-3

36. Jiranek WA, Ruby LK, Millender LB, Bankoff MS, Newberg AH. Long-term results after Russe bone-grafting: The effect of malunion of the scaphoid. *J Bone Jt Surg - Ser A*. 1992;74(8):1217-1228. doi:10.2106/00004623-199274080-00012

37. Bain GI, Bennett JD, MacDermid JC, Slethaug GP, Richards RS, Roth JH. Measurement of the scaphoid humpback deformity using longitudinal computed tomography: Intra- and interobserver variability using various measurement techniques. *J Hand Surg Am*. 1998;23(1):76-81. doi:10.1016/S0363-5023(98)80093-2

38. Singh HP, Forward D, Davis TRC, Dawson JS, Oni JA, Downing ND. Partial union of acute scaphoid fractures. *J Hand Surg Am*. 2005;30(5):440-445. doi:10.1016/j.jhsb.2005.05.007

39. Mathoulin CL, Arianni M. Treatment of the scaphoid humpback deformity – is correction of the dorsal intercalated segment instability deformity critical? *J Hand Surg Eur Vol*. 2018;43(1):13-23. doi:10.1177/1753193417739526

40. Burgess RC. The effect of a simulated scaphoid malunion on wrist motion. *J Hand Surg Am*. 1987;12(5):774-776. doi:10.1016/S0363-5023(87)80067-9

41. Birchard D, Pichora D. Experimental corrective scaphoid osteotomy for scaphoid malunion with abnormal wrist mechanics. *J Hand Surg Am*. 1990;15(6):863-868. doi:10.1016/0363-5023(90)90004-B

42. Lynch NM, Linscheid RL. Corrective osteotomy for scaphoid malunion: technique and long-term follow-up evaluation. *J Hand Surg Am*. 1997;22(1):35-43. doi:10.1016/S0363-5023(05)80177-7

43. T N. Scaphoid Malunion. *J Bone Jt Surg*. 1991;73(1):134-137.

44. Fernandez DL. A technique for anterior wedge-shaped grafts for scaphoid nonunions with carpal instability. *J Hand Surg Am*. 1984;9(5):733-737. doi:10.1016/S0363-5023(84)80025-8

45. El-Karef EA. Corrective osteotomy for symptomatic scaphoid malunion. *Injury*. 2005;36(12):1440-1448. doi:10.1016/j.injury.2005.09.003

46. Gillette BP, Amadio PC, Kakar S. Long-Term Outcomes of Scaphoid Malunion. *Hand*. 2017;12(1):26-30. doi:10.1177/1558944716643295

47. Inoue G, Sakuma M. The natural history of scaphoid non-union Radiographical and clinical analysis in 102 cases. *Arch Orthop Trauma Surg*. 1996;115(1):1-4. doi:10.1007/BF00453208

48. Buijze GA, Goslings JC, Rhemrev SJ, et al. Cast immobilization with and without immobilization of the thumb for nondisplaced and minimally displaced scaphoid waist fractures: A multicenter, randomized, controlled trial. *J Hand Surg Am*. 2014;39(4):621-627. doi:10.1016/j.jhsa.2013.12.039

49. Megerle K, Harenberg PS, Germann G, Hellmich S. Scaphoid morphology and clinical outcomes in scaphoid reconstructions. *Injury*. 2012;43(3):306-310. doi:10.1016/j.injury.2011.08.015

50. Afshar A, Mohammadi A, Zohrabi K, Navaeifar N, Sami SH, Taleb H. Correlation of Reconstructed Scaphoid Morphology with Clinical Outcomes. *Arch bone Jt Surg*. 2015;3(4):244-249. http://www.pubmedcentral.nih.gov/articlerender.fcgi?artid=4628629&tool=pmcentrez&rendertype=abstract.

51. Lalone EA, Willing RT, Shannon HL, King GJW, Johnson JA. Accuracy assessment of 3D bone reconstructions using CT: An intro comparison. *Med Eng Phys*. 2015;37(8):729-738. doi:10.1016/j.medengphy.2015.04.010

52. Lalone EA, Grewal R, King GW, MacDermid JC. Evaluation of an Image-Based Tool to Examine the Effect of Fracture Alignment and Joint Congruency on Outcomes after Wrist Fracture. *Open Orthop J*. 2015;9:168-178. doi:10.2174/1874325001509010168

53. Gammon BM. Arthrokinematics of the Distal Radioulnar Joint in the Normal Wrist and Following Distal Radius Malunion Graduate Program in Medical Biophysics.

2016;(April):166. http://ir.lib.uwo.ca/etd.

54. Wu K, Padmore C, Lalone E, Suh N. An Anthropometric Assessment of the Proximal Hamate Autograft for Scaphoid Proximal Pole Reconstruction. *J Hand Surg Am*. 2018:1-8. doi:10.1016/j.jhsa.2018.04.021

55. Stoesser HL. A Biomechanical Investigation of Scaphoid and Lunate Kinematics During Wrist Motion. 2017;(January).

56. Kim JH, Lee KH, Lee BG, Lee CH, Kim SJ, Choi WS. Dorsal intercalated segmental instability associated with malunion of a reconstructed scaphoid. *J Hand Surg Eur Vol*. 2017;42(3):240-245. doi:10.1177/1753193416680133

57. Berger R, Bishop A, Bettingger P. New dorsal capsulotomy for the surgical exposure of the wrist. *Ann Plast Surg*. 1995;35(1):54-59.

Chapter 3

3 The Impact of Scaphoid Malunion on Carpal Motion: An *In-Vitro* Analysis

As with the kinetic impact of scaphoid malunion on total carpus motion, the importance of scaphoid malunion on wrist kinematics remains largely unstudied. The intent of this chapter is to explore the impact of scaphoid malunion on carpus motion, particularly its effect on the radial-sided carpal bones including the scaphoid, lunate, trapezium, trapezoid, and capitate using a cadaveric active motion simulator.

A version of this work has been submitted to the 2020 Annual Meeting of the American Association for Hand Surgery (AAHS), as well as presented at the 2019 Department of Plastic Surgery Research Day.

3.1 Introduction

The complexity of wrist anatomy has been previously highlighted in **Sections** Error! Reference source not found.-Error! Reference source not found.**.** The delicate interplay between the carpal bones to facilitate a broad range of motion despite limited soft tissue support has been investigated by various authors and prominent theories have been highlighted in **Section** Error! Reference source not found.. There is significant variability within these theories, but each implicates the scaphoid as critical for stability to coordinate motion between the proximal and distal carpal row.

Clinically, the importance of the scaphoid in the coordination of motion and carpus stability is demonstrated in scaphoid non-union advanced collapse (SNAC) post-traumatic arthritis. In this pathology, the distal and proximal rows become uncoupled leading to wrist instability and progressive joint arthrosis.[26] Other alterations to scaphoid morphology may affect wrist kinematics leading to secondary instabilities, such as scaphoid malunion. Despite this, there is little consensus regarding the relationship between scaphoid shape and total wrist motion.

In the late 80s and early 90s, a number of authors published clinical case reports describing patients with scaphoid malunion that had painful limited motion that were successfully treated with operative reconstruction.[34,39,41,42,44,45] More recently however, other authors have attempted to correlate radiographic measures of scaphoid malunion with patient functional status and failed to elucidate a relationship although most of these studies did not investigate total wrist motion specifically.[33,36,46,49,50] To date, there has only been a single report investigating the relationship between wrist motion and scaphoid malunion severity. Burgess used a cadaveric model and found that increasing angulation resulted in decreased extension of the wrist, with all wrist extension being lost with scaphoid angulations of 30° or greater. This study was limited by small numbers, as well as static measures that failed to give insight into dynamic carpal motion.

The purpose of this study was to characterize how progressive scaphoid malunion affects the radial sided carpal bones and investigate the relationship between increasing scaphoid malunion severity on motion during active motion using a previously validated cadaveric biomechanical method. [51–54] The kinematics of these carpal bones were measured during planar motions of

unconstrained wrist flexion and extension with varying degrees of scaphoid malunion severity. By understanding the biomechanical implications of scaphoid malunion, the natural history can be speculated, and further studies targeted more efficiently to determine the importance of this pathology. We hypothesized that increasing scaphoid malunion severity will result in increasingly pathologic motion of the scaphoid and lunate.

3.2 Methods

*The experimental approaches employed herein are similar to those described in **Section 2.2**. They are presented here, re-written to satisfy the manuscript format of this thesis and to avoid duplication for eventual publication.*

Seven (7) male fresh frozen cadaveric specimens (average age 63 years, range: 50-76 years) amputated at the mid humerus were used in this study.

3.2.1 Specimen Preparation

These specimens underwent pre-testing assessment to rule out underlying pathology using fluoroscopy, CT imaging, and direct inspection as previously described in **Section 2.1**.

The carpal bones of interest tracked in this work included the scaphoid, lunate, trapezium, trapezoid, capitate, radius and ulna. Two cortical bone screws were placed in each bone of interest (Ø 2.7mm) to mount the optical trackers. The scaphoid and trapezium-trapezoid were accessed from a volar wrist approach using a combination of an extended carpal tunnel and Wagner incisions. A wrist capsulotomy was created over the lunate and scaphoid using a ulnarly based flap. Tracking screws were placed in the distal scaphoid tubercle, whereas a single set of screws were placed across the trapezium and trapezoid together given the small size of these carpal bones (**Figure** 3.1). Dorsally, screws were placed in the lunate using a midline incision centered on the long axis of the third metacarpal (**Figure** 3.2). The wrist capsule was opened using a method previously described by Berger et al.[57] All screw placements into the carpal bones were verified using fluoroscopy to ensure there was no violation into a joint. (**Figure** 3.3). Placement of trackers into the radius, ulna, and third metacarpal was accomplished under direct visualization using an open surgical approach after each specimen was loaded into the simulator as described below.

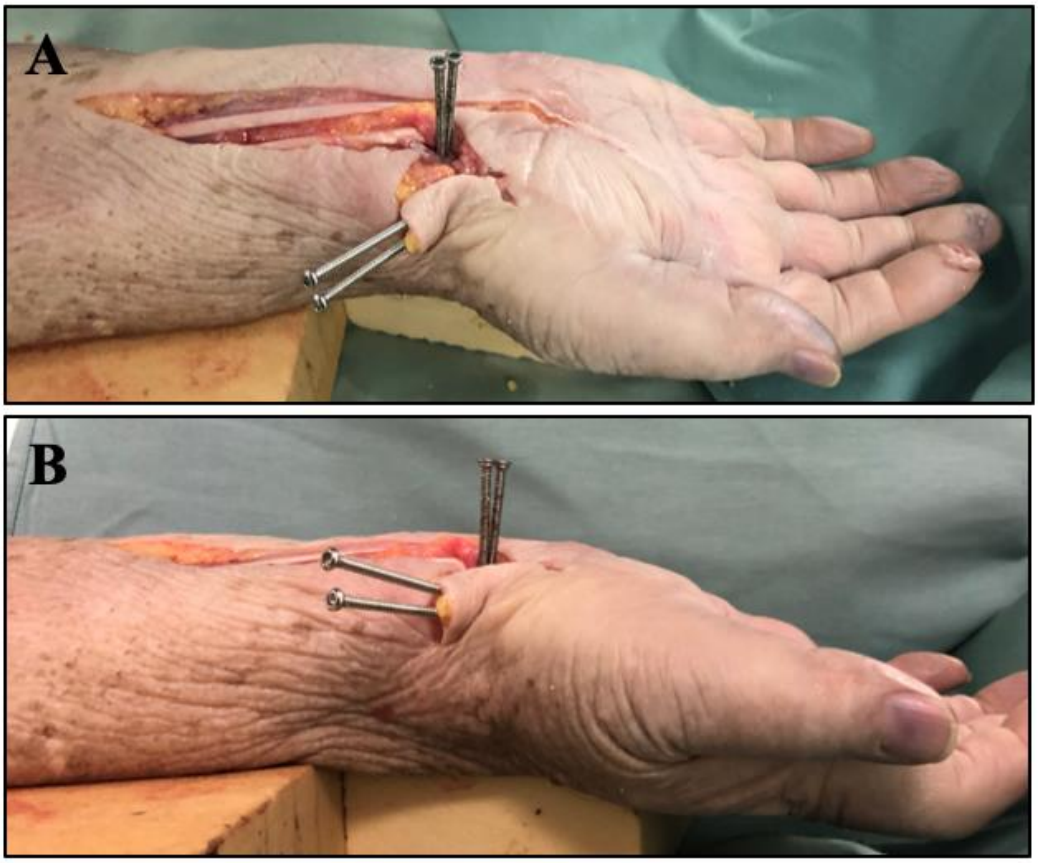

Figure 3.1: Volar Screw Placement for Optical Tracker Attachment. (**A**) Superior lateral picture demonstrating extended carpal tunnel approach with extended Wagner surgical approach with tracking screws in-situ located in the distal scaphoid tubercle & trapezium-trapezoid complex. **(B)** Lateral picture demonstrating tracking screw placement.

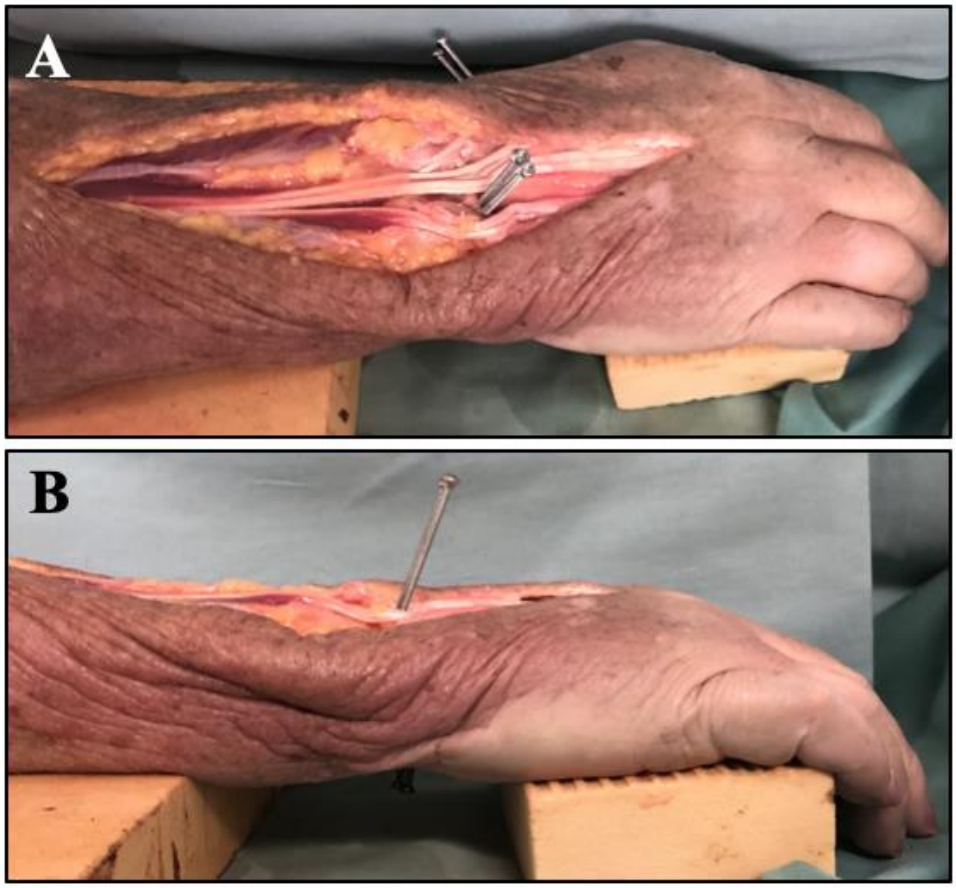

Figure 3.2: Dorsal Screw Placement for Optical Tracker Attachment. A Overhead picture demonstrating midline dorsal surgical approach tracking screws in-situ located in the lunate & trapezium-trapezoid complex. B Lateral picture demonstrating tracking screw placement with screws visible in the lunate.

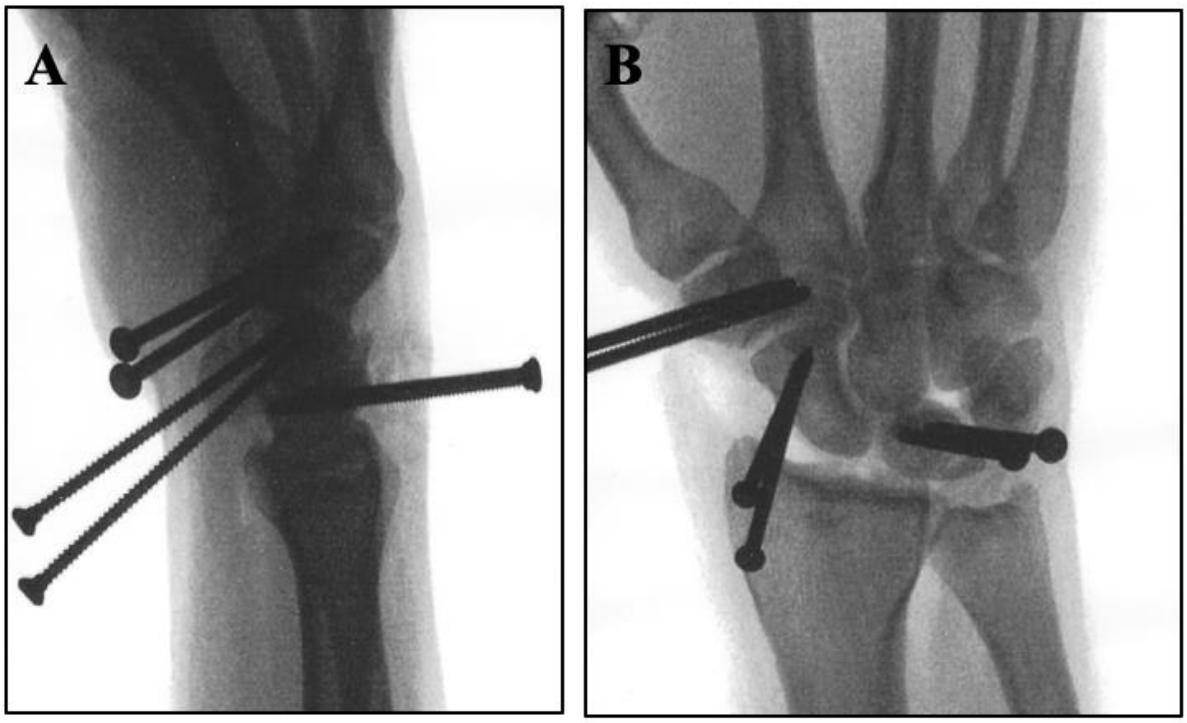

Figure 3.3: Radiographs Demonstrating Placement of Carpal Tracker Mounting Screws. A lateral radiograph demonstrating placement of carpal tracking screws in lunate, scaphoid, and trapezium-trapezoid complex B Anterior-posterior radiograph demonstrating same carpal tracker screw placement.

With all trackers placed, tendons were identified, and sutures were placed in the same method described in **Section 2.2.1.2**. Sutures were placed in the BB, PT, FCR, FCU, ECU, ECR, and ECRB. These sutures were placed at the distal extent of each tendon (taking care not to disrupt soft tissue structures overlying their insertions) and then fed through epicondyle blocks as previously demonstrated in **Figure** 2.4**.**

3.2.2 Testing Protocol

The specimen was then loaded into a custom wrist simulator. The arm was secured first using a humeral clamp then two Steinman pins were used to fix the shaft of the ulna to the support tower aligning the elbow at 90° flexion. The suture lines were tied to their corresponding SmartMotor at the base of the simulator platform as previously depicted in **Figure** 2.5 & **Figure** 2.6.

In order to facilitate feedback for closed loop control of each specimen, local coordinate systems were created for the radius, ulna and third metacarpal. With specimens loaded into the active motion simulator, bony anatomical landmarks of the radius, ulna, and third were identified and their position in space marked using an optical stylus. These points served as the basis for local coordinate systems that were then used as a basis for determining the position of the wrist in terms of flexion-extension. Neutral position was designated as the long axis of the third metacarpal coplanar to the long axis of the radius, as defined by the International Society of Biomechanics.[6] Tone loads were then applied to the biceps brachii and pronator teres suture cables of 45N in order to maintain neutral pronation-supination. In its native state, each specimen underwent five motion trials of planar flexion-extension. Motion was carried out at approximately 5°/sec and proceeded from 45° extension to 45° flexion. Motion data was calculated at 15Hz and later quantized to 5° increments for analysis. Data from the final 3 motion trials was averaged for later analysis. After each specimen was simulated in its native state, the progressive scaphoid malunion protocol was initiated.

The volar surgical incision and capsulotomy was opened, and the scaphoid was exposed. The specimen was extended, and the previously marked waist identified. From this waist, a wedge osteotomy was designed. The size of wedge resection varied from specimen to specimen and was based on measurements acquired from central sagittal images from pre-simulation CT scans (**Figure** 3.4). The width of the scaphoid waist was measured and the resultant height required to create a flexion deformity of 10° was determined using trigonometry.

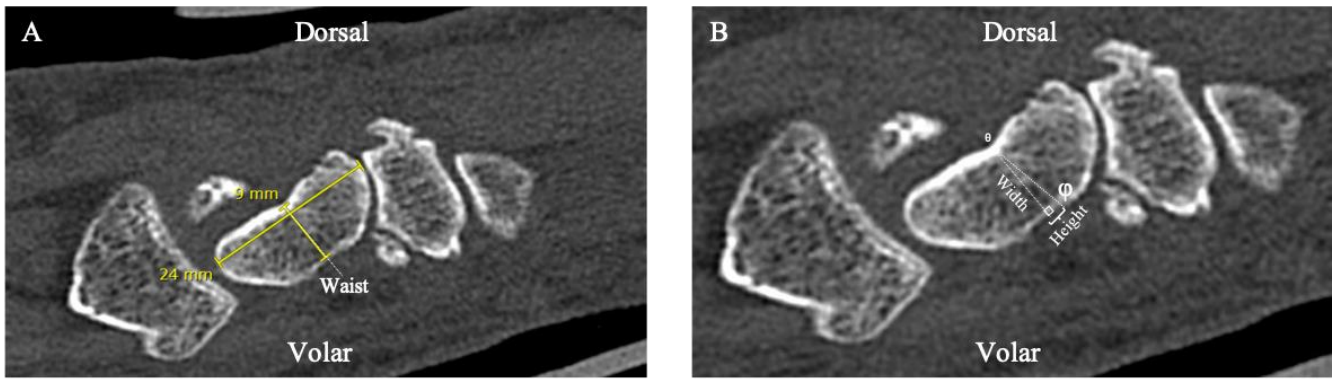

$$(1)\ \frac{\text{Width}}{\sin(\phi)} = \frac{\text{Height}}{\sin(\theta)} \rightarrow \frac{\sin(\theta)}{\sin(\phi)} \times \text{Width} = \text{Height}$$

$$(2)\ \theta + \phi + 90° = 180°$$

$$(2)\ \theta = 10°, \quad \therefore \phi = 180° - (90° + 10°) = 80°$$

$$(1\ \&\ 2)\ \frac{\sin(10°)}{\sin(80°)} \times 9mm = \text{Height} = \sim 1.5mm$$

256

257 **Figure 3.4 :Volar Wedge Size Calculation.** The pre-testing CTs were used to calculate the size
258 of volar wedge that needed to be resected to create the desired malunion deformity. With the
259 desired intrascaphoid angle known, as well as the width of the scaphoid waist the volar height
260 was calculated using Sine law as shown in equations 1 & 2. A Baseline measurement of scaphoid
261 for a central sagittal slice of pretesting CT. B schematic representation of volar wedge osteotomy
262 height calculation.

This measurement was then translated to the specimen and marked prior to carrying out each osteotomy. Bone was resected using a Hall oscillating saw (CONMED, Utica NY), taking care not to damage surround soft tissue structures or other carpal bones. With the osteotomy complete, it was verified that the proximal and distal pole were completely dissociated, and the fracture site was inspected to ensure it was free from debris. The wrist was then flexed, and the fracture reduced under direct visualization **(Figure** 3.5**)**. With the fracture reduced, two 0.45 Kirschner wires (K-Wires) were delivered retrograde from the distal pole to the proximal pole across the fracture site. The radiocarpal joint was then inspected to ensure there was no impingement from K-wires that were placed through the proximal pole. With the wrist capsule open, the specimen was taken through a full range of flexion-extension with the fracture site under direct observation to ensure the fracture site remained reduced and that there was no instability or gapping. Once adequate fixation had been achieved, the capsulotomy and soft tissues were repaired and simulation continued, assessing flexion-extension motion. The scaphoid was once again exposed through the volar incision to ensure fixation had been adequate and the proximal and distal poles were still reduced. If the fixation had failed, the fracture was re-reduced, k-wires were reoriented, and motion trials were restarted. If the scaphoid retained its reduction, further progressive osteotomies in a similar method were created to increased malunion severity. In total, 4 states were tested: native scaphoid topology, 10° malunion, 20° malunion, and scaphoid non-union (K-Wires removed). At the completion of testing each specimen was denuded and joints were dissected. The trackers were diligently protected throughout this process to ensure no movement relative to their respective bones occurred. With all individual bones exposed, landmarks on the studied bones (scaphoid, lunate, trapezium-trapezoid, radius, ulna, third metacarpal-capitate) were digitized using a stylus to be later co-registered with motion data for the assessment of contact in future work.

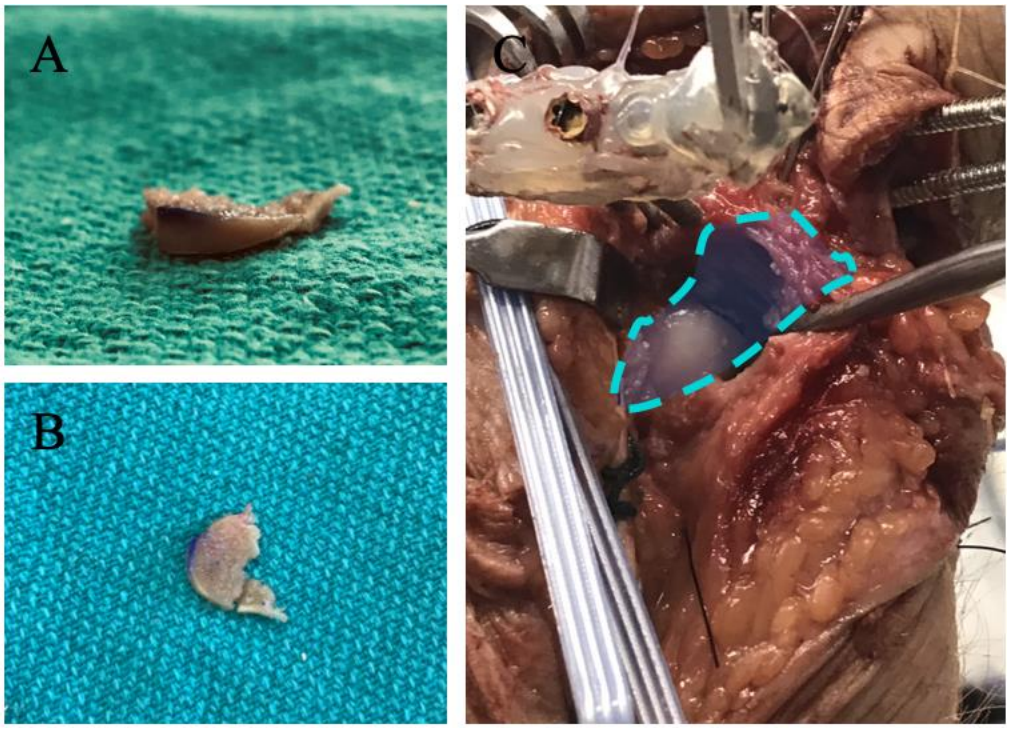

Figure 3.5: Osteotomy Wedge Resection and Resultant Reduction of Osteotomy Site using Kirshner Wires. (**A)** & (**B**) Resultant wedge osteotomy resected from volar aspect of scaphoid (**C)** Reduced fracture line fixated with 2 K-wires in-situ.

3.2.3 Outcome Variables and Statistical Approaches

The flexion and extension of the scaphoid, lunate, and trapezium-trapezoid was evaluated for flexion-extension relative to the distal radius during flexion-extension motion trials such that their motion paths could be compared across trials of differing malunion severity. Scapholunate intercarpal motion was calculated by taking the difference between the scaphoid and lunate motion in the flexion-extensions plane (**Figure** 3.6). Wrist angle was defined as the angle between the long axis of the third metacarpal and the long axis of the radius local coordinate system.

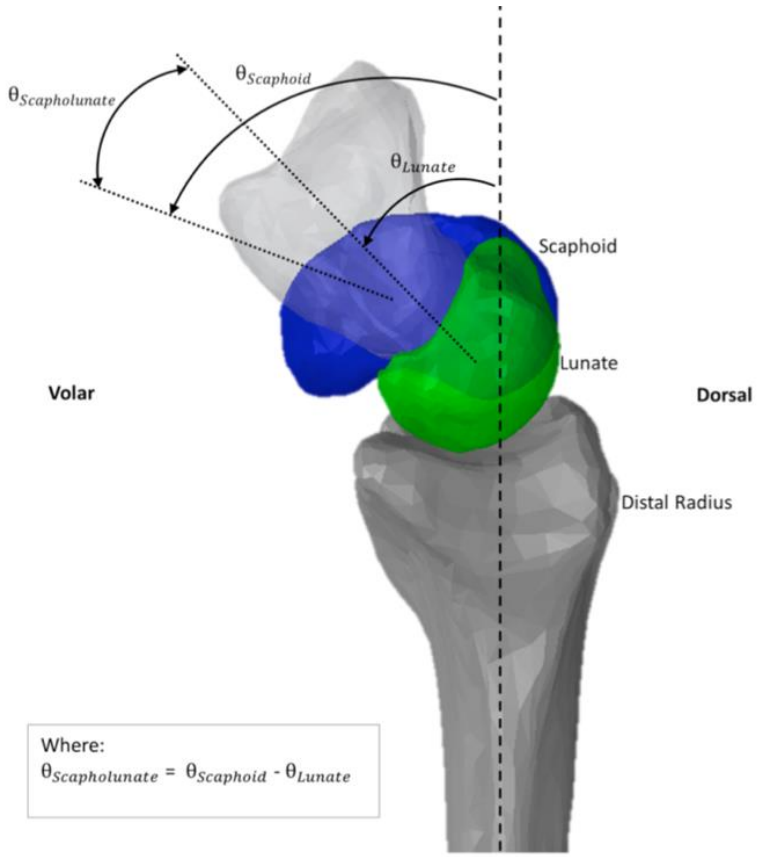

Figure 3.6: Pictorial Representation of Motion Measurements. Position of the lunate, Scaphoid, Trapezium-Trapezoid, and Scapholunate angle were measured during all motion trials. Trapezium-Trapezoid are not pictured here for clarity.

A 2-way repeated measures analysis of variance (RM-ANOVA) was performed using SPSS (SPSS 18, IBM, Armonk NY). The factors included: malunion severity (intact; 10°, 20°, non-union) and wrist motion angle (45° flexion to 45° extension, in 5° increments). Individual analyses were performed for the scaphoid, lunate, and trapezium-trapezoid during wrist flexion-extension. Statistical significance was set at $p<0.05$.

3.3 Results

3.3.1 Scaphoid Kinematics During Flexion-Extension

The motion of the scaphoid remained stable throughout all severities of scaphoid malunion and there was not statistically significant change in motion path compared to its native state ($p>0.05$). (**Figure** 3.7, **Figure** 3.8). During the non-union motion trial, the angular position of the scaphoid had a statistically different angular position compared to the intact state (mean dif. =5.7° ± 3.2, $p=0.04$). Scaphoid motion remained associated with wrist motion during both motion paths during these trials. Flexion-extension non-union $R_2 = 0.99$, extension-flexion non-union $R_2 = 0.99$.

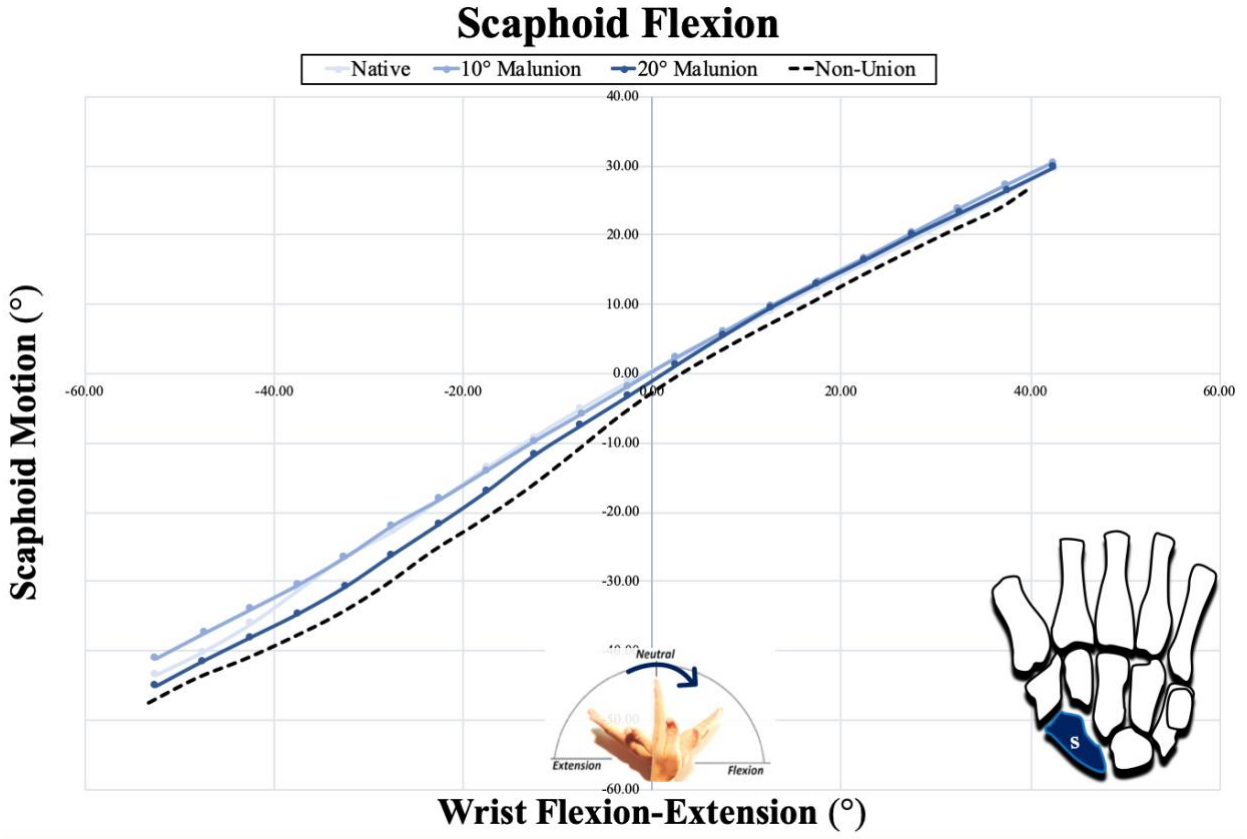

Figure 3.7: Scaphoid Flexion-Extension During Progressive Malunion Severity in During Wrist Extension-Flexion Motion Path. With progressive scaphoid malunion deformity, the motion path of the scaphoid remained unchanged compared to native ($p>0.05$). In the case of scaphoid non-union there was a significant change in motion path compared to the native scaphoid ($p<0.05$).

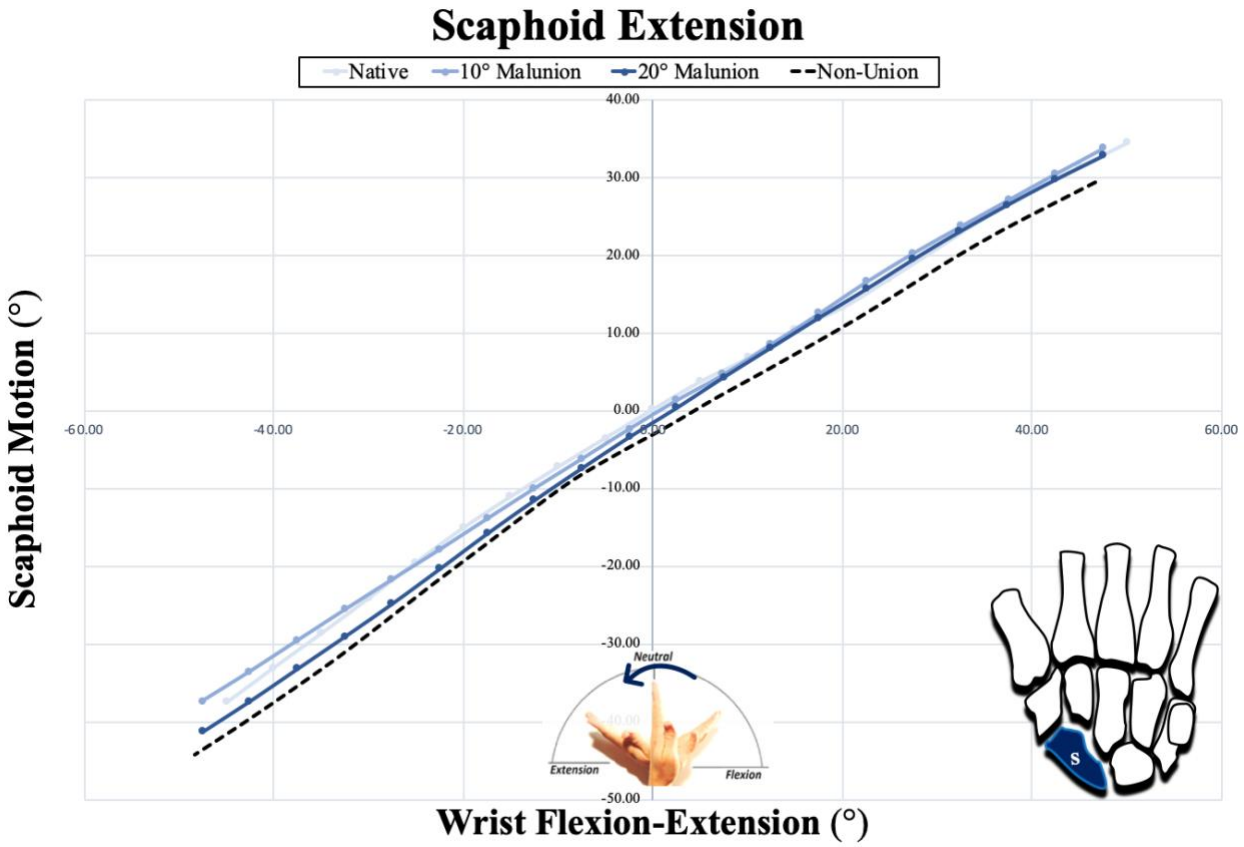

Figure 3.8: Scaphoid Extension-Flexion During Progressive Malunion Severity in During Wrist Flexion-Extension Motion Path. Similar to the extension-flexion motion path, there were no noted changes in scaphoid motion path with progressive scaphoid malunion.

3.3.2 Lunate Kinematics During Flexion-Extension

During malunion trials, there were significant changes in motion of the lunate (**Figure** 3.9, **Figure** 3.10). For progressive degrees of malunion severity, the posture of the lunate became increasingly extended compared to its position in the native wrist (native – 10° malunion: mean dif. = 7.1° ± 1.6, $p<0.05$; native – 20° malunion: mean dif. = 11.2° ± 2.0, $p<0.05$) (**Figure** 3.11).

During the scaphoid non-union trials, the lunate was significantly more extended compared to its position in the native wrist (native – non-union: mean dif. = 13.8° ± 3.7, $p<0.05$).

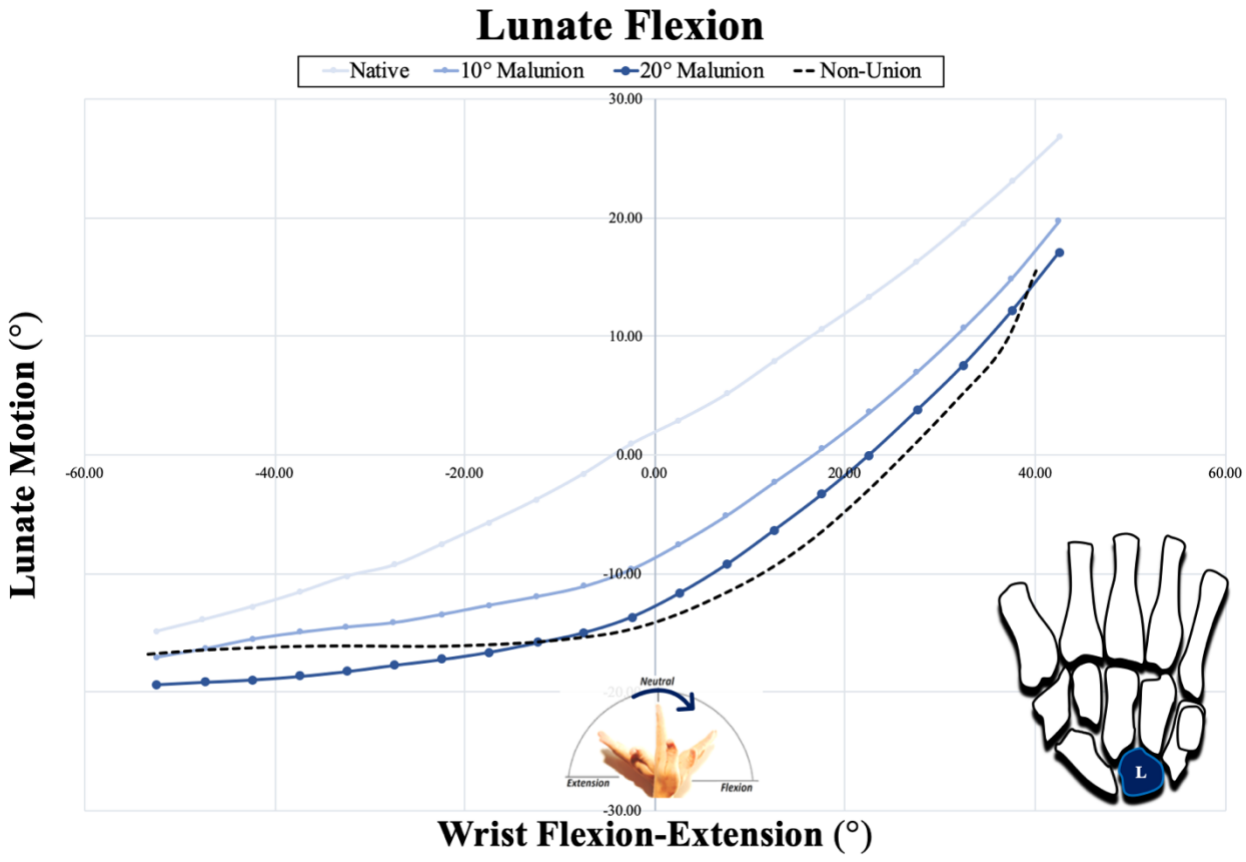

Figure 3.9: Lunate Flexion-Extension During Progressive Malunion Severity in During Wrist Extension-Flexion Motion Path. With progressive malunion, the lunate began to demonstrate increasing extension for all wrist positions.

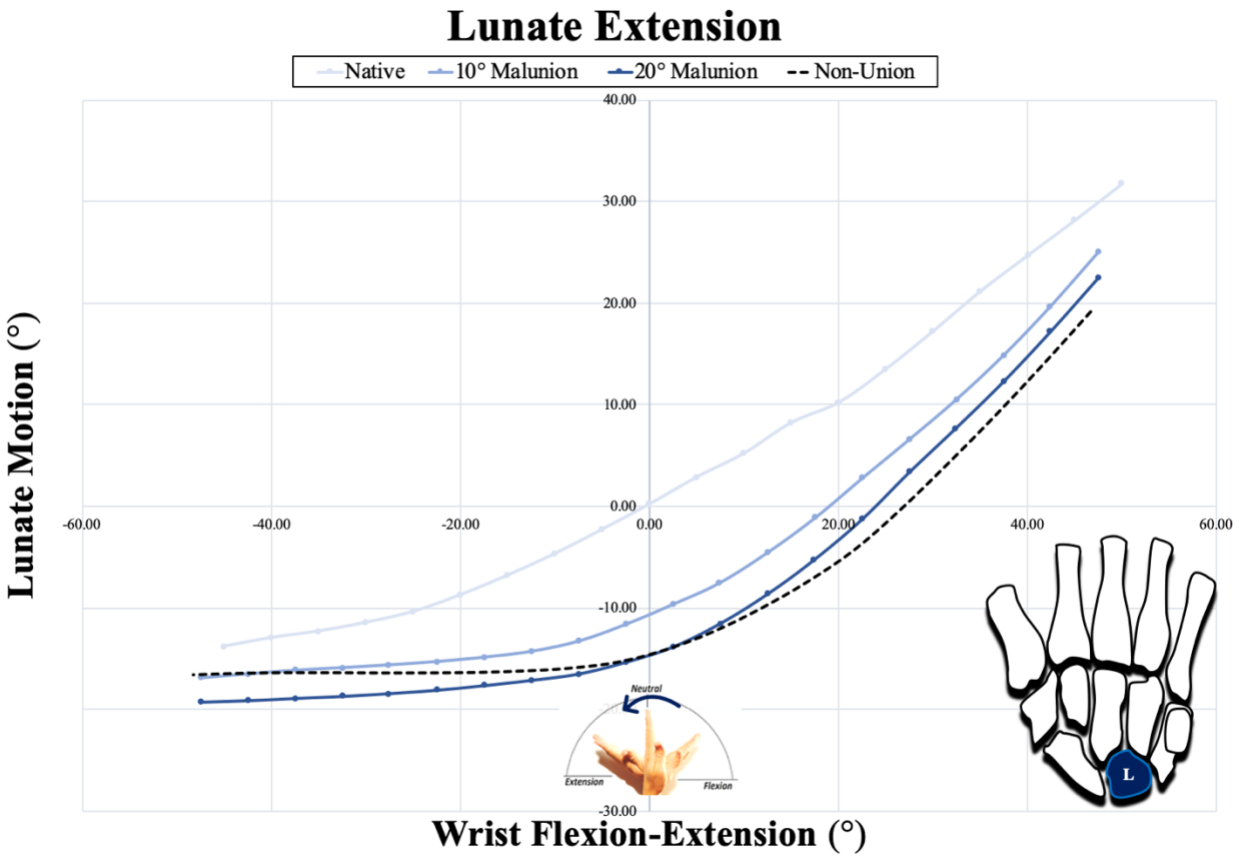

340

341 **Figure 3.10: Lunate Extension-Flexion During Progressive Malunion Severity in During**
342 **Wrist Extension-Flexion Motion Path**. During progressive malunion the lunate's motion
343 became progressively extended for all wrist positions.

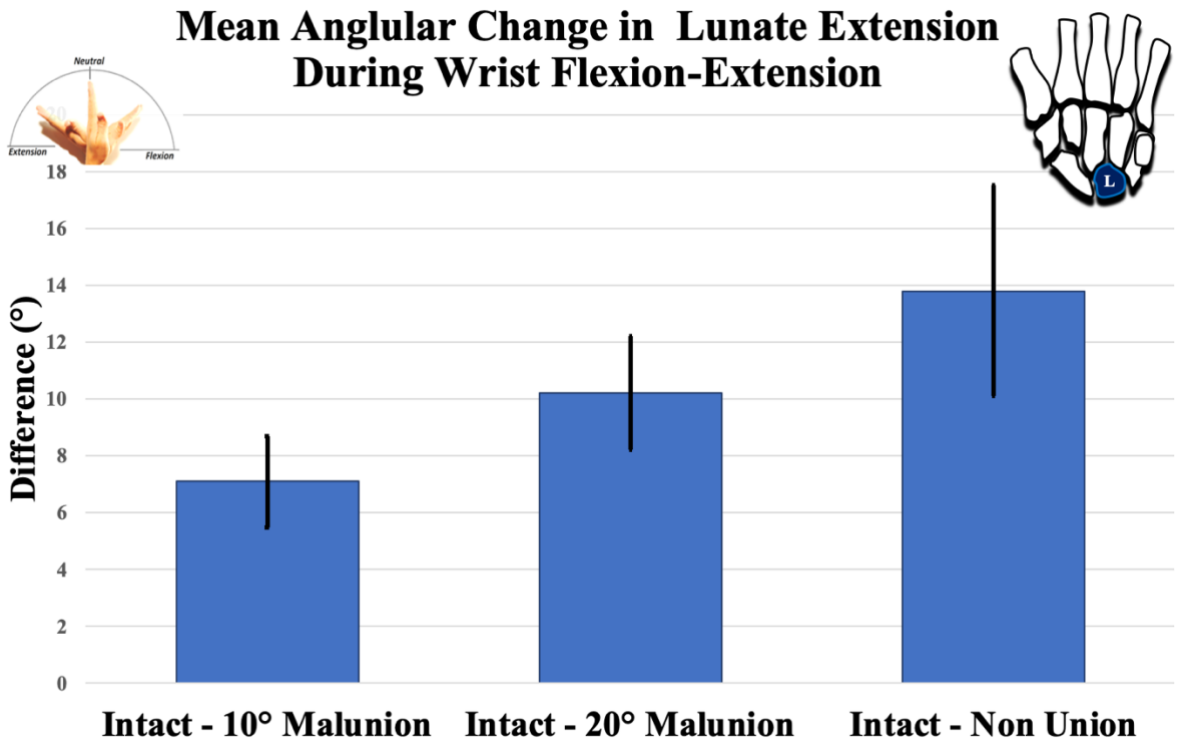

Figure 3.11: Mean Angular Change in Lunate Motion for Planar Wrist Flexion-Extension.

Mean Angular change (± 1 SD) of lunate position compared to intact state for each progressive malunion severity.

3.3.3 Trapezium-Trapezoid Kinematics During Flexion-Extension

During all trials for both motion paths there was no significant difference in trapezium-trapezoid motion for all severities of scaphoid malunion or scaphoid non-union (**Figure** 3.12**, Figure** 3.13).

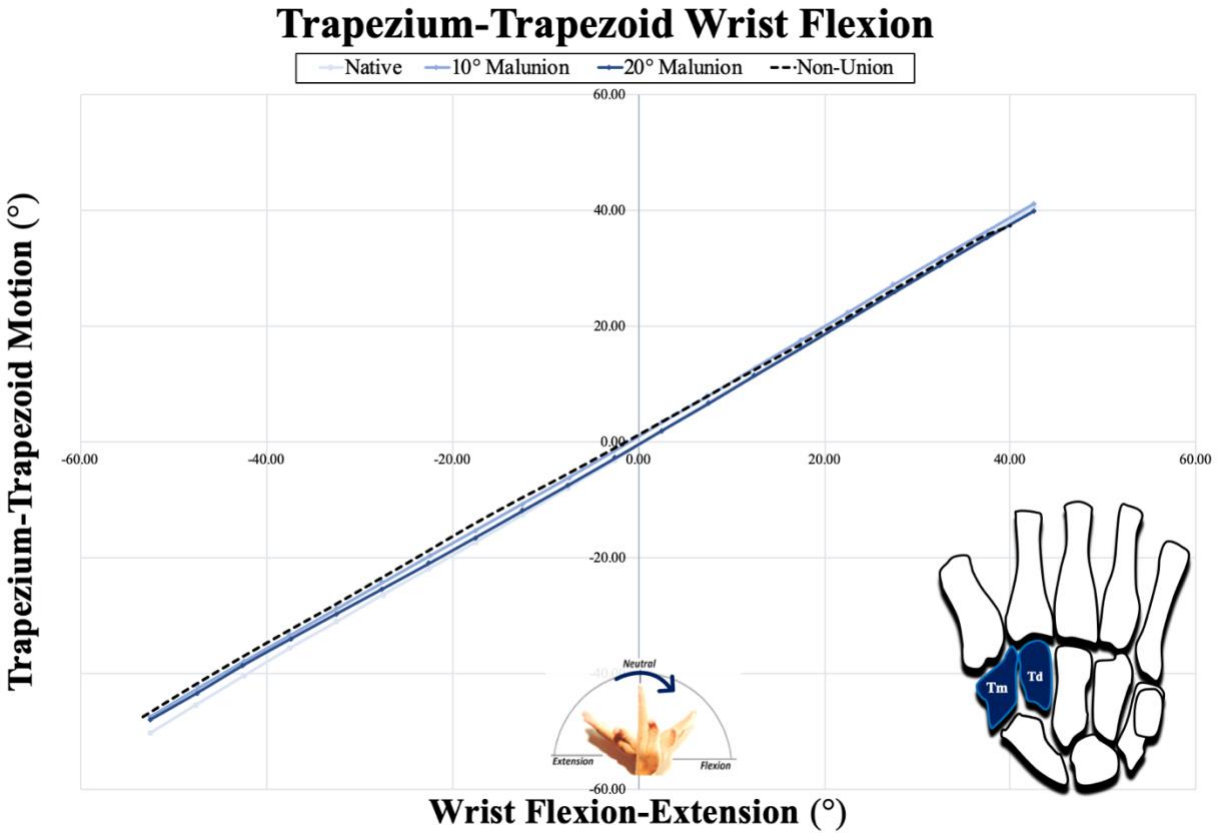

Figure 3.12: Trapezoid-Trapezium Flexion-Extension During Progressive Malunion Severity in During Wrist Extension-Flexion Motion Path. There were no statistically significant differences in trapezium-trapezoid motion paths for all severities of malunion, as well as scaphoid non-union.

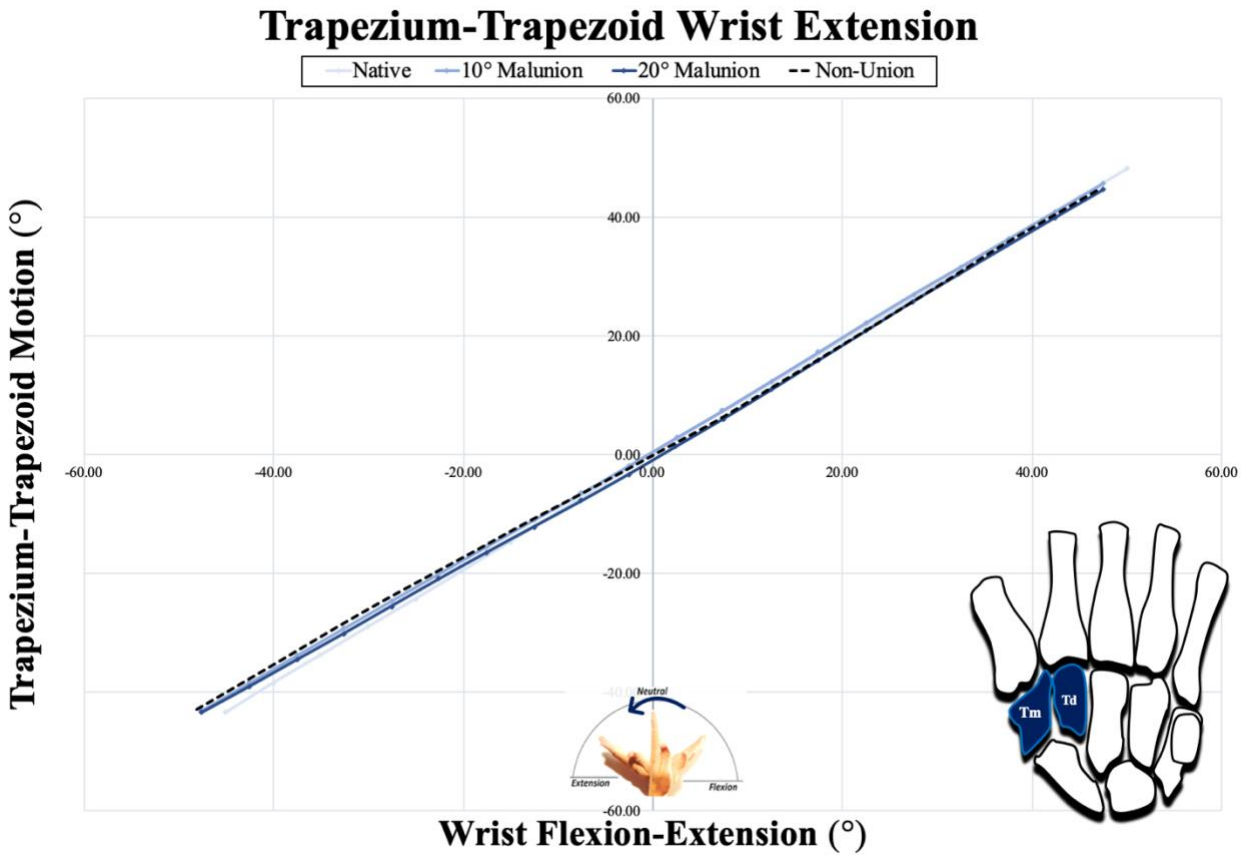

360

361 **Figure 3.13: Trapezoid-Trapezium Extension-Flexion During Progressive Malunion**
362 **Severity in During Wrist Flexion-Extension Motion Path.** Similar to the extension-flexion
363 motion path, there were no statistically significant differences in trapezium-trapezoid motion
364 paths for all treatment protocols.

3.3.4 Scaphoid-Lunate Intercarpal Motion During Flexion-Extension

The SLA demonstrated a statistically significant increase with increasing scaphoid malunion severity (**Figure** 3.14, **Figure** 3.15). The scaphoid became more flexed relative to the lunate with more significant deformities: native – 10° malunion: mean dif. = 6.2° ± 4.0, $p<0.05$; native – 20° malunion: mean dif. = 11.4° ± 6.1, $p<0.05$). As well, there was also a noted change for scaphoid non-union (mean dif. = 6.5° ± 4.1, $p<0.05$) (**Figure** 3.16).

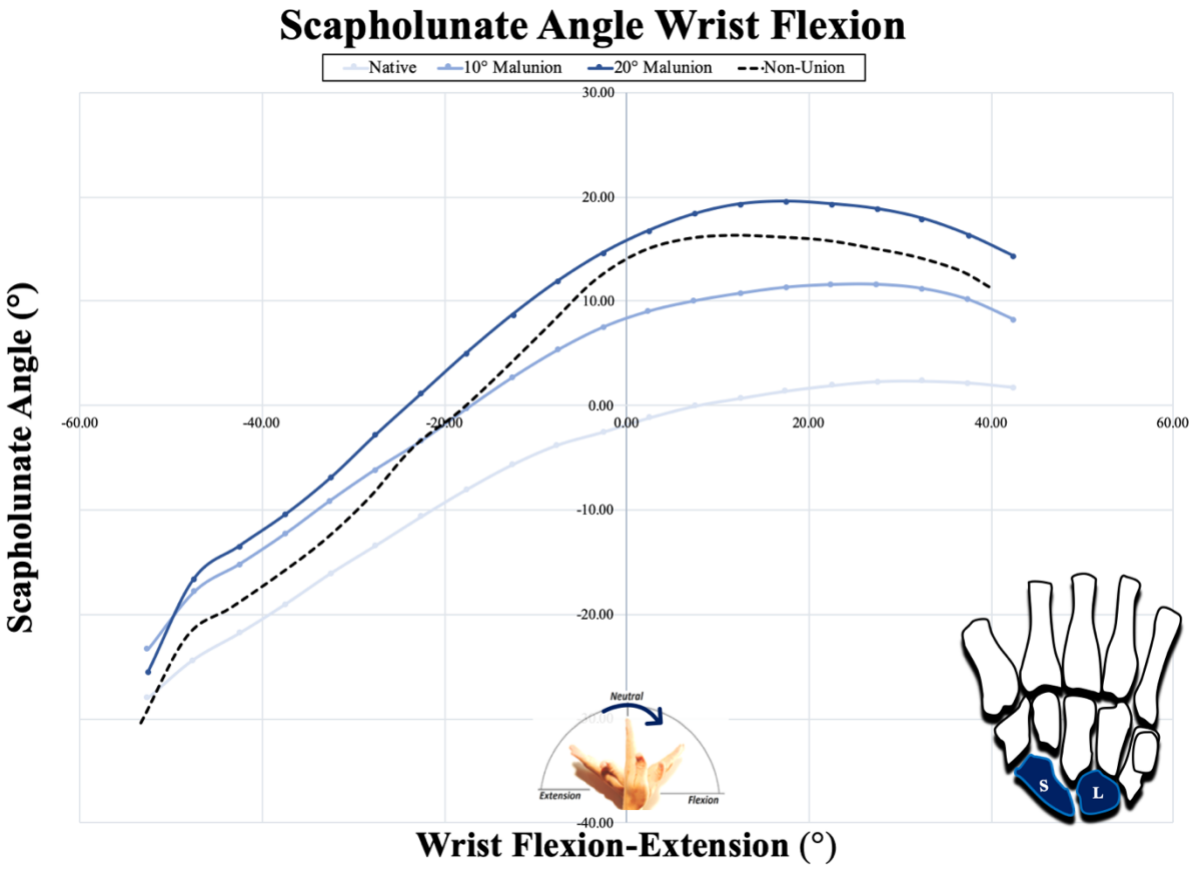

Figure 3.14: Scapholunate Angle During Progressive Malunion Severity in During Wrist Flexion-Extension Motion Path. During wrist flexion-extension, the scapholunate angle increased linearly with wrist flexion until the neutral position after which there was little change in scapholunate angle and in some cases, there was a decrease. With increasing scaphoid malunion, there was a statistically significant increase in scapholunate angle ($p<0.05$).

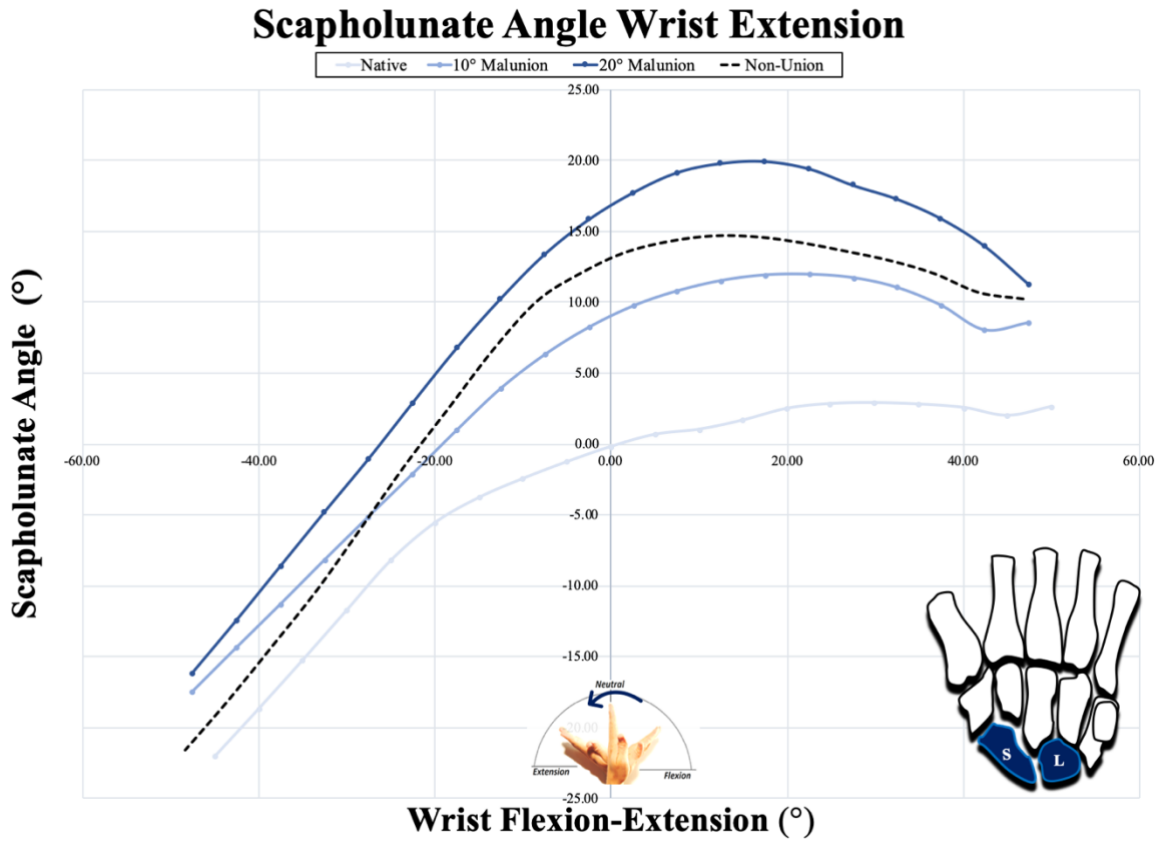

378

379 **Figure 3.15: Scapholunate Angle During Progressive Malunion Severity in During Wrist**
380 **Extension-Flexion Motion Path.** The scapholunate angle followed a similar motion path during
381 wrist extension-flexion comparing to flexion-extension with two common patterns of motion.
382 With increasing scaphoid malunion, there was a statistically significant increase in scapholunate
383 angle ($p<0.05$)

384

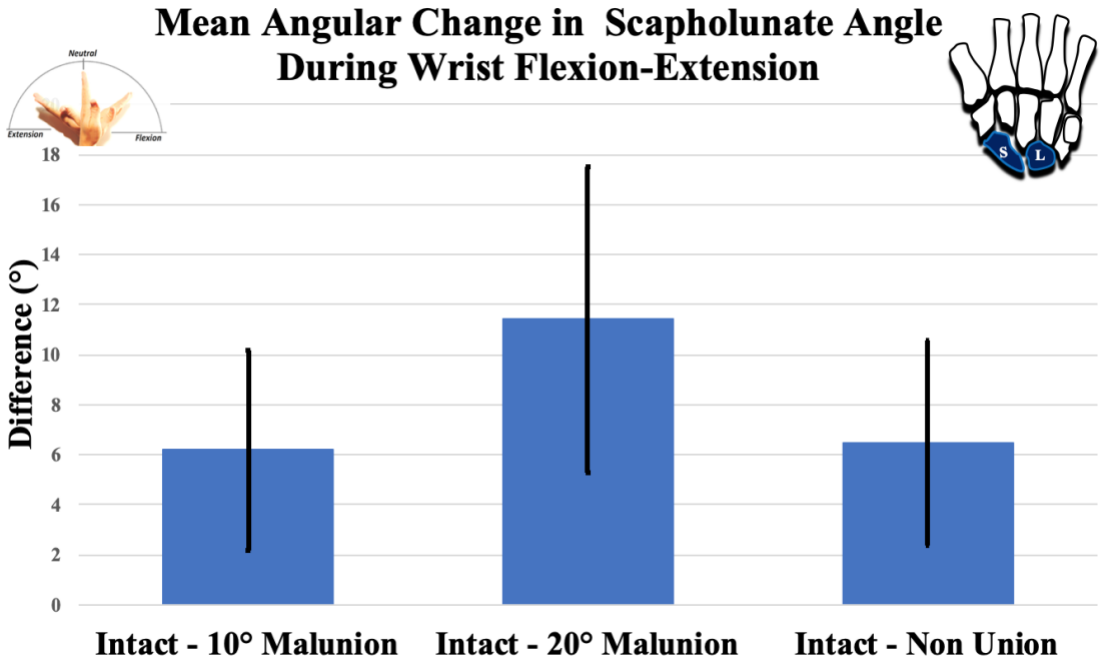

385

386 **Figure 3.16: Mean Angular Change of Scapholunate Angle for Wrist Flexion-Extension.**
387 Mean Angular change (± 1 SD) of scapholunate angle position compared to intact state for each
388 progressive malunion severity. There was also a significant change in SLA for non-union
389 compared to the native scaphoid state although the difference was less compared to 20 °
390 malunion.

3.4 Discussion

The motion of the wrist has been investigated by many but the delicate interactions that occur between the osseous and soft tissue components has yet to be fully elucidated. There is a relative paucity of ligamentous support in the wrist compared to other joints, implying the associations of the carpal bones themselves may be particularly important. From existing studies, it is known that the motion that each carpal bone undergoes as well as its relationship to its surrounding carpal bones may vary from patient to patient and that changes to native anatomy can have significant effects. There have been a number of investigators who have attempted to determine these relationships, as well as numerous theories that attempt to explain carpal motion. A common theme in many theories is the importance of the scaphoid. It is generally agreed that the scaphoid plays an important role in the coordination between the motion of the distal and proximal carpal row due to its position bridging these two groups. The theories of wrist motion have been previously discussed in **Section** Error! Reference source not found.; in each case the scaphoid serves to translate motion from the distal row which is directly impacted by tendinous forces to the intercalated proximal row which is free from tendinous insertions.[1]

When the link provided by the scaphoid is totally disrupted, as is the case of scaphoid non-union or scapholunate ligament disruption, motion is significantly altered and the wrist becomes unstable leading to post-traumatic arthrosis (SNAC and SLAC wrist, respectively). The importance of alterations to native scaphoid morphology with a maintained link, as is the case in scaphoid malunion, is less clear. To date there has been only a single study published investigating the biomechanics of the malunited scaphoid wrist. Burgess demonstrated that increasing scaphoid malunion may be associated with decreased wrist extension of motion based on a small number of cadaveric specimens but did not quantify the motion of other carpal bones in relation to this change.[40]

Clinically, authors have published reports detailing patients with scaphoid malunion manifesting clinically with pain, reduced range of motion, and limited wrist strength. It is unclear the exact pathomechanics causing these symptoms, but it has been hypothesized they may be the result of secondary carpal mal-positioning caused by scaphoid malunion. Kim et el. reported a relationship between a dorsal intercalated segment instability (DISI) deformity and scaphoid

malunion severity and noted that patients with a H/L exceeding 0.73 were at high risk for the development of a DISI deformity.[56] Meagerle et al. published similar results and observed that scaphoid malunion was associated with increasing radio-lunate angle (RLA) and patients with larger RLAs had poorer outcomes.[49] It was hypothesized by Megerle that the extended position of the lunate was a direct consequence of altered scaphoid morphology. With ligamentous injuries between the scaphoid and lunate being uncommon in the setting of scaphoid fracture, it is believed that the rotational position of the lunate represents an angular change in the position of the proximal pole of the scaphoid.[49] Following scaphoid fracture, the distal pole tends to flex, and when this fragment reunites with the proximal pole and is brought back to a neutral position, the proximal fragment must rotate in an extended relative to its native state. This rotation is then translated to the lunate through the stout SL ligament, forcing the lunate into an extended position. This manifests as an increase in RLA and resultant DISI deformity which may in turn may make the carpus unstable causing secondary sequelae.

The hypothesis that scaphoid malunion causes progressive extension of the lunate is congruent with the results of this cadaveric biomechanical investigation. Although increasing scaphoid malunion severity did not significantly alter the motion path of the scaphoid, capitate, or trapezium-trapezoid complex, it was observed that increasing malunion altered the posture of the lunate causing extension in all wrist positions. This change in lunate posture is observed in other wrist pathologies such as SLAC and SNAC wrist and is thought to be the basis of eventual arthrosis. Although the change in lunate position may arise from different pathomechanics, this change may represent an important common pathway for carpal instability. A second finding was a change in SLA with progressive scaphoid malunion. As the distal pole of the scaphoid was progressively flexed, the angle between the lunate and scaphoid also increased. The scaphoid plays a primary role in dictating the position and angular rotation of the lunate throughout wrist motion and it is possible that by altering this relationship the lunate may be further destabilized. The link between the scaphoid and lunate, as well as the relative positioning of these bones varies between patients,[1] which may explain why some patients with scaphoid malunion develop limitations in wrist motion, whereas others are clinically asymptomatic.

To verify the validity of our malunion model, simulations were also carried out with a non-union scaphoid model. In each case, the motion path of the malunited scaphoid was significantly different than non-union state. The lunate's motion path in particular was altered with a distinct pattern of motion unique from both the native and malunited states ($p<0.05$). With an alteration to scaphoid morphology, the transfer of the motion from the distal row to the proximal row becomes alterted, and possibly the lunate was destabilized, and its movement primarily influenced by its ligamentous attachments through the triquetrum and trapezoid. The motion of the triquetrum and trapezoid was not recorded in this investigation, so it is not possible to prove this theory.

As with any biomechanical investigation, there are limitations related to the model of pathology, biomechanical simulation, and other factors. The model of scaphoid malunion was intentionally simplified in order to maintain reproducibility between studies. We attempted to create malunions in a single rotational plane of motion although in reality the humpback deformity is a complex morphological change. The model was also subject to human error, as the osteotomies were created without a guide. The motion path of the wrist was simplified to increase inter-specimen reproducibility when in reality wrist motion is multiplanar. In addition, the wrist was only simulated in a gravity loaded positions. It is known that the topology of the carpal bones is influenced by the magnitude of force transmitted through it and different levels of loading may have accentuated or diminished the magnitude of our findings. The tracker placement only captured the motion of the scaphoid, lunate, capitate, and the fused trapezium-trapezoid. Although it is believed that the trapezium-trapezoid has little impact on total wrist motion, this is a non-physiologic state of the wrist. Finally, the results of this work are based on the assumption that the fixation of the scaphoid malunion osteotomy with k-wires was rigid throughout wrist motion simulation. Although the fracture line position was verified both before and after simulation, it is possible that motion at the fracture side occurred.

This study has strengths despite the limitations of a cadaveric study. We were able to achieve a large range of motion (45° extension - 45° flexion) which exceeds that of other reports studying wrist kinematics that were only able to achieve 30°. This motion was carried out in a highly reproducible motion path due to the closed loop control feedback of our simulator and was also facilitated by an active motion protocol to facilitate *in-vitro* motion. All soft tissues were

preserved with diligent surgical technique and repairs, and all incisions were closed for simulations. The optical tracking recorded high fidelity data that was highly accurate to determines the position and velocity of various bones of interest.

3.5 Conclusion

In this *in-vitro* model of scaphoid malunion increasing scaphoid malunion deformity was associated with progressive extension of the lunate in all wrist positions and also resulted in altered motion between the scaphoid and lunate in this cadaveric biomechanical investigation. This work gives insight into alterations in motion that may occur in the scaphoid malunited wrist and serves to generate targets of future investigation to determine the clinical significance of this injury. Future directions would include clinical investigations assessing for degenerative changes around the lunate or potentially carrying out further modelling of scaphoid malunited wrists with a particularly focus on secondary changes to lunate joint contact.

3.6 References

1. Hirt B, Seyhan H, Wagner and M. *Hand and Wrist Anatomy and Biomechanics : A Comprehensive Guide*.; 2016. doi:4718699

2. Gray H. Anatomy of the Human Body. *Am J Med Sci*. 1919;157(5):704. doi:10.1097/00000441-191905000-00011

3. Wolfe SW (Weill MCU, Hotchkiss RN (Weill MCU, Pederson WC (University of THSCSATHC of SA, Kozin SH (Shriners H for CTUS of M. *Green's Operative Hand Surgery*. 6th ed. (Green DP, ed.). Philadelphia, PA: Elsevier; 2011.

4. Feipel V, Rooze M. The capsular ligaments of the wrist: Morphology, morphometry and clinical applications. *Surg Radiol Anat*. 1999;21(3):175-180. doi:10.1007/BF01630897

5. Hanse J, Saunders JB. *Netters Clinical Anatomy*. 2nd ed.; 2010.

6. Wu G, Van Der Helm FCT, Veeger HEJ, et al. ISB recommendation on definitions of joint coordinate systems of various joints for the reporting of human joint motion - Part II: Shoulder, elbow, wrist and hand. *J Biomech*. 2005;38(5):981-992. doi:10.1016/j.jbiomech.2004.05.042

7. Craigen MAC, Stanley JK. WRIST Row , column or both ? *J Hand Surg Br Eur Vol*. 1995;20(Fig 2):165-170.

8. Garcia-Elias M. Understanding Wrist Mechanics: A Long and Winding Road. *J Wrist Surg*. 2013;02(01):005-012. doi:10.1055/s-0032-1333429

9. Johnston H. Varying positions of the carpal bones in the different movements al the wrist PART II. *J Anat Physiol*. 1907;4:280-292.

10. Navarro A. Anatomy and physiology of the carpus [in Spanish]. *Imprenta Artist Dornaleche Hnos*. 1935:166-189.

11. Taleisnik J. The Ligaments of the Wrist. *J Hand Surg Am*. 1976;1(2):110-118.

12. Lichtman DM, Schneider JR, Swafford AR, Mack GR. Ulnar midcarpal instability—Clinical and laboratory analysis. *J Hand Surg Am*. 1981;6(5):515-523. doi:10.1016/S0363-5023(81)80115-3

13. Dunning C, CS L, RT B, PattersonSD, JA J, GJ K. Supplemental pinning improves the stability of external fixation in distal radius fractures during simulated finger and forearm motion. *J Hand Surg Am*. 1999;24(5):992-1000.

14. Werner FW, Palmer AK, Somerset JH, et al. Wrist Joint Motion Simulator. *J Bone Jt Surg*. 1996;14(6):639-646.

15. Iglesias DJ. Development of an in-vitro passive and active motion Simulator for the investigation of wrist function and Kinematics. 2015.

16. Rikli DA, Honigmann P, Babst R, Cristalli A, Morlock MM, Mittlmeier T. Intra-Articular Pressure Measurement in the Radioulnocarpal Joint Using a Novel Sensor: In Vitro and In Vivo Results. *J Hand Surg Am*. 2007;32(1):67-75. doi:10.1016/j.jhsa.2006.10.007

17. W GW, H BR, C. L. Mechanism of wrist joint with special reference to fractures of the scaphoid. *Guys Hosp Rep*. 1943;92:52–59.

18. Landsmeer J. Studies in the anatomy of articulation. I. The equilibrium of the "intercalated" bone. *Acta Morphol Neerl Scand*. 1961;3:287-303.

19. Fisk G. The wrist. Review article. *J Bone Joint Surg Br*. 1984:396-407.

20. JM K. The interdependence of carpal articulation chains. *Acta Anat*. 1974;88:481-501.

21. Stormont TJ, An KN, Morrey BF, Chao EY. Elbow joint contact study: Comparison of techniques. *J Biomech*. 1985;18(5):329-336. doi:10.1016/0021-9290(85)90288-X

22. Pogue DJ, SF V, RM P, et al. Effects of distal radius fracture malunion on wrist joint mechanics. *J Hand Surg Am*. 1990;15(5):721-727.

23. Nishiwaki M, T N, T N, Y T, Ikegami H. Ulnar-shortening effect on distal radioulnar joint pressure: a biomechanical study. *J Hand Surg Am*. 2008;33(2):198-205.

24. Wan L, Deasla R, Rubash H, Li G. Determination of in-vivo articular cartilage contact areas of human talocrural joint under weightbearing conditions. *Osteoarthr Cartil*. 2006;14(12):1294-1301.

25. GE M, DH L, C D, S A, CM G, Crisco JJ. Estimating Joint Contact Areas and Ligament Lengths From Bone Kinematics and Surfaces. *IEEE Trans Biomed Eng*. 2004;51(5):770-779.

26. Sendher R, Ladd AL. The Scaphoid. *Orthop Clin North Am*. 2013;44(1):107-120. doi:10.1016/j.ocl.2012.09.003

27. Herbert J, Fisher E. Management of the fractured scaphoid using a new bone screw. *J Bone Jt Surg*. 1984;66(1):114-123.

28. Cooney W, Dobyns J, Linscheid R. Fractures of the scaphoid: a rational approach to management. *Clin Orthop*. 1980;149(149):90-97.

29. Russe O. Fractures of the Carpal Navicular. *J Bone Jt Surg*. 1960;42(5):759-768.

30. Ten Berg P, Drijkoningen T, Strackee S, Buijze G. Classifications of Acute Scaphoid Fractures: A Systematic Literature Review. *J Wrist Surg*. 2016;05(02):152-159. doi:10.1055/s-0036-1571280

31. Cooney WP. *The Wrist: Diagnosis and Operative Technique*. St.Louis; 1998.

32. Russe O. Fracture of the Carpal Navicular: Diagnosis, Non-operative Treatment, and Operative Treatment. *J Bone Jt Surg*. 1960;42(5):759–768.

33. Forward DP, Singh HP, Dawson S, Davis TRC. the Clinical Outcome of Scaphoid Fracture Mal Union At 1 Year. *Hand, The*. 2009:40-46.

34. Lee CH, Lee KH, Lee BG, Kim DY, Choi WS. Clinical outcome of scaphoid malunion as a result of scaphoid fracture nonunion surgical treatment: A 5-year minimum follow-up study. *Orthop Traumatol Surg Res*. 2015;101(3):359-363. doi:10.1016/j.otsr.2014.09.026

35. Amadio PC, Berquist TH, Smith DK, Ilstrup DM, Cooney WP, Linscheid RL. Scaphoid

malunion. *J Hand Surg Am*. 1989;14(4):679-687. doi:10.1016/0363-5023(89)90191-3

36. Jiranek WA, Ruby LK, Millender LB, Bankoff MS, Newberg AH. Long-term results after Russe bone-grafting: The effect of malunion of the scaphoid. *J Bone Jt Surg - Ser A*. 1992;74(8):1217-1228. doi:10.2106/00004623-199274080-00012

37. Bain GI, Bennett JD, MacDermid JC, Slethaug GP, Richards RS, Roth JH. Measurement of the scaphoid humpback deformity using longitudinal computed tomography: Intra- and interobserver variability using various measurement techniques. *J Hand Surg Am*. 1998;23(1):76-81. doi:10.1016/S0363-5023(98)80093-2

38. Singh HP, Forward D, Davis TRC, Dawson JS, Oni JA, Downing ND. Partial union of acute scaphoid fractures. *J Hand Surg Am*. 2005;30(5):440-445. doi:10.1016/j.jhsb.2005.05.007

39. Mathoulin CL, Arianni M. Treatment of the scaphoid humpback deformity – is correction of the dorsal intercalated segment instability deformity critical? *J Hand Surg Eur Vol*. 2018;43(1):13-23. doi:10.1177/1753193417739526

40. Burgess RC. The effect of a simulated scaphoid malunion on wrist motion. *J Hand Surg Am*. 1987;12(5):774-776. doi:10.1016/S0363-5023(87)80067-9

41. Birchard D, Pichora D. Experimental corrective scaphoid osteotomy for scaphoid malunion with abnormal wrist mechanics. *J Hand Surg Am*. 1990;15(6):863-868. doi:10.1016/0363-5023(90)90004-B

42. Lynch NM, Linscheid RL. Corrective osteotomy for scaphoid malunion: technique and long-term follow-up evaluation. *J Hand Surg Am*. 1997;22(1):35-43. doi:10.1016/S0363-5023(05)80177-7

43. T N. Scaphoid Malunion. *J Bone Jt Surg*. 1991;73(1):134-137.

44. Fernandez DL. A technique for anterior wedge-shaped grafts for scaphoid nonunions with carpal instability. *J Hand Surg Am*. 1984;9(5):733-737. doi:10.1016/S0363-5023(84)80025-8

45. El-Karef EA. Corrective osteotomy for symptomatic scaphoid malunion. *Injury*. 2005;36(12):1440-1448. doi:10.1016/j.injury.2005.09.003

46. Gillette BP, Amadio PC, Kakar S. Long-Term Outcomes of Scaphoid Malunion. *Hand*. 2017;12(1):26-30. doi:10.1177/1558944716643295

47. Inoue G, Sakuma M. The natural history of scaphoid non-union Radiographical and clinical analysis in 102 cases. *Arch Orthop Trauma Surg*. 1996;115(1):1-4. doi:10.1007/BF00453208

48. Buijze GA, Goslings JC, Rhemrev SJ, et al. Cast immobilization with and without immobilization of the thumb for nondisplaced and minimally displaced scaphoid waist fractures: A multicenter, randomized, controlled trial. *J Hand Surg Am*. 2014;39(4):621-627. doi:10.1016/j.jhsa.2013.12.039

49. Megerle K, Harenberg PS, Germann G, Hellmich S. Scaphoid morphology and clinical outcomes in scaphoid reconstructions. *Injury*. 2012;43(3):306-310. doi:10.1016/j.injury.2011.08.015

50. Afshar A, Mohammadi A, Zohrabi K, Navaeifar N, Sami SH, Taleb H. Correlation of Reconstructed Scaphoid Morphology with Clinical Outcomes. *Arch bone Jt Surg*. 2015;3(4):244-249. http://www.pubmedcentral.nih.gov/articlerender.fcgi?artid=4628629&tool=pmcentrez&rendertype=abstract.

51. Lalone EA, Willing RT, Shannon HL, King GJW, Johnson JA. Accuracy assessment of 3D bone reconstructions using CT: An intro comparison. *Med Eng Phys*. 2015;37(8):729-738. doi:10.1016/j.medengphy.2015.04.010

52. Lalone EA, Grewal R, King GW, MacDermid JC. Evaluation of an Image-Based Tool to Examine the Effect of Fracture Alignment and Joint Congruency on Outcomes after Wrist Fracture. *Open Orthop J*. 2015;9:168-178. doi:10.2174/1874325001509010168

53. Gammon BM. Arthrokinematics of the Distal Radioulnar Joint in the Normal Wrist and Following Distal Radius Malunion Graduate Program in Medical Biophysics.

2016;(April):166. http://ir.lib.uwo.ca/etd.

54. Wu K, Padmore C, Lalone E, Suh N. An Anthropometric Assessment of the Proximal Hamate Autograft for Scaphoid Proximal Pole Reconstruction. *J Hand Surg Am*. 2018:1-8. doi:10.1016/j.jhsa.2018.04.021

55. Stoesser HL. A Biomechanical Investigation of Scaphoid and Lunate Kinematics During Wrist Motion. 2017;(January).

56. Kim JH, Lee KH, Lee BG, Lee CH, Kim SJ, Choi WS. Dorsal intercalated segmental instability associated with malunion of a reconstructed scaphoid. *J Hand Surg Eur Vol*. 2017;42(3):240-245. doi:10.1177/1753193416680133

57. Berger R, Bishop A, Bettingger P. New dorsal capsulotomy for the surgical exposure of the wrist. *Ann Plast Surg*. 1995;35(1):54-59.

Chapter 4

4 General Discussion and Conclusions

This chapter will briefly review the hypothesis and objectives set forth in the first chapter of this thesis. The conclusions of each study will then be summarized as well as their strengths, weaknesses and implications. Directions for future works, as well as the current understanding of this area will be discussed

4.1 Summary

The purpose of this work was to elucidate the impact of scaphoid malunion on wrist motion and joint mechanics as well as to characterize this relationship for progressive severities of scaphoid malunion. Presented in this thesis are the results of an *in-silico* study examining joint contact changes at the radioscaphoid joint as well as *in-vivo* analysis examining the kinematics of the scaphoid, lunate, capitate, and trapezium-trapezoid complex during simulated unrestrained planar wrist flexion-extension for progressive scaphoid malunion severities. The specific objectives detailed at the beginning of this work have been accomplished with results presented that were anticipated, as well as others that were unexpected.

The objectives of this thesis were:

1. Characterize how wrist contact is altered with progressive scaphoid malunion
2. Characterize how progressive scaphoid malunion affects the radial sided carpal bones.

The findings of the studies detailed in **Chapter 2&3** are reviewed and summarized below, as well as limitations of each study design.

4.2 Chapter 2: The Impact of Scaphoid Malunion on Radioscaphoid Joint Contact: An *In-Silico* Analysis

The first objective of these thesis was to characterize the association between scaphoid malunion severity and joint contact at the radioscaphoid joint. This was achieved using computational methods employing high fidelity models created from an active motion wrist simulator and a simplified model of scaphoid malunion. Using previously derived carpal bone models, various scaphoid models with increasing severities of scaphoid malunion were created. These malunited scaphoids were then simulated in their native wrist and the resultant changes in contact at the radioscaphoid joint was characterized.

The results presented in **Chapter 2** suggest that increasing scaphoid malunion severity is associated with increasing joint contact at the radioscaphoid joint. The of increase in contact varied from specimen to specimen but each showed similar progressive changes. One specimen in particular demonstrated a substantially different pattern of joint contact with larger changes occurring for each incremental increase in scaphoid deformity. This wrist had a unique topology of the radioscaphoid joint, implying that patients with a prominent inter-fossa ridge may be particularly prone to contact changes following injury. These results confirm the first hypothesis that increased scaphoid malunion severity would be associated with increasing joint contact.

4.3 Chapter 3: The Impact of Scaphoid Malunion Carpal Motion: An *In-Vitro* Analysis

The second objective of this work was to understand the impact of scaphoid malunion on radial sided carpal bone motion including the scaphoid, lunate, trapezium, trapezoid, and capitate. This was accomplished using a cadaveric model and an active motion wrist simulator. Planar flexion-extension was achieved using a force-position algorithm for 7 specimens placed in a gravity loaded position by exerting forces through tendons of interest. Optical trackers were placed on the aforementioned carpal bones to track carpal motion throughout wrist motion and between increasing severities of simulated scaphoid malunion.

The results presented in **Chapter 3** refute the hypothesis that increasing scaphoid malunion would be associated with altered scaphoid kinematics. The motion path of the scaphoid, capitate, as well as the trapezium-trapezoid complex were not significantly altered throughout all severities of scaphoid malunion. Interestingly, the motion path of the lunate was significantly altered with increasing scaphoid malunion severities. The lunate assumed a more extended posture for all wrist positions, and this extension became greater with increasing malunion severities. In addition, there was also an observed increase in scapholunate angle with progressive severities of scaphoid malunion implying the change in morphology to the scaphoid alters the positional relationships between the scaphoid and lunate. These changes imply that the morphology of the scaphoid influences the position of the lunate and alterations to native scaphoid morphology may cause secondary carpal malposition.

4.4 Strengths and Limitations

The work presented in this thesis has numerous strengths and limitations largely related to its *in-silico* and *in-vitro* nature. In both cases, although high fidelity measuring techniques were used to ensure accurate characterization, the models of scaphoid malunion were intentionally simplified to increases reproducibility between specimens. Specifically, the computational study employed a model of scaphoid malunion with a fixed axis of rotation and shortening, when in reality these injuries are complex processes with changes in geometry that is multiplanar. The malunion model used in the biomechanical study was carried out without the use of a jig due to the variability in size and morphology of carpal bones between specimens and as such is subject to error in surgical technique. As well, the motion studied in each case was simple planar flexion-extension. In reality, the wrist undergoes a large range of multi-planar motion, and as such the presented results may not represent true *in-vivo* interactions. The computational study assessed inter-bone interactions, which although this is related to joint contact, is not a direct surrogate for this measurement.

These investigations both had many strengths as well. Each study achieved statistical significance despite small numbers. This is a consequence of the RM-ANOVA statistical analysis in the setting of highly reproducible trials. Care was taken to preserve anatomical relationships and soft tissue structures whenever possible and all structures that were surgically incised were appropriately repaired. All specimens included in both studies were devoid of underlying pathologies as confirmed by both CT and fluoroscopy imaging.

4.5 Current and Future Directions

This current study serves to supply insight into carpal changes that occur following a scaphoid malunion and corroborate previous clinical studies that have suggested that altered scaphoid morphology results in significant changes to wrist mechanics. Future work is needed to further understand carpal mechanics and kinetics with a more precise model of scaphoid malunion, as well as to study secondary changes that occur at the lunate in this pathology.

Chapter 2 examined the inter-bone interaction of the scaphoid using highly accurate computational models of the wrist, these results were limited to the radioscaphoid joint and also subject to errors introduced in simplified planes of motion and models of malunion. Further work should investigate joint contact between the scaphoid and other surrounding bones including the trapezium and trapezoid.

In **Chapter 3,** it was demonstrated that scaphoid malunion did not significantly impact biomechanics of the scaphoid, capitate, trapezium, or trapezoid but did alter the lunate motion path. These changes in lunate motion need to be further quantified during multiplanar motion to better understand their significance.

Ideally, long term clinical investigations should be undertaken to determine if the observed alterations in carpal mechanics as a result of varying severities of scaphoid malunion, can prognosticate symptomatic arthrosis or carpal mal-positioning *in-vivo*. The time to post-traumatic arthritis following scaphoid malunion is not well known and as such, this work would need to be undertaken for a prolonged period of time to detect subtle changes.

4.6 Significance

Carpal motion and the relative contribution of each carpal bone to total wrist motion has been studied previously, but carpal kinetics and kinematics in pathologic states is relatively unknown. The natural history of scaphoid malunion remains a relatively unexplored area of wrist injuries, with only one documented basic science paper to date. This thesis serves as the framework to better understand the changes that occur in the wrist following scaphoid malunion and allows for the targeting of future works to determine factors that may be clinically important. A detailed understanding of how wrist mechanics change in the setting of scaphoid injury also contributes to the overall understanding of native wrist mechanics and the scaphoid's role in the coordination of this motion.

The scaphoid is the most commonly fractured carpal bone. With the majority of these injuries impacting young healthy individuals, it is paramount to understand the natural history following fracture to direct clinical treatment in an effort to avoid secondary complications and arthrosis.

This study has shown that increasing scaphoid malunion severity is associated with altered contact at the radioscaphoid joint and progressive extension of the lunate in all wrist positions. The exact clinical impact of these changes has yet to be investigated, but these findings serve as the basis for understanding carpal kinetics and kinematics following scaphoid malunion. By targeting future clinical work to better characterize these changes, treatment guidelines may be developed to better serve patients and inform surgical decision making.

Appendices

Appendix A: Glossary

Active Motion	Motion accomplished by transmitting forced through tendons of interest that cause movement in normal physiologic conditions
Arthritis	Disorder impacting joints leading to inflammation, incongruity of joint surfaces and limitations in motion
Arthrosis	Degenerative change of a joint or articular surface
Arthrodesis	The fusion of a joint to remove motion
Anterior	Towards the front of the body
Biomechanics	The study of the forces produced or applied to biological structures and organisms
Casting	Immobilizing a part of the body by placing it in a rigid external construct, typically made of plaster or fiberglass
Coronal	In plane with the face
Cranial	Towards the head of the body
Cephalad	Towards the foot of the body
Distal	Away from the origin or attachment of a structure
Extension	Motion bringing two parts of the body farther apart

Flexion	Motion bringing two parts of the body closer together
Inferior	Located below
Lateral	Towards the outside of the body
In-Silico	Latin; an experiment conducted by means of computer modelling
In-Vitro	Latin; an experiment conducted outside of a living organism
In-Vivo	Latin; an experiment conducted within a living organism
Kinematics	The study of motion
Kinetics	The study of forces acting on mechanisms
Ligament	A fibrous structure made of connective tissue connecting one bone to another
Malunion	Union of a fracture in a non-anatomical position
Medial	Towards the center of the body
Non-Union	Failure of a fracture to unite within a predefined time frame
Passive Motion	Motion accomplished by exerting force externally
Posterior	Towards the back of the body
Proximal	Towards the origin or attachment of a structure

Pronation	Rotation of the hands downwards at the level of the forearm
Reduction	Repositioning components of a fracture to an anatomic position
Sagittal	A plane which divides a structure into left and right
Servomotor	An electronic motor capable of producing precise forces and movement
Superior	Located above
Supination	Rotation of the hands upwards at the level of the forearm
Tendon	A fibrous structure made of connective tissue connecting muscle to bone
Union	Healing of a fracture

Spencer Chambers

Education

Plastic and Reconstructive Surgery Residency Schulich School of Medicine & Dentistry, Western University, London ON	2017 – Current
Masters of Science in Surgery (MSc) Western University, London ON	2018 – Current
Doctor of Medicine (MD) Schulich School of Medicine & Dentistry, Western University, London ON	2013 – 2017
Electrical and Biomedical Engineering (B.Eng.) *Graduated Summa Cum Lade*, McMaster University, Hamilton ON	2009 – 2013

Awards

James Roth Resident Research Award: Best Academic Paper. Department of Plastic and Reconstructive Surgery, Schulich School of Medicine & Dentistry Awarded to best research paper within the division of Western Plastic & Reconstructive Surgery	2019
Master of Science in Surgery Colloquium Best Presentation Paper. Department of Surgery, Schulich School of Medicine & Dentistry Awarded to best research presentation within the Master of Science in Surgery Program of Western Department of Surgery	2019
Western University Graduate Student Innovation Scholar (GSIS) (1500$). Ivey School of Business: Pierre L Morrissette Institute for Entrepreneurship Graduate scholarship aimed to foster collaboration within multidisciplinary teams targeting opportunities for innovation and entrepreneurship	2018
Frederick Banting and Charles Best Canada Graduate Scholarship (17500$). Canadian Institute of Health Research (CIHR). National organizations funding high quality graduate health research	2018
Ontario Graduate Scholarship (15000$) **(***Declined*), Western University. Based on cumulative undergraduate performance and potential to succeed in postgraduate training	2018
Dr. Donald and Christina Jolly Medical Student Bursary (1200$). Schulich School of Medicine & Dentistry. Based on academic accomplishments and financial need	2015
Summer Studentship Award (4500$). Technology Evaluation in the Elderly Network. Selected in top ten of applicants based on research proposal, CV and reference letters	2015
Dr. Alexander Graham Award (900$). Schulich School of Medicine & Dentistry. Based on academic accomplishments and financial need	2014

Western University Entrance Award (3400$), Schulich School of Medicine & Dentistry. Based on academic accomplishments and financial need — 2013

Ontario Graduate Scholarship (15000$) (*Declined*), Western University. — 2013
Ontario Graduate Scholarship (15000$) (*Declined*), McMaster University. — 2013
Based on cumulative undergraduate performance and potential to succeed in postgraduate training.

McMaster University Provost Honor Roll, McMaster University. Achieved a sessional GPA of 4.0, awarded to <1% of student body — 2013

McMaster University Deans Honor List, McMaster University. Awarded for achieving a sessional GPA of 3.5 or greater — 2010–2013

Scholarly Activities

Publications

Pavlosky A, Glauche J, **Chambers SB**, Al-Alawi M, Yanev K, Loubani T. Validation of an effective, low-cost, high-quality, Free/open access 3D-printed stethoscope. *PLOS ONE* 2017 — 2017

Chambers SB, Martin C, Ball I, Morgan B. Glycemic Variability and Delirium in the Critically Ill Patient. (Abstract) *Canadian Geriatrics Journal 2017;20(3): 126* — 2017

Chambers SB, Grant A. Skin Cancer: An Ideal Candidate for Preventative Medicine *University of Western Ontario Medical Journal. November 2016; 86(2): 37-40* — 2016

Invited Presentations

The Impact of Scaphoid Malunion on Carpal Kinematics: A Biomechanical Study, Presentation at Western Department of Surgery Resident Research Day 2019 Meeting, London, ON — 2019

Posters and Presentations

Assessing Success of Implant Based Breast Reconstruction Following Radiation Therapy, Poster at Canadian Surgery Forum 2019 Meeting, Montreal, QC — 2019

Analysis of Scaphoid Malunion Clinical and Radiographic Outcomes at a Minimum of 4 Years Follow-Up, Presentation at American Association of Hand Surgeons (AAHS) 2019 Meeting, Palm Desert CA — 2019

The Impact of Scaphoid Malunion on Radioscaphoid Joint Contact: A Computational Study, Poster at American Association of Hand Surgeons (AAHS) 2019 Meeting, Palm Desert CA — 2019

Analysis of Scaphoid Malunion Clinical and Radiographic Outcomes at a Minimum of 4 Years Follow-Up, Poster at American Society for Surgery of the Hand 73rd annual meeting, Boston Massachusetts — 2018

Association between Scaphoid Malunion and Radioscaphoid Joint Contact: A Computational Study, Presentation at Resident Research Day, Department of Plastic and Reconstructive Surgery, London ON — 2018

Traumatic Spinal Cord Injuries, Presentation at Presentation at Victoria Hospital, Department of Traumatology Grand Rounds, London ON	2017
Stenosing Flexor Tenosynovitis (Trigger Finger), Presentation at Toronto Western Hospital, Department of Plastic Surgery Rounds, Toronto ON	2016
Skin Cancer Screening in Primary Care, Presentation at St. Josephs Family Health Team, Department of Family Medicine Grand Rounds, London ON	2016
PKU: Challenges of Diet in the Aging Patient, Presentation at Victoria Hospital, Department of Genetics and Metabolic Medicine Grand Rounds, London ON	2015
Glycemic Variability and Delirium in the Critically Ill Patient, Poster at Technology Evaluation in the Elderly Network Annual Conference, Toronto ON	2015
Glycemic Control and Delirium in the Intensive Care Unit, Presentation at Victoria Hospital, Critical Care and Trauma Center Grand Rounds, London ON	2015
Different Paths to Medical School, Presentation at Kincardine District Secondary School, Kincardine ON	2014

Professional Memberships

American Society of Plastic Surgeons (ASPS) Resident Member	2018 – Current
Professional Association of Residents in Ontario Plastic & Reconstructive Surgery Division Representative	2018 – 2019
Canadian Society of Plastic Surgeons (CSPS) Resident Member	2017 – Current
Canadian Federation of Medical Students (CFMS)	2014 – 2017
American Society of Plastic Surgeons (Student Member)	2016 – 2017
Canadian Medical Association (CMA)	2013 – Current
Ontario Medical Association (OMA)	2013 – Current
Golden Key Honors Society	2013 – Current

Research Experience

Clinical Research Studentship - Glycemic Variability and Delirium in the Critically Ill. 2015-2018
Victoria Hospital, Critical Care and Trauma Centre, London ON

Supervisors: Dr. Ian Ball MD & Dr. Claudio Martin MD

Delirium is a well-known disorder that occurs in the critically ill. Despite its prevalence, the pathophysiology is poorly understood. I carried out a prospective observational study to evaluate the relationship between glycemic variability and the incidence of delirium. This included writing research proposals, working in a multidisciplinary team, collecting data, creating data analysis software and writing a manuscript.

Hardware Development Engineer - The Glia Project: Free Medical Hardware. Department of Emergency Medicine, London Health Science, London ON 2014-2015

Supervisor: Dr. Tarek Loubani MD

The Glia project is a group of engineers and medical professionals with the common goal of creating medical devices that can be produced at low costs in impoverished areas. I was responsible for the design, prototyping and creation of microelectronic circuits to be used in electrocardiogram and pulse oximetry devices. I was also involved in group management, organizing meetings between global members and creating concise documentation for the end user.

Summer Studentship – Sodium Magnetic Resonance Imaging and Intercellular Pressure Changes in Cervical Cancer. Department of Medical Imaging, Department of Gynecologic Oncology**.** St. Joseph's Hospital & Juravinski Hospital, Hamilton ON 2013

Supervisors: Dr. Mike Noseworthy PhD, PEng & Dr. Raimond Wong MD

There are many known microvascular and physiologic changes that occur in tumors as they develop. In this project I was tasked to create an intercellular pressure monitor as well as a novel sodium MRI coil to study these changes. I worked independently designing, testing and building these devices. I was also responsible for presentations on my research, scheduling progress meetings, and carrying out statistical analysis of my data.

Research and Design Engineer – Myoelectric Upper Limb Orthosis. Department of Engineering**.** McMaster University, Hamilton ON 2013

Supervisors: Dr. Hubert deBruin PhD, P.Eng

In my final year research course, I led a team of fellow engineering students in the design and implementation of a myoelectric driven upper limb orthotic device. This involved coordinated meetings, the delivery of regular status updates, prospective planning, software design, hardware design and numerous presentations. The final product integrated a custom electromyograph system to control a nerve stimulator and restore basic hand function.